Université de Montréal

Biceps Brachii Synergy and Its Contribution to Target Reaching Tasks within a Virtual Cube

par
Liang HE

Institut de génie biomédical
Département de pharmacologie et physiologie
Faculté de médecine

Thèse présentée en vue de l'obtention du grade de
Philosophiae Doctor (Ph.D.)
en génie biomédical

Juillet 2019

Université de Montréal

Institut de génie biomédical
Département de pharmacologie et physiologie
Faculté de médecine

Cette thèse intitulée

Biceps Brachii Synergy and Its Contribution to Target Reaching Tasks within a Virtual Cube

Présentée par

Liang HE

A été évaluée par un jury composé des personnes suivantes

Dr Dany GAGNON
Président-rapporteur

Dr Pierre A. MATHIEU
Directeur de recherche

Dr Fabien DAL MASO
Membre du jury

Dr Philippe ARCHAMBAULT
Examinateur externe

Dr Paul ALLARD
Représentant de la doyenne

Résumé

Ces dernières années, des travaux importants ont été observés dans le développement du contrôle prothétique afin d'aider les personnes amputées du membre supérieur à améliorer leur qualité de vie au quotidien. Certaines prothèses myoélectriques modernes des membres supérieurs disponibles dans le commerce ont de nombreux degrés de liberté et nécessitent de nombreux signaux de contrôle pour réaliser plusieurs tâches fréquemment utilisées dans la vie quotidienne. Pour obtenir plusieurs signaux de contrôle, de nombreux muscles sont requis mais pour les personnes ayant subi une amputation du membre supérieur, le nombre de muscles disponibles est plus ou moins réduit selon le niveau de l'amputation. Pour accroître le nombre de signaux de contrôle, nous nous sommes intéressés au biceps brachial, vu qu'anatomiquement il est formé de 2 chefs et que de la présence de compartiments a été observée sur sa face interne. Physiologiquement, il a été trouvé que les unités motrices du biceps sont activées à différents endroits du muscle lors de la production de diverses tâches fonctionnelles. De plus, il semblerait que le système nerveux central puisse se servir de la synergie musculaire pour arriver à facilement produire plusieurs mouvements. Dans un premier temps on a donc identifié que la synergie musculaire était présente chez le biceps de sujets normaux et on a montré que les caractéristiques de cette synergie permettaient d'identifier la posture statique de la main lorsque les signaux du biceps avaient été enregistrés. Dans un deuxième temps, on a réussi à démontrer qu'il était possible, dans un cube présenté sur écran, à contrôler la position d'une sphère en vue d'atteindre diverses cibles en utilisant la synergie musculaire du biceps. Les techniques de classification utilisées pourraient servir à faciliter le contrôle des prothèses myoélectriques.

Mots-clés: membre supérieur, prothèses myoélectriques, biceps brachial, cube virtuel, synergie musculaire, électromyographie, cibles.

Abstract

In recent years, important work has been done in the development of prosthetic control to help upper limb amputees improve their quality of life on a daily basis. Some modern commercially available upper limb myoelectric prostheses have many degrees of freedom and require many control signals to perform several tasks commonly used in everyday life. To obtain several control signals, many muscles are required, but for people with upper limb amputation, the number of muscles available is more or less reduced, depending on the level of amputation. To increase the number of control signals, we were interested in the biceps brachii, since it is anatomically composed of 2 heads and the presence of compartments was observed on its internal face. Physiologically, it has been found that the motor units of the biceps are activated at different places of the muscle during production of various functional tasks. In addition, it appears that the central nervous system can use muscle synergy to easily produce multiple movements. In this research, muscle synergy was first identified to be present in the biceps of normal subjects, and it was shown that the characteristics of this synergy allowed the identification of static posture of the hand when the biceps signals had been recorded. In a second investigation, we demonstrated that it was possible in a virtual cube presented on a screen to control online the position of a sphere to reach various targets by using muscle synergy of the biceps. Classification techniques have been used to improve the classification of muscular synergy features, and these classification techniques can be integrated with control algorithm that produces dynamic movement of myoelectric prostheses to facilitate the training of prosthetic control.

Keywords: upper limb, myoelectric prostheses, biceps brachii, virtual cube, muscle synergy, electromyography, targets.

Table of Contents

List of Tables

List of Figures

List of Acronyms

ANN: Artificial neural network
AP: Action potential
AR: Augmented reality
BB: Biceps brachii
BMI: Body mass index
CNS: Central nervous system
CoD: Coefficient of determination
DoF: Degrees of freedom
ELM: Extreme learning machine
EM: Expectation-maximization
FA: Factor analysis
FF: Fast fatiguable
FFR: Fast and fatigue resistant
FR: Fatigue resistant
LDA: Linear discriminant analysis
LH: Long head
MAV: Mean average value
MDC: Minimum distance classifier
MN: Motor neuron
MU: Motor unit
MUAC: Mid-upper arm circumference
MVC: Maximal voluntary contraction
NMF: Non-negative matrix factorization
PCA: Principal component analysis
pICA: Probabilistic independent component analysis
RK4: Runge-Kutta 4^{th} order
RMS: Root mean square
ROC: Receiver operating characteristic
SD: Standard deviation
sEMG: Surface electromyography
SH: Short head
SNR: Signal-to-noise ratio
SP: Static postures
SVM: Support vector machine
SVR: Support vector regression
TAC: Targeted achievement control
TLX: Task load index
VAF: Variation accounted for
VR: Virtual reality

Acknowledgements

First, I want to thank the members of my jury. Your scientific opinions matter to me and certainly allow me to improve my thesis. I would like to appreciate my research director, Professor Pierre A. Mathieu for giving me this opportunity to conduct scientific research in his laboratory and for his financial support. I will always be very grateful for our discussions, the conferences for me to attend, and journal articles that we have collaborated on.

I would also like to thank Professor Michel Bertrand and Jean Laurier for their suggestions to improve my research results in numerous group reunions of Electromyography Laboratory. I appreciate the help from Martin Robert during the fabrication of the electronic circuits and the participation in a pilot study of the research.

I would like to thank Professor Alain Vinet for providing advice in the matter of graduate study in biomedical engineering program. I would also like to thank Professors Philippe Comtois, Michel Bertrand, and Maxime Raison for being members of my predoctoral general examination committee. I would like to thank Dr. Gilles Noël and Vice-dean Pierre Belhumeur for providing consultations in the matter of student and research advisor relationship.

I appreciate my friends, my relatives, and my family for their support.

1. Introduction

Following an upper limb amputation, myoelectric controlled prostheses are commonly used by upper limb amputee persons to remediate their incapacity to produce important movements in their daily activities. With technological advancements, new prostheses have many degrees of freedom (DoF), and many surface electromyography (sEMG) signals are needed to use them at their full functional potential.

1.1. Background

The first myoelectric prosthesis was developed in 1960s by the Russians (Sherman, 1964). The prosthesis had a single function: open and close the hand that was realized by contracting 2 different muscles. Nowadays, modern myoelectric prostheses having many DoFs require many control signals to fully benefit from their potential. While for normal subjects, the available muscles to provide sEMG signals are abundant, the situation is different after an upper limb amputation, which could have reduced significantly the number of available sites to generate sEMG signals. With this challenging problem, the method presented in this research is to use surface electrodes positioned across the biceps brachii (BB) muscle of normal subjects and to experiment on whether muscle synergy as neural control signal can be extracted with a non-negative matrix factorization (NMF) algorithm (Lee and Seung, 2001) while the subjects place their upper limbs at different static postures. The BB muscle is used because it is involved in the shoulder stabilization, elbow flexion, and forearm supination, and on its inner surface up to 6 individually innervated compartments were observed (Segal, 1992).

Two research questions

1) From a single muscle such as the BB, is it possible to extract muscular synergy?
2) Could features of the muscular synergy of the biceps be used to control the movement of a small sphere within a cube presented on a screen?

To answer these questions, we initially used a database of sEMG signals from the BB muscle of 10 healthy subjects previously set up by Nejat (2012). With those signals, we wanted to verify if muscular synergy was present in the biceps. Then, an experimental protocol was designed to evaluate if features of the muscular synergy of the biceps could be used to control the displacement of a small sphere in a virtual cube presented on a screen.

1.2. Hypotheses and objectives

Hypothesis #1

Physiological evidence from animals and humans suggested that central nervous system (CNS) could use muscle synergy to simplify its control of task-oriented body movements. The simplification is achieved through the simultaneous activation of a group of muscles working together to produce a movement. Due to its 6 individually innervated compartments and its multifunctional role in the upper limb, the BB can be considered as muscles within a muscle. This leads to the hypothesis that muscle synergy could be extracted from this single muscle to provide multiple control signals. To test the hypothesis, the verifiable criterion is that recognizable patterns should be obtained from features of muscle synergy extracted from different upper limb static postures.

Objective #1

The first objective is to determine whether muscle synergy exists in the multifunctional biceps muscle. To achieve this objective, literature review is to be conducted to determine conventional methods for muscle synergy extraction from muscle activities. Critical review of literature should lead to the synthesis of theoretical method to determine the existence of muscle synergy from single muscle. The method is then used to demonstrate the extraction of muscle synergy from biceps muscle. Another task is to determine whether the identified features of muscle synergy can be used to classify paired static upper limb postures. This includes the use of a classification system (specifically the minimum Euclidean distance classifier) to classify paired static postures. The last task is to determine the performance of the posture classification system based on the classification accuracy.

Hypothesis #2

Features of muscle synergy of the biceps obtained under different upper limb postures are control signals having the potential, within a virtual cube, to move a small sphere toward a target. In terms of control theory, a movement can be considered as a combination of many motor primitives, where the individual motor primitive associated with muscle synergy can be interpreted as a position regulation problem, where synergistic muscles provide the balancing force to maintain a static posture of the upper limb. To test the hypothesis, the verifiable criterion is that individual subject without any previous motor learning experience with a virtual interactive program could produce certain specified motor control tasks with control signals obtained from features of their biceps' muscle synergy.

Objective #2

The primary objective is to develop a pattern recognition based control system to facilitate the control of task-oriented movements. First, a posture classification system that could classify multiple static postures by using features of muscle synergy from biceps muscle is to be developed. This is followed with the development of an intermittent control system that allows the pattern recognition system to be used as a part of the control system for target reaching tasks in a computer simulated virtual environment. Lastly, an interactive program is developed to evaluate the task performance with control signals from biceps muscle.

1.3. Organization of the thesis

Following the Introduction, a Literature Review is presented on the theory of muscle synergy, techniques to extract muscle synergy, and the application to upper limb posture recognition. Next follows is a chapter on Materials and Methods, which describes customized sEMG amplifiers and filters, data processing and classification algorithms, and implementation of online interactive program. Chapter 4 consists of a published article describing how muscular synergy was extracted from pre-recorded sEMG signals obtained from the BB of 10 normal subjects and how features of muscle synergy could be used to determine in which upper limb postures the subjects were when the data was recorded. In Chapter 5, a second article (submitted for publication) is presented, where features of the biceps muscle synergy were used to control the displacement of a red sphere toward a target within a cube presented on a screen. To do this, a clustering algorithm was used to identify synergy features associated with each static upper limb posture among a set of 8. The identified posture is used as input to an intermittent control system to control the displacement of the red sphere. Complementary results from an

experienced subject are presented in Chapter 6, where the control of a small humanoid manipulator with the biceps muscular synergy and dynamic control of upper limb of a virtual avatar are also presented. In the Discussion, limitations of the proposed approach are presented in relation to other myoelectric prosthesis controls and compared with existing technologies. Finally, recommendations are made for improvement of the research methodology, and perspective is provided for future research direction.

2. Literature Review

2.1. Anatomy and physiology of skeletal muscles

2.1.1. Skeletal muscles

Skeletal muscles are made of many grouped muscle fibers (Fig. 2.1a). The average diameter of the muscle fiber is 50 – 60 μm. A muscular fibre is composed of many cylindrical elements called the myofibrils, which are bundled along the length of the muscle fiber with light and dark bands that are called sarcomeres.

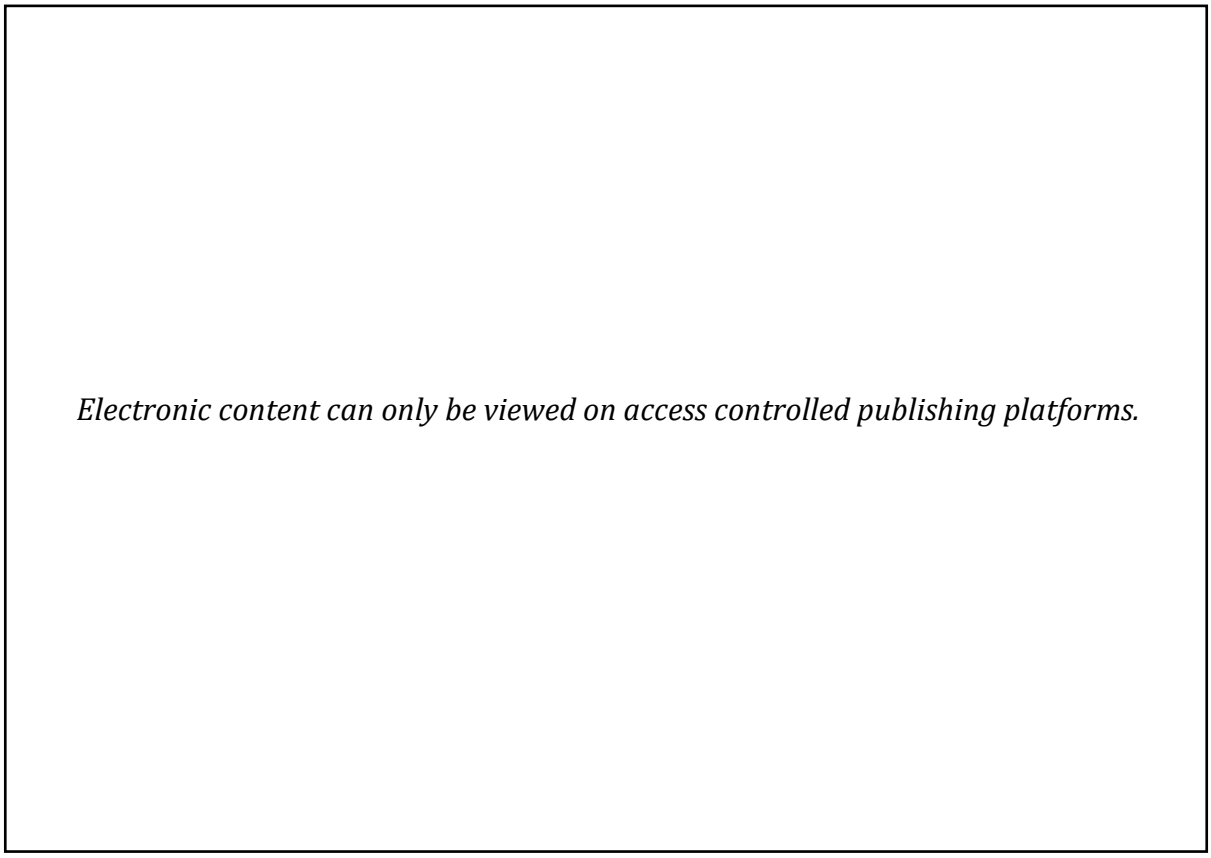

Fig. 2.1 Motor unit innervates the muscle fiber: (a) motor neuron in spinal cord provides innervation to the muscle fibers; (b) photomicrograph of neuromuscular junctions (Human anatomy & physiology 7th ed, Fig. 9.13, p. 296, Marieb and Hoehn, 2007). [Reprinted by permission of Pearson Education, Inc., New York, New York.]

Sarcomeres form the basic contraction mechanism of the muscle with thin and thick myofilament. During the muscle contraction, the thick myosin filament pulls up on the thin actin filament via myosin heads. Attachment of the myosin on the actin is called a cross bridge, and the length of a sarcomere shortens as the myosin pulls on the actin filament toward the center of the sarcomere. This fundamental mechanism of muscle contraction is known as the sliding filament theory (Huxley and Niedergerke, 1954, Huxley and Hanson, 1954).

Muscular fibers are innervated by motor neurons (MNs) located in the spinal cord through neuromuscular junctions (Fig. 2.1b). As shown in Fig. 2.2, the intramuscular action potential (AP) at rest is about -70 mV. The depolarization of the muscle fiber up to + 30 mV is due to the opening of ionic channels on the membrane of the muscle fiber. This AP (-70 to +30 mV) then propagates from the neuromuscular junction in opposite direction toward the 2 ends of each fiber of a motor unit (MU).

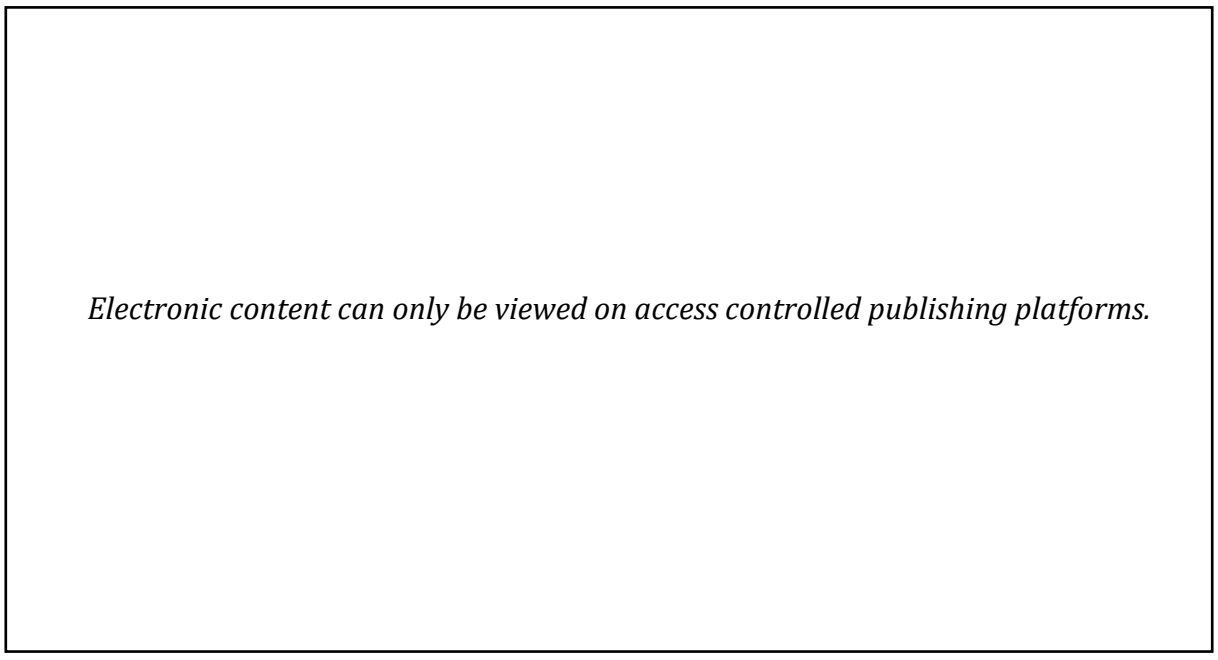

Fig. 2.2 Action potential of muscle fiber (Human anatomy & physiology 7th ed, Fig. 9.9, p. 291, Marieb and Hoehn, 2007). [Reprinted by permission of Pearson Education, Inc., New York, New York.]

Ionic exchanges associated with a muscular AP can be transformed as an electronic potential through an electrode, and the detected signal is known as EMG. The AP of a single muscle fiber can be identified with single fiber electrodes (Sanders et al., 2019). Amplitude of the EMG is inversely proportional to the squared distance between active muscle fibres and the detection sites. EMG amplitude at the skin surface is in the μV range, and its frequency spectrum ranged from 10 to 500 Hz; the intramuscular EMG spectrum can reach up to 3 kHz.

Skeletal muscle fibers can be classified as type I, which is fatigue resistant (FR), type II, fast and fatigue resistant (FFR), and type III, fast and fatiguable (FF). The FR fibers use aerobic metabolism and function mainly to sustain the body postures. The fast muscle fibers use anaerobic metabolism to supply energy, and they are used in fast movements. Majority of the muscles has all the three types of muscle fiber in their composition. The type of muscle fiber is the same in a MU.

The force generation of a MU is directly proportional to the number of innervated muscle fibers. The force generated by a muscle is controlled by the CNS: initially, the MU discharge frequency is increased up to its tetanic level, following which other MUs are recruited from small ones up to large ones according to the Henneman's size principle (Henneman, 1957, Henneman et al., 1965).

2.1.2. Biceps brachii muscle

Under voluntary control, skeletal muscles are attached to the skeleton with tendons (Fig. 2.3A). The point where a muscle attaches to the bony skeleton, which does not move, is called the point of origin, and the point of insertion is the one which crosses an articulation and moves the limb when the muscle is contracted.

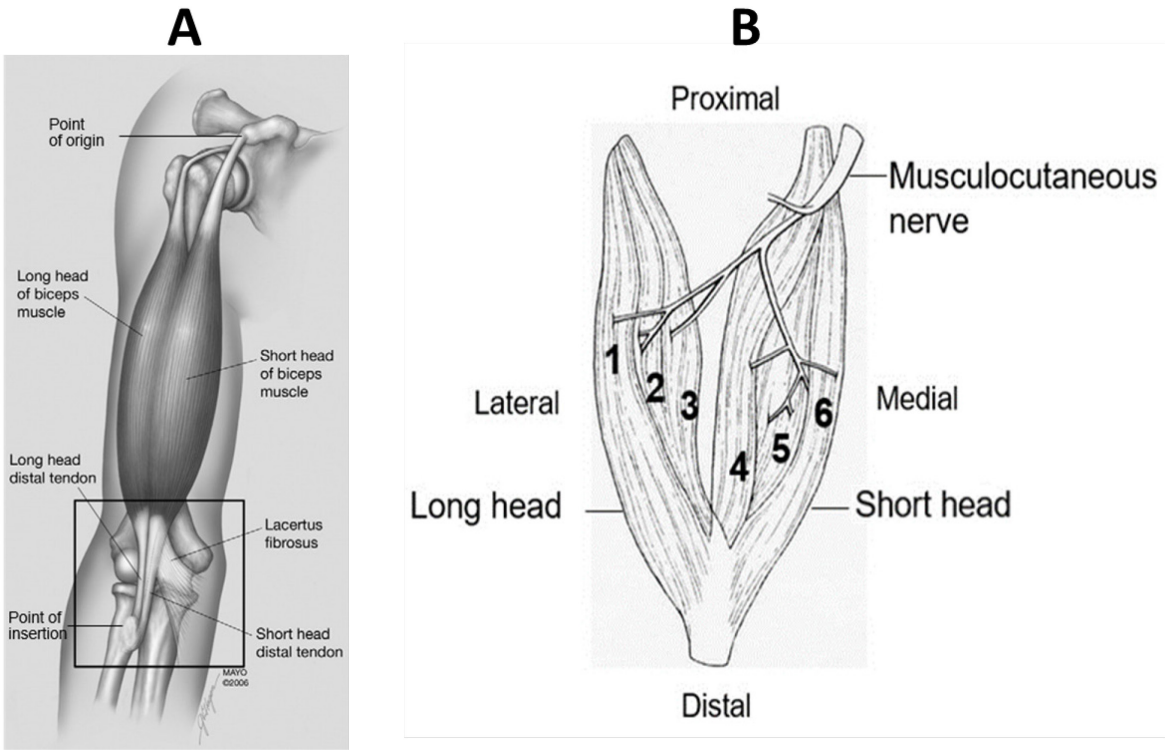

Fig. 2.3 Anatomy of biceps brachii. **A**: Structural attachment (origin and insertion) of the biceps muscle via tendon to the bone (Athwal et al., 2007) [Figure is used with permission of Mayo Foundation for Medical Education and Research, all rights reserved.]; **B**: Illustration of the posterior or deep surface of biceps brachii, where 6 compartments innervated individually by musculocutaneous nerve (Segal, 1992). [Reproduction with minimal alteration of the illustrations with permission of Elsevier.]

As its name suggested, the BB has 2 main divisions: a long head (LH) and a short head (SH). Origin of the SH is the coracoid process of the scapula while origin of the LH is the supraglenoid tubercle just above the shoulder joint. Both heads are inserted along the outer ulnar margin of the bicipital tuberosity (Athwal et al., 2007). However, the SH inserts more distally than LH. According to the origin and insertion points of the two heads, SH of the biceps predominantly acts as a monoarticular muscle while the LH of the biceps predominantly acts as a biarticular muscle. This indicates that LH could be involved in more activities of the upper limb movements than SH.

Schantz et al. (1983) found that the cross-sectional area of BB measured among 26 years old subjects was 23.5 cm^2 for male and 14.4 cm^2 for female. From MRI measurement, Hubal et al. (2005) found the cross section area was 22.5 cm^2 for male and 14.0 cm^2 for female among 585 subjects. The volume of BB was 293.6 cm^3 from MRI measurement and 311.5 cm^3 from ultrasound imaging (Miyatani et al., 2004).

From the investigation of muscle fiber type (Dahmane et al., 2005, Srinivasan et al., 2007), the amount of type I muscle fiber (i.e. FR) in the LH was 39%, and that of SH was 37%. This suggested that the muscle fibers were predominantly type II and III (i.e. FFR and FF). There are 580000 muscle fibers in the BB muscle innervated by approximately 774 MUs (Buchthal and Schmalbruch, 1980).

According to the origin and insertion, SH is a primary elbow flexor and supinator (Jarrett et al., 2012). For LH, it has function of generating force in more direction than the SH (Buchanan et al., 1986). The main function of the BB muscle is the elbow flexion and forearm supination; however, due to the orientation of its tendon attachment, the muscle is also involved in the initial arm elevation at the shoulder joint (Landin et al., 2008) and in the stabilization of the glenohumeral joint (Andrews et al., 1985).

In addition to the presence of 2 heads, Segal (1992) observed on the inner face of cadavers' biceps that the muscle could be further subdivided into 6 individually innervated compartments (as shown in Fig. 2.3B). However, variety in number of compartments could be expected due to muscle architecture and nerve branching pattern. According to the author, the anatomical compartments could be associated with the branching of the nerve that innervates the muscle, and individual compartment within the muscle could supply a mechanically

different function with respect to other compartments. ter Haar Romeny et al. (1984) also found different MU recruitment patterns associated with different functions of the biceps muscle. From anatomical and physiological evidence, English et al. (1993) proposed the compartmentalization hypothesis for multifunctional muscles.

Out of the five terminal nerves of the brachial plexus, the musculocutaneous nerve is responsible for the BB muscle contraction. The nerve originated from C5-C7 spinal segments of the lateral cord (Papin, 2004) has both motor and sensory function. Evidence has shown that this nerve innervates both LH and SH of the biceps muscle as well as the brachialis muscle. Damage to the musculocutaneous nerve causes reduction of function in elbow flexion and forearm supination (Osborne et al., 2000). The variation in formation, origin, and distribution of the nerve is huge. According to Chiarapattanakom's investigation (1998) into 56 cadavers, the branching patterns of the nerve have 3 distinct types: 62% of the nerves have 1 branch to BB muscle, 33% of the nerves have 2 branches, and 5 % have 3 branches. The length of the musculocutaneous nerve innervating the BB ranges from 25 to 88 mm.

2.2. Surface electromyography

Neurons, sensory receptors, and muscle fibers are at the origin of bioelectric phenomena (Malmivuo and Plonsey, 1995). To model a bioelectric phenomenon, ionic currents involved in the generation of APs are usually represented by a dipole source. To reach the skin surface, that source has to travel through a media called the volume conductor which includes nerves, muscle fibers, fat, veins, arteries, etc.

Amplitude of the sEMG is associated with the level of contraction of the muscle under investigation, and sEMG signals are collected with non-invasive surface electrodes. Amplitude

of the sEMG can also be affected by many factors such as the skinfold thickness (De la Barrera and Milner, 1994), placement of the surface electrodes (Staudenmann et al., 2013), and crosstalk from other nearby active muscles (Farina et al., 2004). The volume conductor serves as a low pass filter, which attenuates the sEMG, making itself more easily affected by nearby sources of interference (Kuiken et al., 2003).

Côté and Mathieu (2000) presented a sEMG acquisition system with 3 by 8 Ag/AgCl monopolar electrode matrix that provides optimal spatial resolution to fit on the human upper limb. The system can provide simultaneous representation of the muscular activities during isometric contraction of the upper limb muscles. Authors found that the highest active region depends on elbow torque direction, but the results were also subject dependent. Authors suggested that the sEMG acquisition system could be used to solve inverse problem of muscle activation and to provide valuable information on electrode configuration in volume conduction studies. With such an acquisition system, decision algorithm for multifunctional myoelectric prosthesis can be implemented from the global pattern of muscle activities.

Exploring how the 6 compartments of BB could be used to facilitate the control of a myoelectric prosthesis, Nejat (2012) recorded 10 sEMG signals collected across the BB of 10 normal subjects. Different arm and hand positions were tested; for example, when the subjects were seated with the forearm flexed at $\sim 90^{\circ}$, activity over the SH in 5 of the 10 subjects was higher while their hand was in supination than in pronation. In the standing up position with the arm extended horizontally away from the body, activity was generally higher in the LH than in the SH.

2.3. Muscle synergy

Many muscles are usually activated to produce a movement, and when complex movements are produced, the task of the CNS to execute them rapidly and precisely could be considerable. To reduce the burden of CNS, Bizzi et al. (2000) considered that spinal cord circuits could control a small set of synergistic muscles. Presenting the modular organization of spinal motor systems, Bizzi et al. (2002) pointed out that muscle responses can be explained as a linear combination of a set of muscle synergies for construction of movement by the spinal cord. With evidence collected from frog, Bizzi et al. (2008) demonstrated that muscle synergies are natural structure encoded within spinal networks.

Investigation of neural activities in motor cortex and in spinal cord of several vertebral animals leads Bizzi and Cheung (2013) to hypothesize that CNS uses muscle synergies to activate many muscles in a coordinated fashion. In cats, Ting and Macpherson (2005) explained postural balancing tasks following a perturbation with muscle synergies. Bizzi and Ajemian (2015) explained the production of voluntary movements with terminologies of functional modules in spinal cord and pattern formation contributed from neural signals, such as sensory signals and motor memories. Bizzi (2016) revisited the motor control from the view point of muscle synergy and found that some synergies are shared by multiple motor tasks and others are task specific synergies. Both shared and task specific synergies could be used to facilitate complex movements in the motor control and motor learning.

2.3.1. Extraction of muscle synergy

The first algorithm to extract muscle synergy was proposed by Tresch et al. (1999) who investigated hind limb of the frog. The objective was to extract muscle covariation during

movements. Since muscle activation can only be positive, the activation components can only be positive. Therefore, they constructed a linear combination model, i.e.

$$m_i = \sum_{j=1}^{N} w_{ij} h_j, \quad w_{ij}, h_j \geq 0 \tag{2.1}$$

where m_i is the muscle activities, w_{ij} is the synergy matrix, and h_j is the synergy coefficient.

The synergy coefficient h_j was estimated with the positive constraint with a natural base function, i.e.

$$m_i = \sum_{j=1}^{N} w_{ij} e^{h_j} \tag{2.2}$$

where e^{h_j} assures that the coefficients stay positive. The synergy matrix w_{ij} was estimated with non-negative least squares algorithm. The synergy coefficients were then updated with prediction error in a gradient descent fashion. In each update, the synergy matrix needs to be normalized. The update of coefficient and matrix was repeated until a convergence criterion was met. With this procedure, authors found that the extracted synergies can explain above 90 % of the data variance consistently from different animals.

Non-negative matrix factorization (NMF) is commonly used for extracting synchronous muscle synergies. The factorization algorithm was first used for image processing by Lee and Seung (1999) to learn parts of an object in an image. The multiplicative update rule (Lee and Seung, 2001) used in the factorization algorithm is the most popular one that has been proved to have very good convergence properties as that of the expectation-maximization (EM) algorithm. Given a non-negative matrix (*M*), the algorithm determines two non-negative matrices (*W* and *H*). The multiplicative update rule determines the *H* matrix as follows:

$$H_{ij} = H_{ij} \frac{[W^T M]_{ij}}{[W^T W H]_{ij}} \tag{2.3}$$

and the W matrix as follows:

$$W_{ij} = W_{ij} \frac{[M H^T]_{ij}}{[WHH^T]_{ij}} \tag{2.4}$$

Conventionally, the number of muscle synergies to reconstruct sEMG signals was evaluated from the variation accounted for (VAF) (d'Avella et al., 2006):

$$VAF = 1 - \frac{SSE}{SST} \tag{2.5}$$

where *SSE* is the sum of the squared residuals, and *SST* is the sum of the squared residual from the mean values. The coefficient of determination (CoD) is also used to determine number of muscle synergies in active muscles, and CoD is obtained from the square of the correlation coefficient (Muceli et al., 2010).

To investigate whether muscle synergy could be used to discriminate different motor tasks, Delis et al. (2013) determined the number of task dependent muscle synergies with optimal task discrimination during a single trial hand pointing task experiment. Both simulated and real sEMG data were used to evaluate the method for determination of the optimal number of muscle synergies. The decoding-based method uses linear discriminant analysis (LDA) to evaluate the discrimination power of muscle synergy for different reaching movements as the number of synergies increases gradually. The decoding-based synergy selection method addresses not only the synergy approximation but also the mapping between synergy and task identification; therefore, the new method is more applicable than VAF in terms of task specific synergy selection.

2.3.2. Experimental evidence

Tresch et al. (2002) provided evidence from animal experiments (turtle, frog, and mammals) to support the hypothesis that spinal motor system uses muscle synergies as a strategy. Muscle synergies were also found in other movement behaviours of the animal, such as frog kicking (d'Avella et al., 2003), adduction-caudal extension-flexion rhythm of the frog (Saltiel et al., 2005), and frog swimming and jumping (Cheung et al., 2005). With considerable evidence, d'Avella and Tresch (2006) suggested that muscle synergies could be used to represent motor controls. When investigating the loading effects of frog hindlimb, Cheung et al. (2009) found that muscle synergy patterns are robust.

For Torres-Oviedo and Ting (2007) studying equilibrium strategies for postural response to a perturbation, they demonstrated that despite a high inter-trial variability, a small set of synergy patterns could account for a large variation of muscle activities. Their results suggested that muscle synergy was used consistently by all of their experimental subjects for postural control.

To gain insight of spatiotemporal organization of muscle patterns for fast-reaching movements of human subjects, d'Avella et al. (2006) collected muscle activity data from 19 shoulder and arm muscles during point-to-point movements between a central location and eight peripheral targets in 2 vertical planes. In their experiments, variable loads, variable hand postures, and complex movements were experimented. Spatiotemporal synergies were extracted, and 4 to 5 synergies explained 73-82% of the data variation. They found that amplitude coefficients in extracted time-varying muscle synergies had directional preference and low variation due to changes in load, posture, and target point. The results provided evidence

to support that CNS uses muscle synergy to simplify control tasks from fast-reaching point-to-point movements.

Muceli et al. (2010) investigated whether a set of synchronous muscle synergies of healthy subjects can represent arm movement in a horizontal plane, where shoulder and elbow joints were involved. Muscle synergies were extracted with NMF algorithm from the sEMG of 12 muscles (shoulder, chest, and back muscles). To estimate the non-negative synergy coefficient from a given movement direction, authors used the multiplicative update rule of the NMF while keeping synergy matrix constant. A single synergy matrix was extracted from various segments of a 12-direction reaching movements experiment. The muscle activity reconstruction accuracy with respect to actual muscle activities from sEMG was evaluated with CoD (r^2). The reconstruction of the 12 directional movements was evaluated with 1 to 4 muscle synergies extracted from selected joint movements. When synergies were extracted from a single movement direction, the reconstruction accuracy for the multiple directional movements was lower than that when synergies were extracted from multiple movement directions. This could indicate that synergies are task specific.

Sabzevari et al. (2017) studied the speed effect of the reaching movement during muscle synergy extraction. Six muscles from upper limb and shoulder joints were used to extract the muscle synergy with NMF algorithm at three different movement speeds. They found that three synergies were enough to obtain 99% VAF. Cosine similarity function and mutual information were used to measure the muscle synergy similarity. They found that high similarity can be obtained (above 0.7 for cosine similarity and above 0.75 for mutual information). However, the similarity of synergy coefficient is relatively low compared to those of synergy vectors. From their results, authors concluded that CNS uses muscle synergy to achieve goal directed

movement, and they hypothesized that different speeds of movement use similar muscle synergy with different synergy activation coefficients.

2.3.3. Modularity as movement building block

According to Ting and McKay (2007), body posture and movement can be achieved through “flexible” combinations of muscle synergies, which could be assimilated to building blocks to control body movements.

Reviewing time-varying muscle synergy extracted during coordinated point-to-point upper limb movements and during complex movements, such as via-point and change of direction after initialization of the movement, d'Avella and Lacquaniti (2013) confirmed that information on direction and speed of point-to-point movements can be extracted from time varying muscle synergies. They hypothesized that CNS could implement an intermittent control to perform fast and smooth reaching movement with combination of existing muscle synergies in an open-loop, where motor learning could be achieved from online adjustment from feedback mechanism. This suggests that CNS uses muscle synergy as the modular building block to produce complex movements.

A single muscle, such as the biceps brachii could also consist of different types of building blocks within the muscle that can participate in different motor tasks. For the same task (such as forearm supination), the limited variations in order to fulfill the biomechanical requirement could be expected according the size principle of the muscle recruitment; however, synergy patterns should be similar for the same task because building blocks within the muscle should have relative fixed position (for example, restricted within the same compartment).

When other tasks are performed (such as elbow flexion), changes in synergy pattern should be expected because other building blocks (from a different muscle compartment) become active.

For d'Avella et al. (2015), modularity is a product of evolution for the motor behavior, and authors suggest using it as a general structure from which the human motor control is accomplished. For example, in cognitive robotics, modularity is considered as functional unit exploring the potential of integration to accomplish complex tasks. The regularities (synergy patterns and corresponding activation coefficients) and low dimensionality of muscle synergy could be the by-product of optimization and constraint. To understand how motor control system works, researchers in evolutionary biology, neuroscience, control engineering, and rehabilitation need to work together.

2.4. Upper limb posture recognition with muscle synergy

Two types of posture recognition algorithm are considered usually in the literature. They are regression-based continuous prediction (Bi et al., 2019) and discrete posture classification (Scheme and Englehart, 2011).

Jiang et al. (2009) extracted muscle synergies from sEMG acquired from eight channels of bipolar electrodes placed on forearm and biceps muscles to predict force production from 3 joint axes movement of the wrist. They used the NMF algorithm to extract synergy control from each individual axis movement and then use them to predict simultaneous and proportional force production. With their synergy-based model, authors found that up to 2 DoFs force prediction was very good (78.5%) with 11 healthy subjects, but with the third DoF included in the prediction model the prediction accuracy drops (31.2%). When authors compared their synergy-based linear model with a nonlinear artificial neural network (ANN) model, they found ANN

was able to produce better prediction (64.9%) when all the 3 DoFs were included. This suggests that their proposed synergy-based linear model does not handle nonlinearity very well.

Atoufi et al. (2014) also used muscle synergies extracted from sEMG of 12 forearm muscles to predict force production from ANN that associated with wrist joint with 1 or 2 DoFs at different contraction levels. After examining the synergies extracted from different force levels of their 8 normal subjects, they found that synergy-based force prediction was robust when compared with estimation obtained with mean average value (MAV) of the sEMG. Authors suggested that synergy control could be used to provide proportional control of prosthesis.

Naik and Nguyen (2015) applied NMF algorithm (Lee and Seung, 2001) to sEMG signals to extract features with fourth order autoregression and root mean square (RMS) value function for finger gesture classification. Two types of finger gestures were considered: one type is the simple single finger flexion, and the other is complex finger flexion (combination of two fingers). They used an ANN to evaluate the classification performance. The results showed that simple finger flexion is easier to classify than complex finger flexion. Authors concluded that the less performing classification on complex fingers was associated with the determinant value of the matrix obtained from the NMF algorithm.

Ma et al. (2015) used muscle synergy features extracted from forearm muscles to classify hand and wrist movements with an algorithm previously proposed for simultaneous and proportional estimation of force (Jiang et al., 2009). After observing large fluctuations from the synergy features, authors proposed to apply an expert rule-based posture classification to improve the performance of the posture and movement estimation. The improved posture

classification system with muscle synergy feature gives above 90 % estimation performance for combined hand and wrist movements.

To investigate the simultaneous and continuous estimation of upper limb movements, Gui et al. (2016) used muscle synergy features from upper limb muscles to train the support vector regression (SVR) algorithm that maps the synergy activation to upper limb joint angles. To measure the continuous estimation performance, authors used VAF and absolute estimation error as performance indices. They found that an average VAF value of 88.1% was obtained from SVR model for the continuous estimation of upper limb movements from 6 normal subjects. With absolute estimation error index, the SVR model performed better than conventional ANN model.

Antuvan et al. (2016) compared sEMG with synergy features for movement intention estimation with extreme learning machine (ELM). The sEMG signals were obtained from upper limb, shoulder, and chest muscles of 7 subjects. From the evaluation of five upper limb postures, such as elbow flexion and extension, shoulder flexion, protraction, and retraction, and rest, authors found that sEMG features gave better training in offline mode than synergy features extracted with NMF algorithm (i.e. 99.37% vs 65.73%). For online mode classification, these authors found that synergy-based features gave better classification accuracy than sEMG features (i.e. 91.8% vs 84.1%).

The objective of the research of Rasool et al. (2016) was to implement a real-time hand gestures (1-2 DoF) classification system based on muscle synergy features extracted from sEMG signals of forearm muscles of 12 subjects. Their system consists of a synergy extraction stage and a task discrimination stage. In synergy extraction stage, the probabilistic independent

component analysis (pICA) algorithm was used to extract task specific muscle synergies. To implement the classification system in real-time, Kalman filters were used, where the measurement model was based on extracted muscle synergy, and the system model was based on a rather simple random walk model. Targeted achievement control (TAC) test was used to evaluate the effectiveness of their method for classifying hand and wrist movements. To compare the performance of their method, they also implemented LDA, ANN, and support vector machine (SVM) on the same discrimination tasks. They found that their method performed better than others.

Jiang et al. (2014) have implemented an online application of myoelectric control with synergy features from both able-bodied subjects and subjects with upper limb deficiency. In their application, muscle synergies were extracted from forearm muscles during two DoF movements of the wrist joint to provide simultaneous and proportional control in order to complete target reaching tasks in 2D space. After obtained 95% task completion rate from experiments with their subjects, they concluded that their approach of myoelectric control was more intuitive than other control approaches.

NMF as reviewed in Section 2.3.1 is a clustering algorithm that extracts features from sEMG signals. However, the NMF algorithm does not produce a unique solution, and that is why extracted synergy features need cluster validation (Theodoridis and Koutroumbas, 2009) to select optimal features for posture classification training. The minimum Euclidean distance classifier (MDC) is equivalent to LDA if the variance of the training data is assumed to be equal. However, if this is not the case in the obtained synergy features, then the classifier performance could be affected by the violation of the equal variance assumption. Atoufi et al. (2015) have used LDA with muscle synergies to classify tasks with different force levels with good

performance. In our review, advanced classification algorithm such as ANN, SVM, and ELM have been used to classify body postures from muscle synergy features. Obviously, these advanced classification algorithms could outperform simple classifiers such as MDC when same features are used for training. However, whether validated synergy features will allow a simple classifier to perform better has not been tested.

The above reviewed articles for upper limb posture recognition give simultaneous estimation of movement in two DoF movements; however, when the number of DoFs increases in their experiments, the estimation accuracy decreased. This is in contradiction with the muscle synergy theory, where CNS becomes more efficient with increased number of DoFs. Thus, methods that are consistent with the muscle synergy theory will be pursued in this research. For humans, most of their motor movements involve multiple joints, and modern robotic manipulators can simultaneous move more than 6 DoFs to reach random generated targets in 3D task space. The limitations of the muscle synergy-based estimation algorithm should thus be thoroughly considered to improve the estimation performance with natural human motor control if the algorithm is to be used to facilitate the control of modern prosthesis.

From a clinical perspective, the use of myoelectric prosthesis by amputees needs to be evaluated with a set of available tests, such as box and blocks test, clothespin relocation test, and Southampton hand assessment procedure. Our research is limited to normal subjects in laboratory settings. Thus, testing criteria are different from those used in a clinical setting. In particular, our evaluations are based on emerging pattern recognition based control. For evaluation from the pattern recognition perspective, the posture recognition accuracy is generally used. For evaluation from the control perspective, Fitts's law tasks were usually considered. The tasks include the evaluation of the response time, precision, accuracy, etc. of

the control. In our research, we will consider these testing requirements; thus, for pattern recognition, the posture classification accuracy will be tested, and for task control evaluation, target reaching time, posture changes before reaching a target, trajectory length when a target is reached in a specified time limit, and distance to the target in case of unreached target after a specified time limit are considered. For the control of the number of DoFs, our primary concern is to obtain control signals associated with the biceps muscle, which has three functions, such as flexing the shoulder joint, flexing the elbow joint, and supinating the forearm. Thus, three DoFs control can be provided to a myoelectric prosthesis. In terms of speed or maximum delay, these performance parameters can be calibrated to an arbitrary precision based on the existing control theory if a model-based control is used on the prosthetic device. Pattern recognition based control is an emerging control strategy for modern prostheses. Static posture pattern classification is considered as one component that requires other control components such as the intermittent controller as presented in this research to facilitate the integration of the myoelectric control system with human control.

3. Materials and Methods

3.1. First experimental protocol

To investigate the muscular synergy of the biceps brachii, two experimental protocols were used. In the first protocol, we used data that has been previously collected in our laboratory (Nejat, 2012), where sEMG signals had been collected across the biceps of 5 female and 5 male healthy subjects. Ten pairs of 6 mm surface electrodes were vertically and horizontally separated by 15 mm. To avoid the innervation zone, bottom row of the electrode array was placed 10 mm above the middle portion of the biceps. Two body postures were considered: seated with right arm close to the trunk and elbow flexed at 90°, and standing up with right shoulder abducted by 90° in coronal plane and elbow fully extended. Three to four isotonic and isometric contractions of 5 s were produced at 20% of the maximal voluntary contraction when seated and with a 1kg load applied to the wrist when standing up. In seated and standing postures, recordings were made when the hand was pronated (P), in neutral position (N), or supinated (S). Acquisitions of those signals were obtained with a Grass amplifier system (15LT) and a National Instrument data acquisition unit (NI USB-6225, National Instruments, USA) interfaced with LabView software that saved the acquired signal data in MATLAB files (MathWorks, USA) on a laptop computer. The collected sEMG signals were conditioned with RMS function prior to be used in the NMF algorithm for extraction of muscle synergies.

To make sure that the analyzed signals were from those of BB muscle, only signals from electrode pairs #2 to #9 were used. Processing was done on these 8 sEMG data sets to obtain muscle synergies of BB muscle and identify in which static posture the hand was when a given data set was recorded. A flow chart of our signal processing is shown in Fig. 3.1.

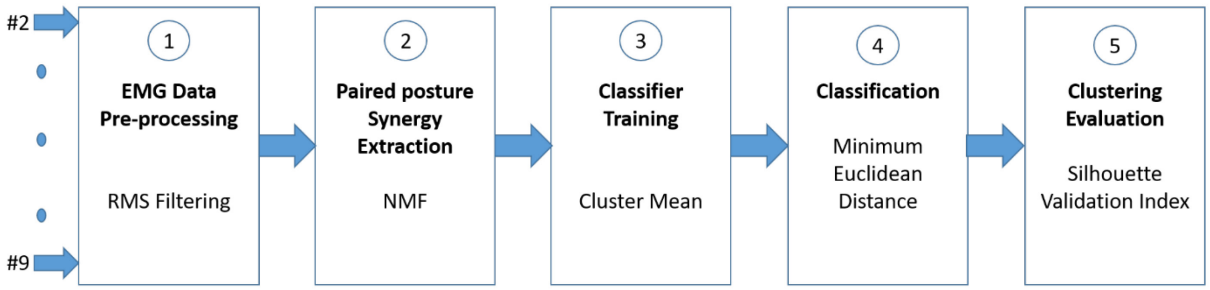

Fig. 3.1 First protocol flow chart: ① raw EMG signals from the biceps are smoothed with a RMS filter. ② sEMG signals from paired postures are concatenated before extracting muscle synergy. ③ mean values of muscle synergy from pairwise postures are used to train a minimum Euclidean distance classifier. ④ classification of paired postures is obtained with the trained classifier. ⑤ formation of the clusters is evaluated with silhouette clustering index to increase the discrimination power.

In the first stage, each channel of the EMG is filtered with a window of 815 ms over which RMS values are obtained, and the window has a moving step size of 0.5 ms. The sEMG signals from two hand postures are pairwise concatenated (②) before extracting muscle synergies. Each extraction provides one muscle synergy matrix that is shared by the paired postures, and it also provides mean value of synergy coefficients associated with each posture. That information is used to train the classifier in stage ③. For pairwise posture classification, two mean synergy coefficient values are determined: each mean value is obtained from the respective hand posture of the pair. After the MDC is trained, a classifier is used to classify a posture at stage ④. The stage ⑤ of the offline posture classification is associated with the attempt to search for better muscle synergy representation such that the results give better discrimination for hand posture classification. Here, the clustering validation index of silhouette (Rousseeuw, 1987) is used on muscle synergy coefficients to determine if better clustering formation has been obtained.

3.1.1. Muscle synergy extraction

Muscle synergy is obtained with NMF algorithm (Lee and Seung, 1999), where the multiplicative update rule (Lee and Seung, 2001) is used to obtain the muscle synergy coefficient and muscle activation matrix as follows

$$E = W \cdot H \tag{3.1}$$

where H represents the synergy coefficient, W is the muscle activation matrix, and E is the concatenated, RMS valued multichannel sEMG signals from a pair of static postures. The NMF DTU toolbox (Joergensen, 2006) is used to extract muscle synergies. The algorithm iteratively optimizes both synergy coefficients and muscle activation matrix, and it ensures that the obtained synergies are non-negative because the nerve innervation to the muscle can either be active or at rest.

3.1.2. Discrimination power

The silhouette clustering index (Rousseeuw, 1987) is used to measure the ability of the trained classifier to define different postures. The nature of the synergy extraction described in the above section is to produce clusters appear to be that the extracted features are invariant at the vicinity of stationary points. Duda et al. (2001) considered reinforcement learning as a tentative approach for learning when the only information from a reward system is right or wrong. In this research, the silhouette clustering index is used as the reward function for the reinforcement learning because compact clusters increase the discrimination power.

To demonstrate the process, muscle synergies was extracted from the recorded sEMG data of pairwise static hand postures (Pronation vs Neutral) of a subject. The raw sEMG signal were processed with a RMS window of 250 ms, and 3 muscle synergies were extracted from 8

channels of sEMG recordings of BB muscle. Multiple extractions of the synergies were performed with the NMF DTU toolbox (Joergensen, 2006). Synergies with different silhouette value are presented in Fig. 3.2.

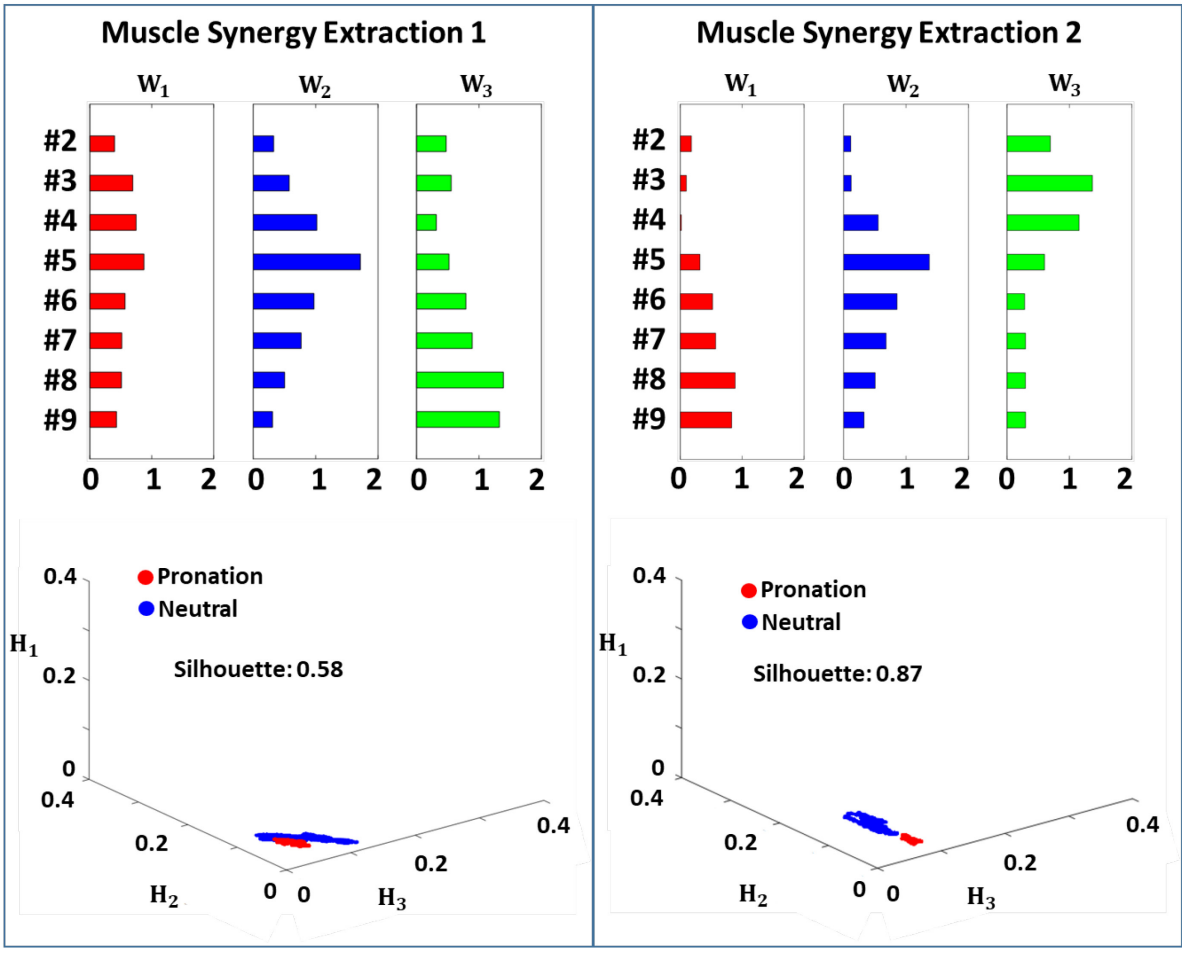

Fig. 3.2 Two synergy extractions (shown in left and right panels) from concatenated sEMG signals when hand was pronated and when it was in the neutral posture. The synergy matrices are presented on top row and synergy coefficient clusters on the bottom row. From the same sEMG signals, the synergy clusters are very different, and their compactness is measured with the silhouette index. A higher index value means higher compactness of the clusters.

From two muscle synergy extractions presented in Fig. 3.2 (one presented at the left panel and the other on the right), the sEMG signal recordings were the same; however, the resulting synergy matrices (as presented on the top row) have different values, which give

different clustering formation as shown in the bottom row of the Fig. 3.2. For both synergy extraction, the reconstructions gave very similar CoD value (0.99) and absolute error (0.68). However, when the silhouette clustering index was used to evaluate the clustering formation of the two synergy extractions, we found that the index values are quite different. As a distance base measure for the discrimination power, the silhouette clustering index provides indication on the compactness of the synergy coefficients. When the synergy coefficient clusters are well formed, they become easier to classify even with simple classifiers, such as the MDC. With this evidence, the multiple muscle synergy extractions are considered to select muscle synergy coefficients with higher discrimination power from same sEMG of paired upper limb postures.

3.2. Second experimental protocol

The objective of the second experiment is to determine whether muscle synergies of the biceps could be used to produce target reaching movements in an interactive virtual environment. All acquisitions were made in a seated body posture and with 8 static upper limb postures involving joint position changes at shoulder, elbow, and wrist (human hand supination and pronation are caused by a crossing over of the radius and ulna; thus, changes of hand supination and pronation are produced at the elbow joint. However, modern prostheses usually have the pronation and supination produced at their wrist joint. To be consistent with the application perspective, pronation and supination of the hand are considered at the wrist joint in this research). Each of the 8 postures of the upper limb is represented by a 3-tuple ([*, *, *]) as shown in Fig. 3.3A. The first element in the tuple indicates the position of shoulder joint, the second element in the tuple indicates the elbow joint position, and the third indicates the wrist position. For shoulder and elbow joints, the available positions are flexion (F) and extension

(E). The wrist joint can be at pronation (P) or supination (S). Synergy features extracted from BB of a subject is then used to control the dynamic movement of the left arm (initialized at FEP) of an avatar simulated in MATLAB virtual environment (Fig. 3.3B). The right arm of the avatar is the target arm posture (FFS).

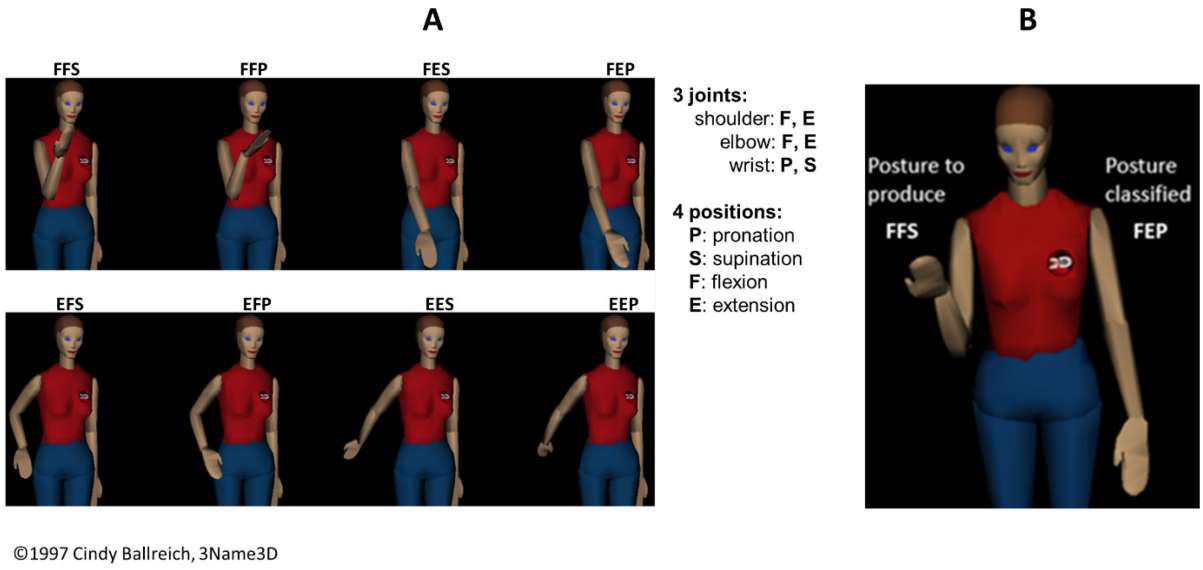

Fig. 3.3 Static postures of virtual avatar. **A**: 8 static postures with 3-tuple notation. **B**: position of the left upper limb of the avatar is changed by the subject's biceps muscle, and right upper limb posture of the avatar is the anticipated posture. An anticipated posture is considered as reached when the controlled left upper limb is a mirror image of the anticipated right upper limb of the avatar with respect to the sagittal plane.

The control signals for upper limb posture changes are obtained from the posture classification where training and testing of the paired posture classifier is the same as those presented in the first protocol (Fig. 3.1, steps ① to ⑤). In addition, to classify more than 2 postures, an ensemble classification method then uses all the paired posture classifiers. The method of ensemble classification that we used in this protocol is presented in Section 3.2.1.

Since online signal processing is required in this protocol for interactive experiment (system used in previous protocol does not have online signal processing function), customized analog circuits were assembled with the circuit design from Muscle Sensor v3 (Advancer Technologies, North Carolina, USA). The analog system has been compared with commercial signal acquisition system by Heywood et al. (2018) who found that the low cost system performed comparatively well with respect to the commercial system (TeleMyo DTS, Noraxon, Arizona, USA). The AD8226 (Analog Devices, Massachusetts, USA) amplifiers, which have a common mode rejection ratio of > 90 dB, were used for differential amplification, and a 6.67 to 1240 band-pass filter was obtained with TL084 op-amps (Texas Instruments, Texas, USA). Following differential amplification (Fig. 3.4A, gain = 200), signals are rectified (Fig. 3.4B) and smoothed (Fig. 3.4C). A second amplification stage uses the same op-amp, and it has an adjustable gain of 1 to 10 (Fig. 3.4D).

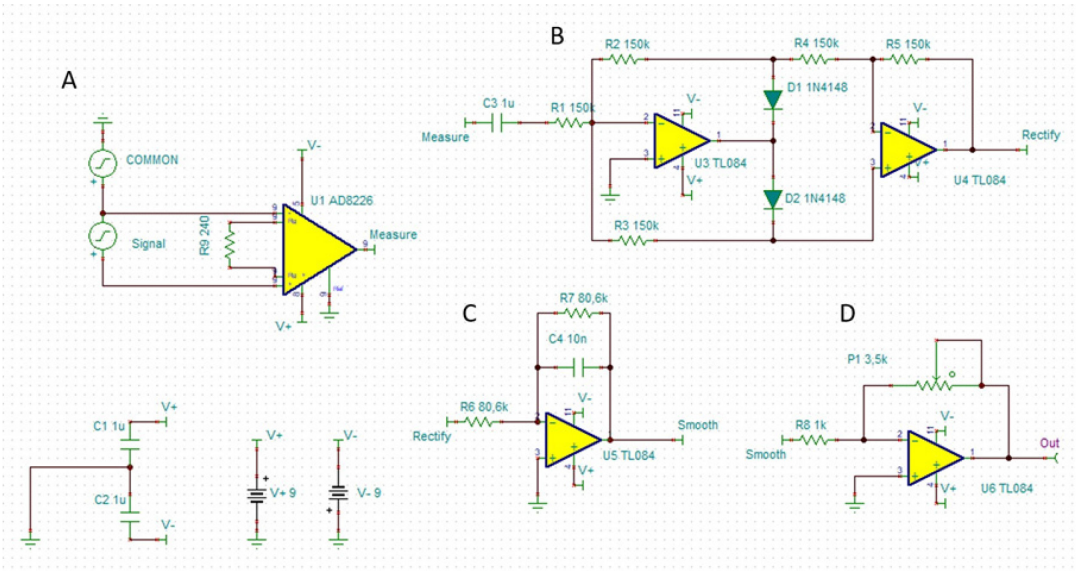

Fig. 3.4 Analog circuits used for preconditioning the sEMG signals. **A**: Differential amplifier AD8226, **B**: signal rectification and high pass filter with TL084 op-amp. **C**: low pass filter with TL084 op-amp. **D**: second stage adjustable amplification with TL084 op-amp (Muscle Sensor v3, Advancer Technologies, North Carolina, USA).

Analog signals are digitized at 2000 Hz (12 bits resolution) by using a microcontroller (OpenCM9.04, ROBOTIS, Seoul, Republic of Korea). The digital signals are processed with a RMS window of 250 ms with a 70 ms step size in an ARM Cortex-M3 processor (72 Mhz clock) incorporated by the microcontroller. Besides processing signals, the embedded microprocessor also provides a communication interface to a MATLAB program on a laptop computer. With a serial communication port, 15 subsampled signals are transferred per second from the microcontroller to the MATLAB program.

During the experiment, the training samples were obtained from a 10s recording from a subject who held his or her upper limb at one of the 8 static postures. The amplitude level of the sEMG was displayed on a computer screen as a visual feedback to keep the signal drift to its minimum. After the training data from all the static postures, required to be used for control, is collected, a winner-takes-all classifier can be obtained (Section 3.2.1). During the classifier training, if any static posture is not recognized, the posture data could be rerecorded in order to obtain a recognizable posture training data.

In this protocol, NMF algorithm serves as two functions: one is to extract the muscle synergy features from the sEMG, and the other is to provide an instantaneous estimate of the muscle synergy coefficients. This instantaneous estimate is obtained from the pseudo inverse of the synergy matrix because the non-negative least square without distribution information does not give a very good fit for the sEMG signals. The Moore-Penrose pseudo inverse was used to invert the synergy matrix, and the resulting matrix is a non-square matrix that serves to project the sEMG to synergy feature space. Muscle synergy was obtained only from paired static postures, thus the sEMG signals during the movement of the arm from one static posture to another static posture were not used for synergy extraction. In this way, the muscle synergy

matrix can be assumed to be unchanged for the paired postures, and only synergy coefficient changes according to which static posture it belongs to. This allows the sEMG obtained from the pairwise postures to be instantaneously projected to the feature space using the pseudo inversed synergy matrix without too much stability issue due to nonlinearity.

The online classification of static postures was accomplished with 3 sets of 5 seconds recording of each static posture. During this operation, the classified postures were duplicated by the avatar, and subjects used that information to correct their biceps contraction to improve the classification accuracy.

3.2.1. Combining classifiers (synergism)

The muscle synergy coefficient with high silhouette value is used to train the simple classifiers, i.e. MDC. The training of the classifier is relatively easy because it only requires the mean value of each muscle synergy cluster from pairwise postures. The simplicity to implement is one of the justifications initially. When tested the performance online, good classification accuracy (95%) were obtained from paired posture classification of two subjects (He and Mathieu, 2017). Thus, the MDC was used for the interactive control program. As mentioned in the literature review, if advanced classifiers, such as ANN or SVM are used, then improved classification performance could be expected. The resulting pairwise posture classifier is called a component classifier (Duda et al., 2001). The winner-takes-all method is used to learn the activation of paired posture classifiers at the pooling stage. As shown in Fig. 3.5, three hand postures (P: pronation; N: neutral; S: supination) are considered for classification with 3 component classifiers, where the same input sEMG signal from a pronated hand is classified. For each component classifier, one estimate is produced, where the identified posture is given a

positive vote (i.e. 1), and the other posture does not receive any vote (i.e. 0). The cumulative sum of positive votes for each posture is determined at the pooling stage to produce the estimated output. As an ideal case shown in Fig. 3.5, where all the component classifiers make the correct classifications, the classifier produces the correct classification, i.e. input from the bottom (P) is reproduced by the output at the top. This suggests that the learning of the network can produce good classification accuracy; otherwise, the network needs to relearn the pattern until the correct posture is reproduced. This procedure is applied to Neutral and Supination hand postures to complete the training of the classifier.

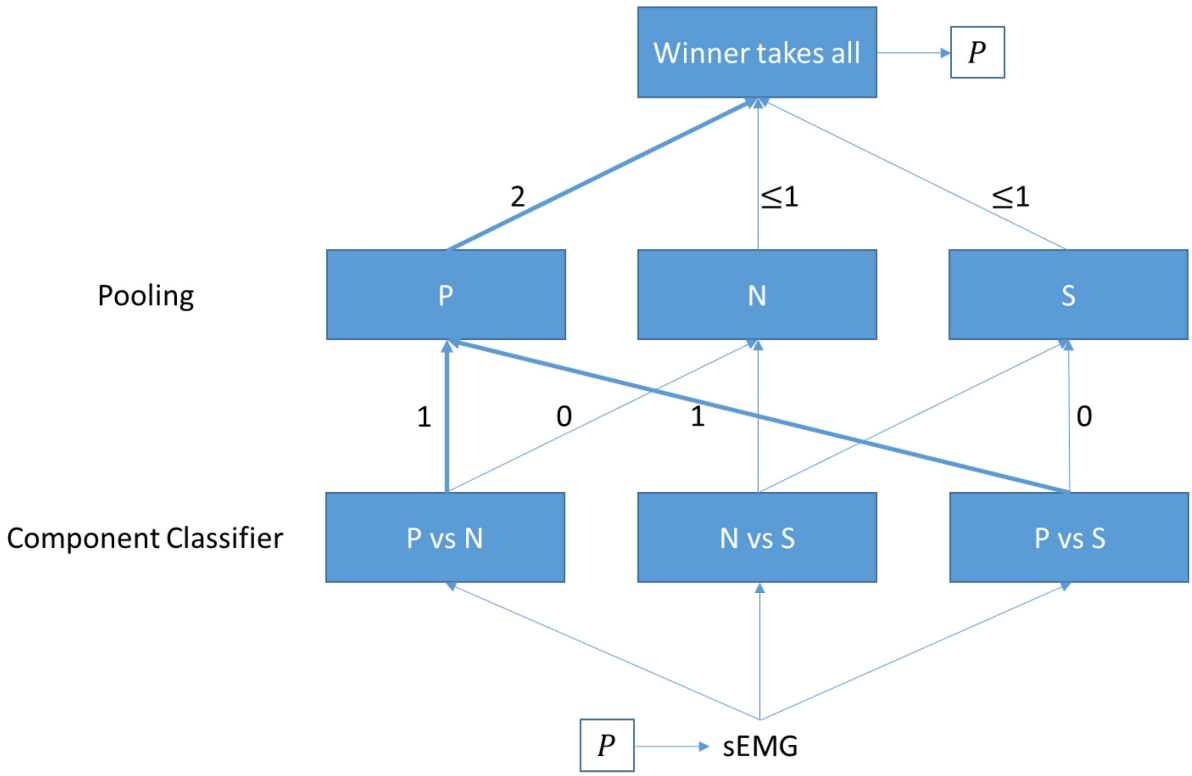

Fig. 3.5 Winner-takes-all method to provide classifier training. Three hand postures (P: pronation; N: neutral; S: supination) were considered. A testing sEMG from pronated hand was used as input. If all the component classifiers produce the correct classification, then the pronated hand receives the highest positive votes at the pooling stage. The posture classifier selects the posture with highest votes as its output of posture classification (i.e. pronation has highest number of votes at the pooling stage, and the classifier produces pronation as its output).

The combination of pairwise classifiers (Fürnkranz, 2002) to produce posture classification is based on round robin method (Park and Fürnkranz, 2007) by using component classifiers in a synergism approach to classify 8 different postures of the upper limb. As a simple demonstration of how the classifier makes estimation, an example is shown in Fig. 3.6. The pairwise classifiers associated with FFS posture are indicated with thick blue lines, and those associated with FFP posture are indicated with orange lines. The shared pairwise classifier between FFS and FFP is indicated with a red line. So, after the initial votes, both FFS and FFP

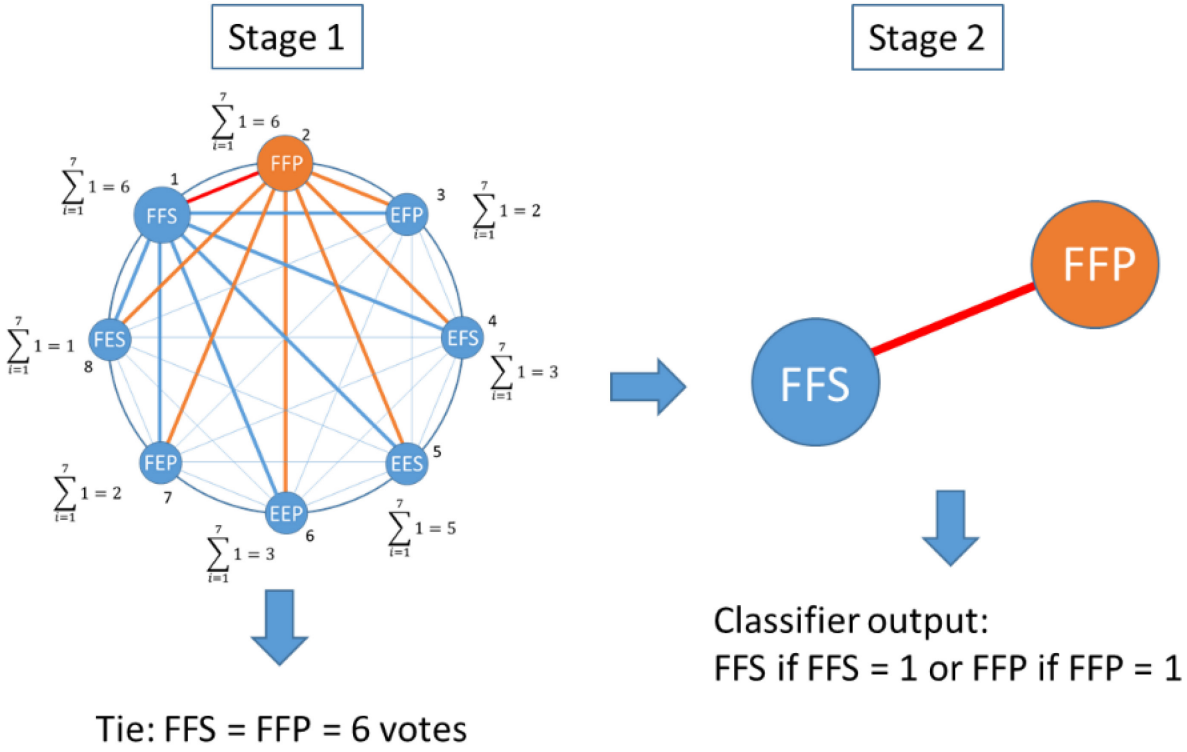

Fig. 3.6 Combining the pairwise posture classifier to produce multiple posture classification. 8 upper limb postures are labelled as 3-tuples. When two postures receive equal votes from their corresponding classifiers (Stage 1, dark colored lines), the tie break will be automatically determined by the pairwise classifier (Stage 2) associated with the postures having equal votes, as in this instance: FFS-FFP paired posture classifier. After the tie break, the winning posture will be the final estimate from sEMG.

postures received 6 votes from their corresponding classifiers. This is a tie condition, and to break the tie and produce final posture estimate, the paired posture classifier indicated with the red line is used to make the final estimate of the posture (as shown in Fig. 3.6, second stage) after the equal votes in the first stage. If the red line pairwise classifier classifies the posture as FFS (i.e. FFS = 1), then the final estimate will be FFS posture, and vice versa for FFP.

As the number of classified postures increases, signal variation between some postures reduces. For pattern classification, this means that posture patterns become similar to each other. Thus, the discrimination power of each paired posture classifier reduces. The cumulative effect to the posture classifier, that consists of many paired posture classifiers, is the reduction of the overall classification performance.

3.2.2. Mapping the upper limb joint position to virtual cube

In order to evaluate the capability of muscle synergy, extracted from biceps muscle, to produce movement in an interactive environment, the normalized joint angular positions of the upper limb in degrees associated with the BB muscle function are mapped to the axes of a virtual cube (displayed on the computer screen) as shown in Fig 3.7A. The 8 static postures of the upper limb (Fig. 3.3A) are associated with the 8 corners of the virtual cube. These static postures represent the extreme positions of the joint movement of the upper limb. The intermediate positions within the cube can be mapped to the joint angular positions as shown in Fig. 3.7B. The parameter mapping between the virtual cube (x, y, z) and the joints of the upper limb (q_1, q_2, q_2) is one-to-one and onto, so the solution from one parameter set is uniquely mapped to the other parameter set. Thus, a joint angular position of the upper limb, that can be produced by the upper limb, can be represented by a position in the virtual cube.

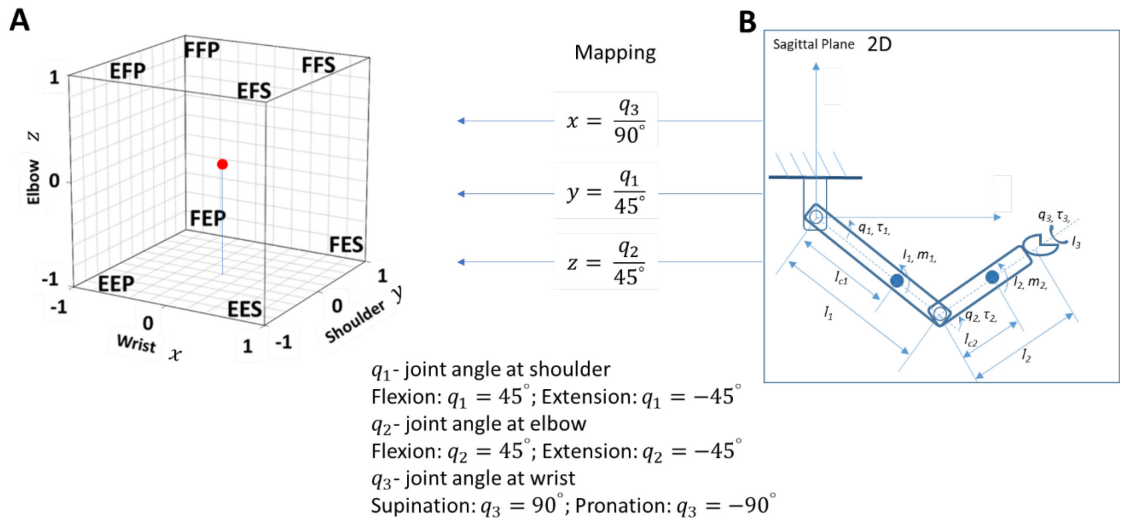

Fig. 3.7 Mapping of the joint parameters of the upper limb to virtual 3D joint space parameters. **A**: a 3D virtual cube, where each corner of the cube is associated with a static posture of the upper limb. **B**: joint angles (q_1, q_2, q_3) of the upper limb in sagittal plane that represent the shoulder, elbow, and wrist joint positions in degrees.

During an experiment, a subject uses 5 (a subset of 8) or all the 8 static postures, as shown in Fig. 3.3A, to move, in the virtual cube, a red sphere from its initial position (Fig. 3.7A) to a target (not shown). Each red sphere displacement in the cube is controlled with one of the 8 static postures taken by the subject.

3.2.3. Joint movement model and intermittent control

The subject's forearm static posture in supination or pronation in joint space was modeled as a standard second-order system (Ogata, 2010). The block diagram is shown in Fig. 3.8A, where the input R(s) is the desired position, C(s) is the system output, and E(s) is the system error. After simplification, the transfer function of the second-order system is given as follows:

$$\frac{C(s)}{R(s)} = \frac{{\omega_n}^2}{s^2 + 2\delta\omega_n s + {\omega_n}^2} \tag{3.2}$$

The step response and impulse response of the system is shown in Fig. 3.8B. The critical damped condition is used for the system, i.e. $\delta = 1$. The natural frequency (ω_n) of the system being considered as a variable, the response time of the system can be changed through the change of natural frequency of this system. In Fig. 3.8A, the natural frequency of the system is set at $\omega_n = 5$ to produce the system response (as shown in Fig. 3.8B). The same second-order system is also used to model the movement of elbow joint and shoulder joint in the joint space.

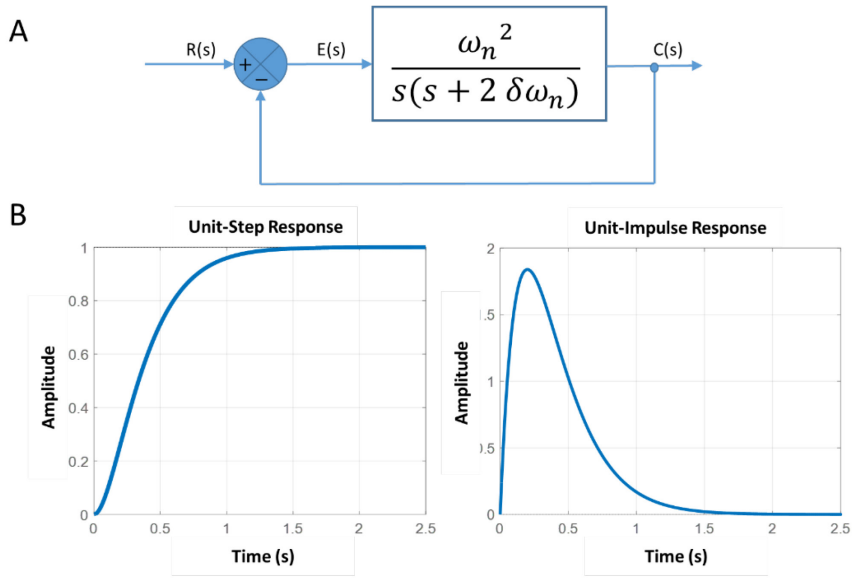

Fig. 3.8 Second-order system. **A**: block diagram of a second-order system, R(s) – input, E(s) – error, C(s) – output, ω_n is the natural frequency of the system, and δ is the damping ratio. **B**: unit step input response and unit impulse response of the system when $\omega_n = 5$ and $\delta = 1$.

A virtual simulator was developed from the second-order system model for three joint movements indicated by the red sphere position change in the cube (Fig. 3.7A). The movement of the red sphere can be obtained from control signal restricted to the 8 discrete static postures from the posture classifier. For static postures in the corners of the cube, coordinated movement control can be solved as a position regulation problem with a proportional controller. The red

sphere can rest at any position in the cube if there is no control input (i.e. muscle is relaxed), and the initialization position of the red sphere is always in the center of the cube (Fig. 3.7A).

The transition of the control signal from one posture to another is modeled with an intermittent control (Gawthrop et al., 2011). In the experiment, a subject can observe the movement of the red sphere in the virtual cube and change control signal by altering static arm postures from one to another. The observation of the red sphere movement in the cube allows the subject to track the movement of the red sphere as considered in (Neilson et al., 1988) such that a trajectory of the red sphere can be planned to reach a targeted position in the cube.

With the position regulator at each axis of the virtual cube, the red sphere can be positioned anywhere in the virtual cube. However, to reach a position target within the virtual cube with this position regulator is difficult because it requires good anticipation of the movement of the red sphere in all of the three joint axes of the virtual cube. To reduce the difficulty during the target reaching, the control system needs to be decoupled; thus, individual joint movement can be obtained by switching from one discrete posture to another.

3.2.4. Individual joint control

In the control system presented above, each estimated posture provides coupled input at three joints of the upper limb through position regulators. For such control system, postures at predefined positions, such as the static postures at the 8 corners of the virtual cube, can be reached automatically. However, to attend an arbitrary position with certain accuracy in the cube (or to place the upper limb in an arbitrary posture with the available three joint movements), the control system needs to be decoupled. Therefore, we consider a 2-stage reaching. The first stage of the reaching is to initiate the movement toward the target with the coupled control in all axes.

When the red sphere moves near the target, a switching algorithm is used to decouple the movement to fine tune the position of the red sphere in order to reach the target. The control system is decoupled by using the transition from consecutive control inputs from the posture classifier. For a demonstration, the motion of the red sphere can be controlled with 4 upper limb postures (FFS, FFP, FES, and FEP) in a plane as shown in Fig. 3.9A. Both coupled (Fig. 3.9B) and decoupled control (Fig. 3.9C) are used to reach a target as a comparison.

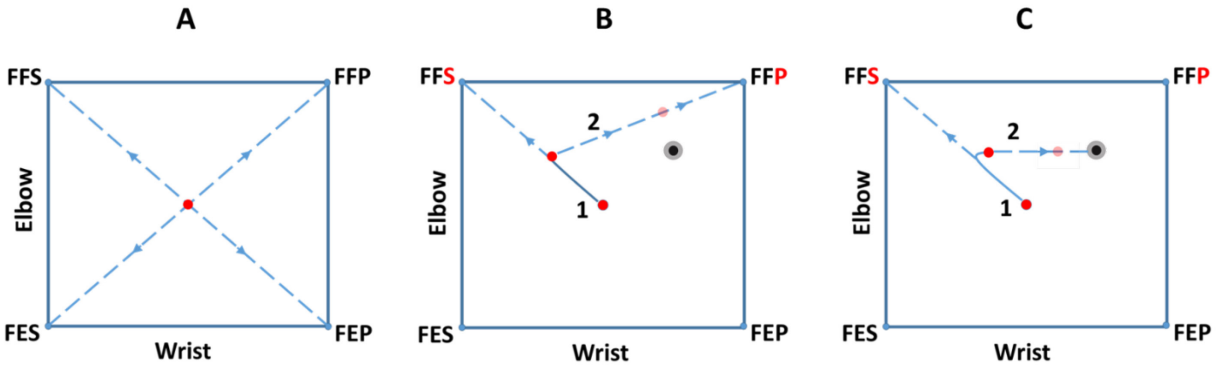

Fig. 3.9 Two stages target reaching methods in a plane. **A**: the red sphere is controlled by 4 estimated upper limb postures which direct the red sphere toward a corner of the plane. **B**: no target reached where control input is switched too late from FFS to FFP. **C**: the FFS motion is inhibited earlier in the elbow axis by a switch from FFS to FFP, and the black target is reached.

With each first static posture, the red sphere is moved from its initial position at the center of the plane toward the corner corresponding to that posture (Fig. 3.9A). When a second static posture is taken, the red sphere immediately moves in the direction associated with the second posture. As illustrated in Fig. 3.9B, target is not reached when a second posture (2) is taken as the red sphere moves toward the FFS corner (1) because the subject failed to anticipate the red sphere trajectory that could reach the target before the posture switch was made. In Fig. 3.9C, the target was reached because the posture switch occurred earlier. This control approach can be extended to 3D displacement of the red sphere in the cube.

4. Static Hand Posture Classification Based on the Biceps Brachii Muscle Synergy Features

This is a published article (J. Electromyogr. Kines., (43): 201-208, 2018), where we used a database of surface EMG signals obtained from the biceps brachii of 10 healthy subjects when their upper limbs were in different static postures (Nejat, 2012). This research was under the supervision of Professor Mathieu. It's Professor Mathieu who has suggested using the concept of muscular synergy on biceps brachii muscle, from its contribution of several different movements and the presences of 6 individually innervated compartments, which could represent several muscles working together. For extraction of muscle synergy from BB muscle for posture classification, I developed the computer program that analyzed the surface EMG signals in the database.

Static Hand Posture Classification Based on the Biceps Brachii Muscle Synergy Features

Liang He, Pierre A. Mathieu
Biomedical Engineering Institute, University of Montreal
Montreal, QC, H3T 1J4, Canada

Abstract

With modern upper limb myoelectric prostheses, many movements can be produced when many control signals are available. Some of them could originate from the multifunctional biceps brachii which appears to be composed of up to six individually innervated compartments. Given its compartmental nature, this muscle behaves as if composed of many individual muscles acting in synergy to achieve a given motor task. Through an appropriate synergy model, its EMG signals could thus be used to produce some of the many control signals required with modern upper limb myoelectric prostheses. Exploring that possibility, muscular synergy which is usually applied to a group of different muscles, was tested on the biceps brachii only. A non-negative matrix factorization method was applied on pre-recorded data consisting of 8 surface electromyographic signals collected across the biceps of 10 normal subjects who, in Seat or Stand posture, held their hand in 3 different postures. We found that muscular synergies can be extracted from the biceps brachii. With a learning process and a classifier, it was also possible, between a pair of static hand postures, to identify which one was used when a given record was made. The mean score of correctly detected hand posture was >80% for our subjects.

Keywords: biceps brachii, compartments, non-negative matrix factorization, muscle synergy, myoelectric prostheses.

4.1. Introduction

From shoulder to the fingertips, many muscles and articulations are spanning the upper limb. Due to that redundancy, the central nervous system (CNS) would have a huge task of identifying rapidly and efficiently which muscles to contract at a given time with a given intensity level while an intended movement is in progress. With trained movements for which high degrees of precision and repeatability are easily observed, the kinematic analysis suggests that an efficient global approach has to be used by the CNS to plan and realize such movements (d'Avella et al., 2006). The same applies to the repetitive activation of the lower limb muscles involved in stepping up and locomotion (Santuz et al., 2007, Yang et al., 2007). To reduce the CNS workload and increase its efficiency in executing a given movement, it has thus been proposed that cooperative muscle interaction has to be involved. Such interaction is defined as muscular synergy (Bizzi and Cheung, 2013, d'Avella and Lacquaniti, 2013).

Muscle synergies cannot be directly observed from electromyography (EMG) signals be-cause individual muscle activation amplitude and timing are difficult to associate with direction and speed of a movement. Synergies are therefore inferred from models where various matrix factorization methods, such as non-negative matrix factorization (NMF), principal component analysis (PCA), factor analysis (FA), independent component analysis (ICA), probabilistic independent component analysis (pICA) and others are used. When Tresch et al. (2006) tested all of these methods on simulated EMGs and on signals collected from frogs, they found that those models produced quite similar synergies. However, the non-negative matrix factorization is usually preferred with EMG signals since muscles can only be at rest or contracted. For example, to analyze the balance control of cats standing on a platform submitted to randomly oriented perturbations, Ting and Macpherson (2005) measured the response of 8 to

15 hindlimb muscles and found with NMF that four synergies could explain the cats' hindlimb postural responses. Studying the human wrist articulation, Jiang et al. (2009) developed a physiologically based surface EMG model where synergistic muscles shared spinal drives that act as time-varying force functions. With 8 EMG signals (biceps and 7 forearm muscles) from 12 subjects who realized tasks involving up to 3 simultaneous degrees of freedom (DoFs), they used a NMF algorithm and their detection success was 78.5±7.62% for 2 DoFs movements and 31.2±17.4% for 3 DoFs demonstrating the feasibility of simultaneous and proportional control of a prosthesis. To study gestures associated with grasping, Günay et al. (2007) applied NMF and PCA algorithms on the EMG signals of 6 forearm muscles. For 14 hand postures classification, they found better results with NMF than with PCA. NMF was also used by Muceli et al. (2017) to study the simultaneous and proportional control of wrist flexion/extension and forearm pronation/supination. With the extracted synergies obtained from 16 monopolar EMG signals of the forearm of 10 subjects, they got a mean task completion rate of 95% at a higher speed than with an industrial control where each DoF is controlled by 2 different EMG signals.

In the above articles, muscle synergy was used to describe the coordinated simultaneous activity of many distinct muscles either in response to a perturbation or involved in a movement. Here, we investigated if muscular synergy could also be extracted from a single muscle the biceps brachii (BB). Our interest was attracted to this muscle because it contributes to the shoulder stability, to the arm abduction, to its adduction and internal rotation, to the elbow flexion and to the hand supination (Ken Hub Channel, 2017). This results in different EMG signals recorded over the muscle as the arm is set in different postures (ter Haar Romeny et al., 1984). Our interest was also drawn by the presence of up to 6 individually innervated compartments which can be visually observed on its inner surface (Segal, 1992). Considering

those compartments as muscles within a muscle, we investigated if muscular synergy could be extracted with NMF from surface EMG signals collected across the contracted biceps while shoulder, elbow and wrist joints were in different static postures. This being the case, a learning process and a classifier were used to determine, between two hand static postures, which one was taken by the subject when the EMG signals were recorded.

4.2. Methods

4.2.1. Experimental data

Pre-recorded data (Nejat, 2012) from 26 to 32 years old healthy subjects (5 females, 5 males) with a mean body mass index of 23.9±0.89 were used. Borders of their BB had been identified by palpation and their mid-point was considered separating the short (SH) from the long head (LH). Five pairs of surface electrodes were positioned across each head (Fig. 1A). The lower electrode row was located 10 mm above the mid-portion of the BB to avoid the neuromuscular junction zone. In one body posture, EMG signals were acquired while subjects were in Seat posture with the right arm close to the trunk and the elbow flexed at 100° (left of Fig. 1B). Constant isotonic and isometric contractions of 5 s were produced at 20% maximal voluntary contraction (MVC) while the hand (Fig. 1C) was pronated (P), in neutral position (N) or supinated (S). In the other body posture (right of Fig. 1B), subjects were in Stand posture with the right shoulder abducted by 90°, the arm held horizontally in the coronal plane (out to the side) with a 1 kg load attached at the wrist level[1] with hand also pronated, in neutral position or supinated. In each of those different experimental conditions, three or four 5 s EMG records

1 While in Stand posture, it was easier to hold a weight as opposed to maintain a constant strain gauge reading. The 1 kg load was judged to be equivalent to the 20% MVC of the Seat posture.

were acquired. Following amplification (×2000), band-pass filtering (10-1000 Hz, second-order) with a 15LT Grass system, signals were sampled at 2 kHz with LabView (National Instrument, USA) and saved as MATLAB file (Mathworks, USA). Arm circumference differing among subjects (25 to 31 cm), the biceps synergy analysis was restricted to the inner eight EMG signals, i.e. those from electrode pairs 1 to 8 (Fig. 1A); this ensured that only signals over the BB were analyzed.

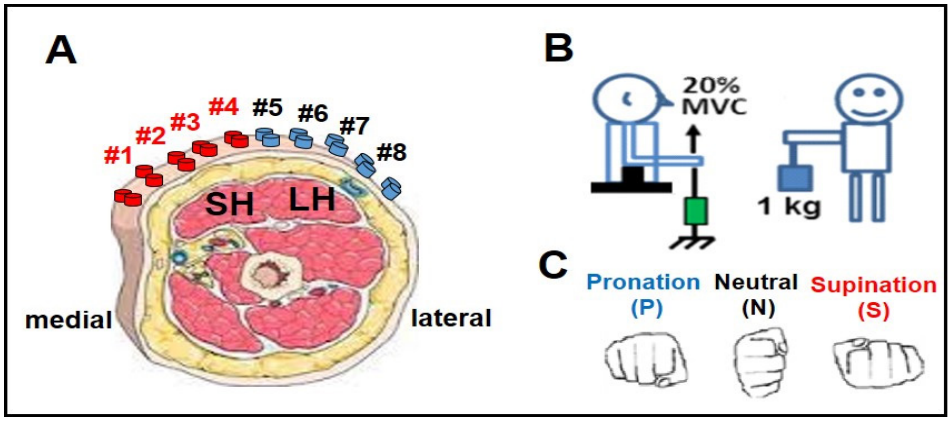

Fig. 4.1 Electrode placement and static postures. **A**: Ten pairs of surface electrode pairs have been equally positioned over the short head (SH) and long head (LH) of the biceps brachial. Due to different arm circumferences among the subjects, only 8 EMG signals were considered to extract the biceps muscular synergy. **B:** Tested postures: Seat with force produced at 20% MVC (Maximum Voluntary Contraction) and Stand with a 1 kg load considered to be equivalent to 20% MVC in the Seat posture. **C:** Three hand postures tested in each body posture.

A 815 ms rectangular window was moved in steps of 0.5 ms along each sampled EMG signal in a set and a RMS value obtained for each window. This resulted in a 8 × 8371 matrix (E) to be factorized. Factorization was achieved on concatenated RMS profiles of signals acquired with the hand pronated and neutral (P+N) and in neutral and supinated (N+S) postures (Fig. 2A). Concatenation can be used for different purposes. For example, Oliveira et al. (2014) assembled the synergies of repeated EMG cycles exercise in a single stream to improve the synergies estimation. Gatti et al. (2008) concatenated processed EMG signals of muscles acting

at the shoulder level to evaluate 3 methods used to predict muscle forces. In contrast to those purposes, concatenation is used here to estimate synergies involved with the control of two hand postures P and N or N and S, where certain contractile elements of the biceps are assumed to be shared but activated at different degrees. Levels of those synergies were used as a posture classification method.

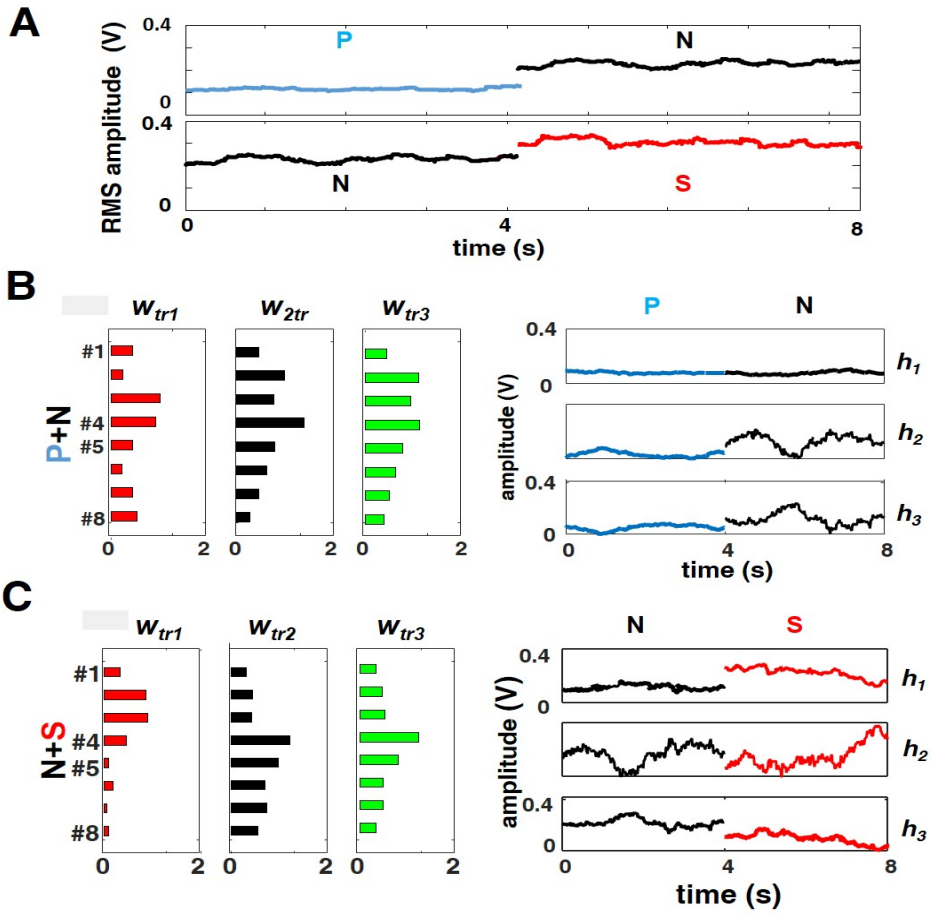

Fig. 4.2 Synergy extraction. **A**: S6 training concatenated RMS values (channel 4) of the biceps EMG signals (P+N: pronation+neutral; N+S: neutral+supination). **B**: For P+N concatenated EMG signals, three training muscle synergies (w_{tr1}, w_{tr2}, w_{tr3}) and concatenated synergy coefficients (h_1, h_2, h_3). **C:** Results for the N+S concatenated signals. Subject was in the Seat posture and EMG signals are those following amplification with a gain of 2000.

4.2.2. Muscle synergy extraction

A set of RMS EMG signals obtained from a multichannel recording forms a matrix *E* for which the NMF factorization is:

$$E = W \times H \quad (1)$$

where all elements of W (the biceps synergy) and H (synergy coefficients) are non-negative. Here, those matrices are estimated with the NMF DTU toolbox (Joergensen, 2006). Using the multiplicative update rule of Lee and Seung (2001), the factorization algorithm proceeds iteratively with a maximum of 50000 iterations to minimize the least squares error between original RMS EMG signals and their reconstruction from the product of synergies *W* and coefficient matrix *H*. The coefficient of determination (Yang et al., 2017) was used to determine the number of muscle synergies. Synergy extraction serves two purposes here: to identify the parameters that will be used to train a classifier (see below) and to evaluate the classifier performance.

i) Classifier training

In each hand posture, the first dataset out of the 3 or 4 available ones was always used to train the classifier. Those training sets are respectively labelled ${}^{(P+N)}_{tr}E_i$ and ${}^{(N+S)}_{tr}E_i$ where the left superscript specifies the type of concatenation while the *tr* subscript indicates the trial used for training; in the paper tr=1 and the subscript i at the right of *E* is the EMG channel number. An example of two concatenated signals from the training set is shown in Fig. 2A (top: ${}^{(P+N)}_{tr}E_4$ and bottom: ${}^{(N+S)}_{tr}E_4$). The NMF decomposition of ${}^{(P+N)}_{tr}E_i$ or ${}^{(N+S)}_{tr}E_i$ was constrained to three components which provided the 8x3 training synergy matrices, respectively ${}^{(P+N)}_{tr}W$ and ${}^{(N+S)}_{tr}W$, and their associated 3xn training synergy coefficient matrices, labeled respectively

${}^{(P+N)}_{tr}H$ and ${}^{(N+S)}_{tr}H$. Fig. 2B and 2C illustrates the three column vectors w_i of the training synergy matrices W and the three row vectors h_i of the training synergy coefficient matrices H.

In Fig. 3A, the training synergy coefficients are shown in a 3D plot. The plot shows the clusters associated to a concatenated N and S segment. Each cluster's center of gravity in the 3D feature space was used to represent the N and S posture. As an example of the notation used, the coordinate vector for the center of gravity for the N cluster from the N+S concatenated data of the training trial *tr* is

$$ {}^{N+S}_{tr}\bar{\boldsymbol{h}}_N = \left\{ {}^{N+S}_{tr}\bar{h}_{1,N} , {}^{N+S}_{tr}\bar{h}_{2,N} , {}^{N+S}_{tr}\bar{h}_{3,N} \right\} \quad (2) $$

where $\bar{h}_{n,N}$ is the mean value for the n[th] components of the synergy coefficient vector. For the S cluster of the same data, we have ${}^{N+S}_{tr}\bar{\boldsymbol{h}}_S$. And for P+N concatenation we have the two clusters' center of gravity, ${}^{P+N}_{tr}\bar{\boldsymbol{h}}_P$ and ${}^{P+N}_{tr}\bar{\boldsymbol{h}}_N$. These centers of gravity define the reference, against which testing postures are compared for classification.

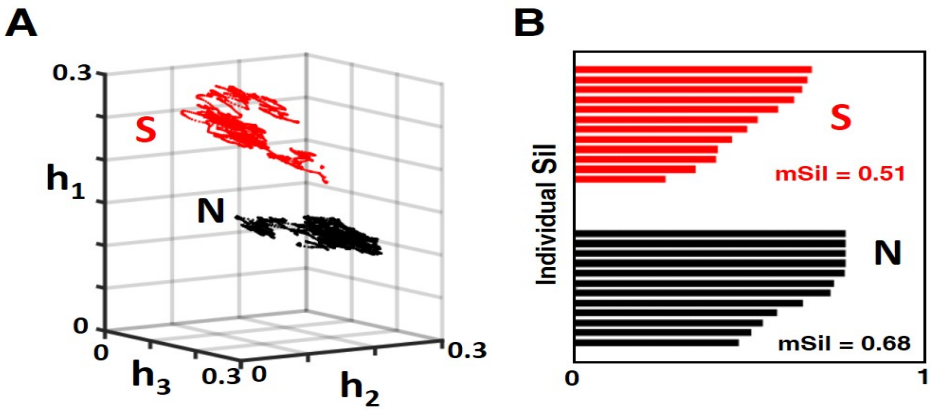

Fig. 4.3 3D plot of synergy coefficient and silhouette. **A**: 3D plots of the training h1, h2, h3 coefficients (units in V) for concatenated N and S clusters of a training trial. **B:** display of decimated (1/750) silhouette indices of each cluster (0 to 1). With the more compact N cluster, its mean silhouette index value (0.68) is higher than for the S cluster (0.51). MATLAB silhouette function was used where distance between points in a cluster is squared. Results of subject S6 in the Seat posture.

ii) Feature extraction method

The classifier operates on the NMF features extracted from the RMS EMG data. Here, these features are synergy estimates. Given the data from the i^{th} trial to be classified, ${}_{i}E$ with $i \neq tr$, we solve the linear overdetermined equation system for H by:

$$ {}_{i}E = {}_{tr}W \, {}_{i}H \tag{3}$$

where ${}_{i}E$ is either ${}^{(P+N)}_{i}E$ or ${}^{(N+S)}_{i}E$ and correspondingly ${}_{tr}W$ is the training synergy matrix, either ${}^{(P+N)}_{tr}W$ or ${}^{(N+S)}_{tr}W$. A general solution can be obtained by minimum lease square inversion, which in its simplest form can be written as:

$$ {}_{i}\widehat{H} = {}_{tr}W^{-1} \, {}_{i}E \tag{4}$$

where $\widehat{H}$ indicates that we have an estimate of H in the least square sense. The MATLAB function *mldivide* is used to determine the inversion, ${}_{tr}W^{-1}$ during the program execution. The right-hand side of equation (4) performs the projection of eight-dimensional E data onto the three-dimensional synergy coefficients feature space. Each jth column of E is a point on the time axis, and therefore we denote this point by $E(j)$; the projection being done on a time sample by sample basis, the corresponding feature vector estimate will be noted $\widehat{H}(j)$.

4.2.3. Hand posture classification

In each dataset, 3 or 4 trials were available and the first one was always used for training. After the training, the 2nd, 3rd and 4th trial were classified by using the minimum Euclidean distance (D) between the training coefficients and the testing coefficients

$$ {}^{P+N}_{i}D_P(j) = \left\| {}^{P+N}_{i}\widehat{H}(j) - {}^{P+N}_{tr}\overline{\boldsymbol{h}}_P \right\| \tag{5}$$

$$ {}^{\mathrm{P+N}}_{i}\mathrm{D_N(j)} = \left\| {}^{P+N}_{i}\widehat{H}(j) - {}^{P+N}_{\mathrm{tr}}\overline{\boldsymbol{h}}_N \right\| \tag{6}$$

$$ {}^{N+S}_{i}D_N(j) = \left\| {}^{N+S}_{i}\widehat{H}(j) - {}^{N+S}_{tr}\overline{\boldsymbol{h}}_N \right\| \quad (7) $$

$$ {}^{N+S}_{i}D_S(j) = \left\| {}^{N+S}_{i}\widehat{H}(j) - {}^{N+S}_{tr}\overline{\boldsymbol{h}}_S \right\| \quad (8) $$

where *j* is a point on the time axis of trial *i*. Operation of the classifier in each paired posture is as follows:

- if ${}^{P+N}_{i}D_P(j) < {}^{P+N}_{i}D_N(j)$, then point j is of class P, otherwise it is of class N
- if ${}^{N+S}_{i}D_S(j) < {}^{N+S}_{i}D_N(j)$, then point j is of class S, otherwise it is of class N

Good classification rates (%) are obtained for each class in a trial by checking the real hand posture against the hand posture inferred from ${}^{P+N}_{i}D_P(j)$ and ${}^{P+N}_{i}D_N(j)$ for a P+N concatenation for example.

While the same NMF and classifier models were used to analyze both the Seat and the Stand posture datasets, the training signal used to detect a hand posture in Seat posture was chosen within the Seat datasets, and chosen within the Stand datasets to detect a hand posture in Stand posture.

4.2.4. Silhouette clustering validation index

To quantify how good the clustering is in a trial, the Rousseeuw's silhouette index (1987) was used:

$$ Sil_i = \frac{b_i - a_i}{max(a_i, b_i)} \quad (9) $$

where a_i is the average distance from the ith point to the other points in the same cluster (i.e. in a given hand posture) and b_i is the minimum average distance between this *i*th point and all other points in the other cluster (i.e. in the other hand posture of concatenated data). It varies

between 1 and -1. A Sil_i index indicates how much each value of the synergy coefficient associated to a hand posture is close to the same ones and is distant from synergy coefficients of the other hand posture. The silhouette index values are obtained based on the true hand posture label. Within a trial, a mean silhouette clustering index is obtained with:

$$mSil = \frac{1}{n}\sum_{i=1}^{n} Sil_i \quad (10)$$

where n is the total number of points in the clusters. Silhouettes obtained for a N+S training trial are displayed in Fig. 3B with mean silhouette index mSil of each cluster. For each training set, the mean of its two mSil values was used while for each tested trial, the mSil of each hand posture was considered with respect to the opposite hand posture cluster in the training dataset.

4.2.5. Processing time

On a personal computer (i7-3820 processor, 3.6 GHz clock), extraction of muscular synergy and associated coefficients of a training trial were obtained in ~2 minutes following 50000 iterations, which assured that convergence of the optimization process was attained. For each tested trial, classification took only 20 ms since it only required comparing trained and testing synergy coefficients.

4.3. Results

4.3.1. Synergy clusters and silhouettes

With 3 synergies, the coefficient of determination between original EMG RMS signals and those obtained by summation of the synergies was always >90%. Samples of 3 synergies (w_{tr1}, w_{tr2}, w_{tr3}) and associated coefficients (h_1, h_2, h_3) obtained in a training trial of subject S6 in the Seat posture are shown in Fig. 2B and 2C. For the P+N situation (panel B), muscular

synergy w_{tr2} and w_{tr3} are slightly larger under channel 1 to 4 (over SH) than under 5 to 8 (over LH). For the same P+N situation in the Stand posture (not shown), more synergy is present in the LH than in the SH. This is in agreement with earlier observations on SH vs LH activity as a function of body and hand postures (Nejat, 2012, Fig. 4.2.2, p.76). Here, for the N+S situation (Fig. 2C), synergy coefficients are larger than in B because EMG activation levels are relative higher in supination than in pronation. An illustration of the 3D plots of the N and S coefficients is presented in Fig. 3A and the silhouette index of one point out of 750 within each cluster is presented in panel B as a horizontal bar within a 0 to 1 scale. When mean value of the N and S silhouette indices (mSil) are calculated, the N index is better (closer to 1) than the S index.

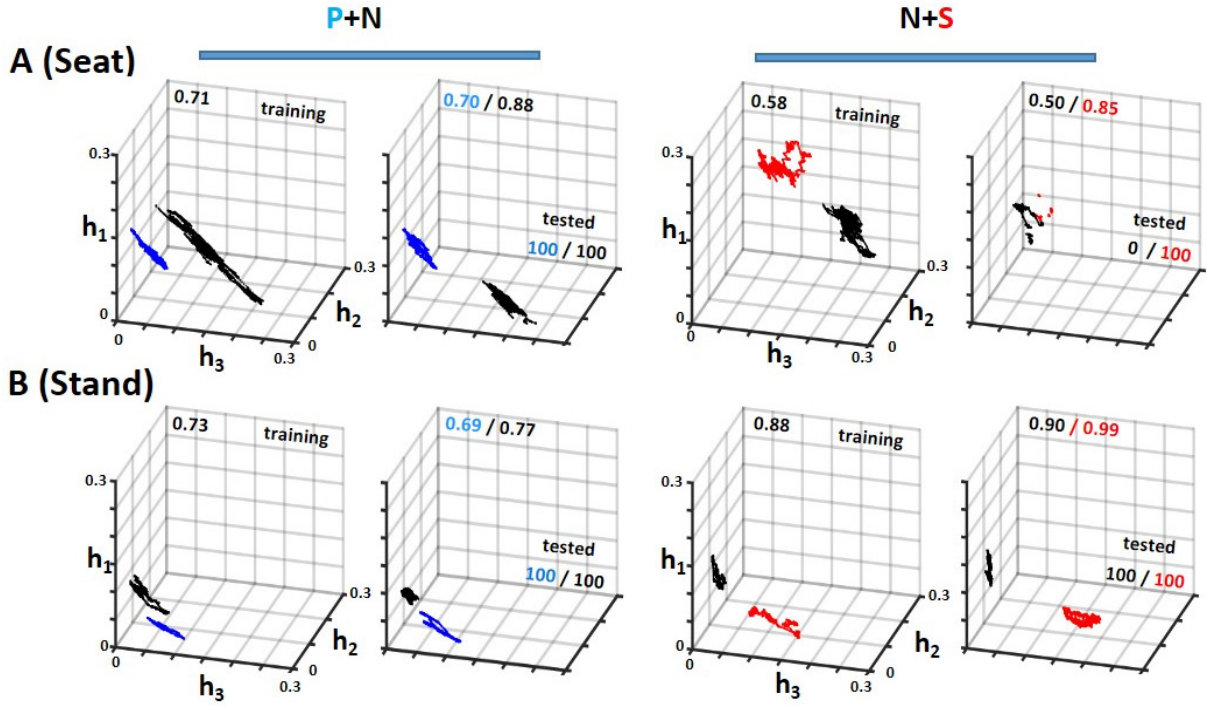

Fig. 4.4 3D plots of the h coefficient clusters of S6 obtained for concatenated P+N and N+S EMG signals in the Seat (**A**) and Stand (**B**) postures. In each of those 4 conditions, plots on the left columns are those of the training trial and those at the right of a tested trial. Numbers near the top of each 3D display are mSil values. Integer numbers near the bottom of the tested trials represent the classification results (%) for each tested hand posture. Units of h_1, h_2, h_3 are in volt.

In Fig. 4, synergy coefficient clusters of a subject obtained in the Seat and Stand postures are presented for the training and for one tested trial. Generally, classes appear well separated in each training and testing trial. When mean silhouette index shown at the top of each plane in the back is >0.70, a good classification performance is obtained as shown at the bottom right of the 3D back plane. In the Seat posture for the N+S condition, a 0% classification result was obtained for the N cluster due to the low silhouette index of the training (0.58) and of the testing trial (0.50); also, the testing trial clusters have moved at the left of the training clusters. For this particular case, the projection of the EMG to the synergy space produced a large number of negative h2 synergy coefficients, clearly defeating the NMF model.

Table 4.1 Classification results (%) obtained for each tested trial of the 10 subjects who are ordered from perfect results to the lower mean performance ones in the Seat posture. The numerous 100% results are represented by an asterisk (*) while the few cells with 0% results are greyed. Large standard deviation (SD) is due to skewness of the distribution of the results.

	SUBJECTS										
	S1	S10	S2	S4	S3	S5	S6	S9	S7	S8	
A (Seat)											Mean±SD(%)
P + N	*	*	*	91	44	*	*	63	0	12	72±34
	*	*	*	82	96	25	*	40	*	78	
		55				41	*	48	9	*	
	*	*	*	*	92	98	*	88	*	13	90±23
	*	*	*	*	72	99	*	98	*	18	
		95				83	*	*	*	83	
N + S	*	*	88	96	*	*	91	*	*	*	87±28
	*	*	*	73	*	*	0	78	*	*	
		*				*	0	55	*	*	
	*	92	71	99	*	94	*	72	*	*	87±28
	*	*	*	87	*	*	*	92	0	61	
		*				*	*	*	*	0	
mean (%)	100	95.2	94.8	91.1	88.0	86.7	82.6	77.8	75.7	63.7	84.4±28.9

B (Stand)	S1	S10	S2	S4	S3	S5	S6	S9	S7	S8	Mean±SD(%)
P + N	36	0	*	55	*	81	*	52	*	*	78±32
	49	*	*	65	*	99	*	*	59	*	
		*				39	*	*	6	*	
	*	62	64	51	*	64	*	*	47	75	80±25
	*	*	82	98	74	46	*	27	85	*	
		*				*	*	18	*	*	
N + S	*	59	*	*	0	*	*	8	82	*	84±32
	*	*	*	65	0	*	*	87	*	*	
		*				*	*	92	*	*	
	66	72	57	*	86	*	*	48	*	*	76±33
	25	0	79	*	96	99	*	72	95	*	
		0				*	*	81	11	*	
mean (%)	71.9	66.1	85.3	79.1	69.6	85.7	100	65.4	73.7	97.9	80.8±29.2

4.3.2. Classification

Results obtained in each tested trial of the 10 subjects are shown in Table 1, where the subjects' presentation order is based on the best classification percentage obtained in panel A for the P+N and N+S condition. Among the 4 tested pairs of hand postures, classification results ranged between 100% and 0%. Out of the 208 results presented in that table, a perfect classification (100%) was obtained in 118 trials (57%) while a complete failure (0%) was observed only in 10 trials (5%). Between those 2 limits, there were 80 trials (38%).

As shown in the bottom line of each panels of Table 1, two subjects obtained excellent results in P+N and N+S situations: S1 got a 100% mean classification results in the Seat posture and S6 in the Stand posture. Less performing subjects were S8 in Seat (63.7%) and S9 in Stand (65.4%) posture. Histograms of those results are presented in Fig. 5 where the 90-100% results outnumbered all the other ones.

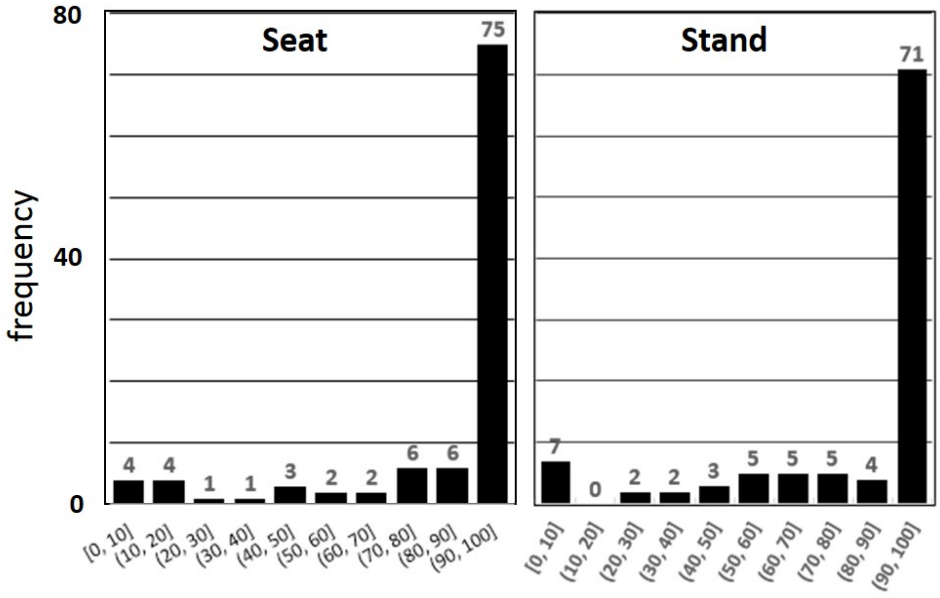

Fig. 4.5 Histograms of the classification results of Table 1. Distributions are skewed to the left due to the many 90-100% results.

Relationship between trained and tested mSil values are displayed in Fig. 6. It can be seen that when trained mSil values are high, high tested mSil values are also obtained. Relatively to the diagonal (dashed green line representing the trained mSil results), tested mean mSil values are sometimes above or under the diagonal. For instances, in the (P+N) situation, 8 tested mSil N values were larger than the trained ones and 9 tested mSil P values smaller than those of the trained mSil. In the N+S situation, best correlation values where obtained when the hand was in neutral position (R^2 = 0.93 and 0.97).

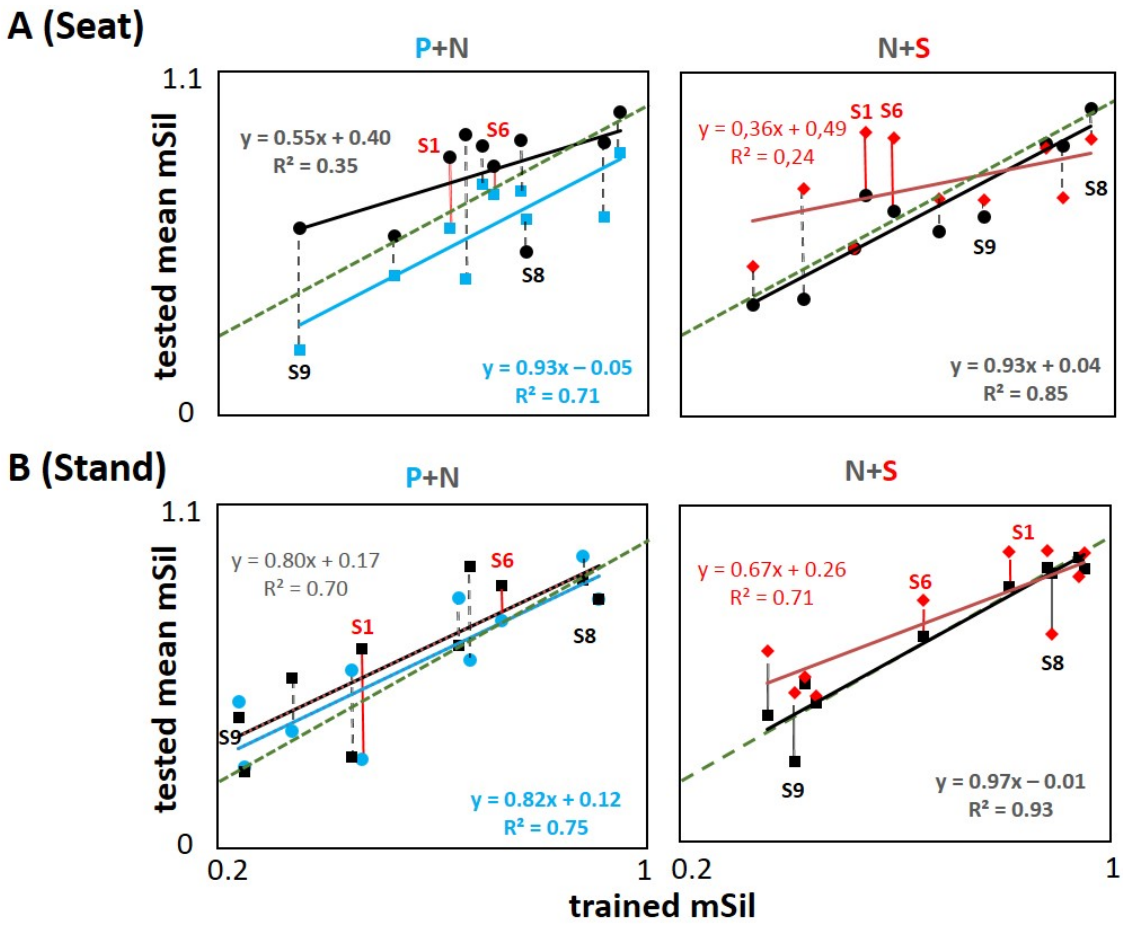

Fig. 4.6 Regression analysis between trained and tested mSil values of the 10 subjects for the concatenated tested hand postures (P: blue squares; N: black circles; S: red circles). In each panel, some of the 2 hand tested postures results are linked by a vertical dashed or solid line for easy pairing. The 2 best (S1, S6) and 2 worst (S8, S9) performers are identified. Green dashed lines represent diagonals.

4.4. Discussion

Studies on muscle synergy are usually related to the activity of many muscles acting together to perform a given motor task. For the first time to our knowledge, synergy results are reported for a single multifunctional muscle, the biceps brachii. This suggests that activity of this muscle is representative of the activity of different "muscles" which could be anatomically associated to the individually innervated compartments observed on its posterior view (Segal, 1992). From the signals collected from 8 equidistant electrode pairs placed across the biceps, three muscle synergies were sufficient to provide a coefficient of determination of 90% with the recorded signals of those "muscles". With those 3 synergies, it was possible to identify, between 2 static hand postures, which one was taken by the subject when a given set of EMG signals were recorded. Those muscular synergies results are comparable to those of other authors, such as Rasool et al. (2016) who collected 5 signals at equal distance around the forearm and found that 2 and 3 synergies were needed to detect respectively 1 and 2 DoFs of wrist movements. Likewise, Torres-Oviedo and Ting (2007) with 16 legs and lower back muscles found that 4 to 6 synergies were involved in the postural standing reflex following a perturbation randomly oriented around their subjects.

Two arm postures, two elbow angles and three hand postures were tested. As can be observed in 3D views of Fig. 4, positions of the synergy coefficient clusters in the Seat (100° elbow angle) are quite different than in Stand (180°elbow angle) posture. If a similar situation can be observed with the biceps of below elbow amputees, they will have the possibility to control more than one action of their prostheses with that muscle. In the event that separable clusters could still be observed with intermediate elbow angles, additional control signals would then be obtained.

As can be observed in Table 1, the presence of many 100% scores indicates that some subjects could produce successively very similar 3 or 4 contractions. This was the case for S1 in the Seat posture and S6 in the Stand posture. That ability was not shared by everyone since a 0% classification result (greyed cells in the table) occurred 10 times for 5 sub-jects. In Table 1, mean classification result of the 10 subjects in Seat posture is higher (84.4±28.9%) than in Stand posture (80.9±29.2%)[2] indicating that it is more difficult in the Stand posture to produce similar contractions when the arm is fully extended horizon-tally to the side than when it is close to the body with an elbow angle of 100° when Seat. We have unpublished data, where similar classification results were obtained by 3 below elbow amputees tested in similar experimental conditions.

In each experimental dataset, the first trial out of 3 or 4 was always used for training. To verify if this was an appropriate strategy, mSil values obtained with the trained trials of each subject were compared with their mean mSil values obtained from the 2 or 3 tested trials. As observed in Fig. 6, the mean tested mSil values of some subjects were, in certain conditions, above the dashed diagonals representing the trained trials. This suggests that having chosen a training trial with a mSil value in the middle of the 3 or 4 mSil values in a dataset, better classification results could have been obtained. In the Seat posture (Fig. 6A) when P and N signals are concatenated, a low R^2 coefficients (0.35) is obtained for the N results while for the same N data concatenated with the S posture, it is the S results which present a low R^2 coefficients (0.24). A somewhat similar situation can be observed in the Stand posture (Fig. 6B) where lower R^2 values (0.70 and 0.71) are also obtained for the N posture when concatenated

[2] High standard deviation values are due to the skewness of the classification results as shown in Fig. 5.

with P and for S posture when concatenated with N. Since similar contractions in the Seat posture are easier to produce than in the Stand one, less compact clusters were expected in the Stand posture not in the Seat one. We presently have no explanation for those results. So, to control a myoelectric pros-thesis, it has to be expected that some subjects will perform better than others and that in some postures, signals generated by the biceps will lead to easier production of a movement than when in other postures.

Table 4.2 Effects of EMG window size on mean classification results of the 10 subjects. Window size reduction induces a small reduction in the classification rate.

	window width (ms) mean±sd (%)		
Seat	**815**	**400**	**200**
P + N	72±34 90±23	71±34 87±23	70±31 80±24
N + S	87±28 87±28	83±28 83±28	78±28 82±23
mean±sd	**84±29**	**81±29**	**78±27**

Stand	**815**	**400**	**200**
P + N	78±32 80±25	78±29 75±28	77±31 70±19
N + S	84±32 76±33	84±31 75±29	83±30 76±27
mean±sd	**81±29**	**78±29**	**77±30**

Raw EMG signals were processed here with a 815 ms window width because it provided the best classification results with our EMG signals recorded under a constant biceps' contraction level. However, such window would be too large for real-time myoelectric control application where the maximal acceptable delay is 200-300 ms including processing time of the algorithm. Hence, we tested smaller window widths of 400 and 200 ms and found that this resulted in only a small reduction in the classification rate (Table 2). As for the processing time,

it takes approximately 20 ms to classify a tested trial; so, this time can be neglected being in the range of acceptable delay.

Here, the synergy of 8 signals of the biceps were used off-line with simple tasks, i.e. for the classification of 2 pairs (P+N, N+S) of hand postures. This at first would be no better than what is already achieved by two channels commercially available prostheses operating without any elaborated signal processing or machine learning algorithms. However, the potential of the synergy model being part of machine learning methods, more complex motor tasks can be foreseen. This is supported by works we reported elsewhere (He and Mathieu, 2017a, He and Mathieu, 201b) with results from pilot studies showing that our method can not only off line classify three hand static postures, as in this paper, but also can online classification any of eight different arm postures.

Recognizing that this still misses an important aspect of prosthetic arm operations, namely a proportional control, further work must be done to investigate its implementation in the synergy model. This will be initiated in an upcoming online data acquisition of different 2D movements of the arm of 10 normal subjects, results on proportional control and the effects of holding two different loads will be obtained.

4.5. Conclusion

For the first time to our knowledge, muscle synergy was extracted from a single muscle, the biceps brachii as if there are muscles within that multifunctional muscle. Applying silhouette clustering index and Euclidean distance classifier on muscular synergy coefficients, a mean classification success rate of >80% was obtained between two static hand postures. Besides offline classification of three static hand postures, the approach can also be used for online

identification of pairs of 8 arm postures as demonstrated in two pilot studies. It thus appears that information in the biceps' synergies coefficients could facilitate the control of myoelectric prostheses when amputation is close to the elbow joint while for an amputation close to the wrist joint, it would be simpler to flex the elbow joint with the biceps and use forearm muscles to activate wrist articulation and prepare the hand to pick up an object. For a trans-humeral amputation, close to the shoulder, the multifunctional deltoid, trapezius or the pectoralis major could be at the origin of many EMG signals.

We believe our approach has the potential to open new avenues in upper arm prosthetic control and in other controls where multifunctional muscles are involved. We recognize that to convincingly become clinically relevant, a larger number of classes, a combination with (clinically required) proportional control should be investigated. The encouraging results we currently obtain provides a valuable support to reach this goal.

4.6. References

Bizzi, E., Cheung, V.C.K., 2013. The neural origin of muscle synergies. Front. Comput. Neurosci. 7 (51), 1–6.

d'Avella, A., Lacquaniti, F., 2013. Control of reaching movements by muscle synergy combinations. Front. Comput. Neurosci. 7 (42), 1–7.

d'Avella, A., Portone, A., Fernandez, L., Lacquaniti, F., 2006. Control of fast-reaching movements by muscle synergy combinations. J. Neurosci. 26 (30), 7791–7810.

Gatti, C., Doro, L.C., Langenderfer, J.E., Mell, A.G., Maratt, J.D., Carpenter, J.E., Hughes, R.E., 2008. Evaluation of three methods for determining EMG-muscle force parameters estimate for the shoulder muscles. Clin. Biomech. 23 (2), 166–174.

Günay, S.Y., Quivira, F., Erdoğmuş, D., 2017. Muscle Synergy-based Grasp Classification for Robotic Hand Prosthetics. In: Proc. 10th Intl. Conf. on Pervasive Technologies Related to Assistive Environments. Association for Computing Machinery, New York, pp. 335–338.

He, L., Mathieu, P.A., 2017a. Environnement Virtuel et Petit Robot pour Apprendre à contrôler une Prothèse myoélectrique du Membre Supérieur. 2nd Congress in Adaptation-Rehabilitation Research (RÉPAR), Montreal.

He, L., Mathieu, P.A., 2017b. Muscle synergy of biceps brachii and online classification of upper limb posture. In: Intl. Conf. on Virtual Rehabilitation (ICVR), Montreal, pp. 1–6. https://doi.org/10.1109/ICVR.2017.8007484.

Jiang, N., Englehart, K.B., Parker, P.A., 2009. Extracting simultaneous and proportional neural control information for multiple-DOF prostheses from the surface electromyographic signal. IEEE Trans. Biomed. Eng. 56 (4), 1070–1080.

Joergensen, K., 2006. NMF DTU Toolbox.<http://cogsys.imm.dtu.dk/toolbox>(Consulted on January 2016).

Ken Hub Channel. Biceps Brachii. Origin, insertion, innervation, function. <https://www.youtube.com/watch?v= v0GJltQp6R0> (Consulted on March 2018).

Lee, D.D., Seung, H.S., 2001. Algorithms for non-negative matrix factorization. In: Leen, T.K. (Ed.), Advances in Neural Information Processing Systems. MIT Press, Cambridge, MA, pp. 556–562.

Muceli, S., Vujaklija, I., Jiang, N., Amsuess, S., Graimann, B., Aszmann, O.C., Farina, D., 2017. A biologically-inspired robust control system for myoelectric control. In: Ibáñez, J. (Ed.), Converging Clinical and Engineering Research on Neurorehabilitation II. Springer International Publishing, Cham, Switzerland, pp. 975–979.

Nejat, N., 2012. Study on the activation of the biceps brachii compartments in normal subjects (Master's thesis). Université de Montréal.

Oliveira, A.S., Gizzi, L., Farina, D., Kersting, U., 2014. Motor modules of human locomotion: influence of EMG averaging, concatenation, and number of step cycles. Front. Hum. Neurosci. 8 (335), 1–9.

Rasool, G., Iqbal, K., Bouaynaya, N., White, G., 2016. Real-time task discrimination for myoelectric control employing task-specific muscle synergies. IEEE Trans. Neural Syst. Rehabil. Eng. 24 (1), 98–108.

Rousseeuw, P.J., 1987. Silhouettes: a graphical aid to the interpretation and validation of cluster analysis. J. Comput. Appl. Math. 20, 53–65.

Santuz, A., Ekizos, A., Janshen, L., Baltzopoulos, V., Arampatzis, A., 2017. On the methodological implications of extracting muscle synergies from human locomotion. Int. J. Neural Syst. 27 (5) 17500071(1–15).

Segal, R.L., 1992. Neuromuscular compartments in the human biceps brachii muscle. Neurosci. Lett. 140 (1), 98–102.
Ting, L.H., Macpherson, J.M., 2005. A limited set of muscle synergies for force control during a postural task. J. Neurophysiol. 93 (1), 609–613.

ter Haar Romeny, B.M., van der Gon, J.J.D., Gielen, C.C.A.M., 1984. Relation between location of a motor unit in the human biceps brachii and its critical firing levels for different tasks. Exp. Neurol. 85 (3), 631–650.

Torres-Oviedo, G., Ting, L.H., 2007. Muscle synergies characterizing human postural responses. J. Neurophysiol. 98 (4), 2144–2156.

Tresch, M.C., Cheung, V.C., d'Avella, A., 2006. Matrix factorization algorithms for the identification of muscle synergies: evaluation on simulated and experimental data sets. J. Neurophysiol. 95 (4), 2199–2212.

Yang, N., An, Q., Yamakawa, H., Tamura, Y., Yamashita, A., Asama, H., 2017. Muscle synergy structure using different strategies in human standing-up motion. Adv. Rob. 31 (1–2), 40–54.

5. Biceps Brachii Muscle Synergy and Target Reaching in a Virtual Environment

This article has just been submitted to the Journal of Frontiers in Neurorobotics. Within a virtual cube presented on a computer screen, a red sphere position is controlled by the signals from biceps brachii of 12 subjects in order to reach 4 different targets. The control signals are obtained with muscle synergy extracted from the biceps of each subject when 8 different static postures were taken by their right upper limb. In this project, I realized all the programs and graphic interfaces for the human computer interaction, recruited 12 subjects, collected the experimental data, and prepared the preliminary draft of the article. Professor Mathieu supervised the research, designed the evaluation routine, and revised the article. Both authors contributed to the final version of the article. With this project, we demonstrated that muscular synergy from the biceps brachii could facilitate the control of myoelectric prosthesis with which upper limb amputees could produce movements frequently used in their daily activities.

Biceps Brachii Muscle Synergy and Target Reaching in a Virtual Environment

Liang He, Pierre A. Mathieu
Biomedical Engineering Institute, Université de Montréal,
Montréal, QC, H3T 1J4, Canada

Abstract

A muscular synergy is a theory suggesting that the central nervous system uses few commands to activate a group of muscles to produce a given movement. Here, we investigate how a muscle synergy extracted from a single muscle can be at the origin of different signals which could facilitate the control of modern upper limb myoelectric prostheses with many degrees of freedom. Five pairs of surface electrodes were positioned across the biceps of 12 normal subjects and electromyographic (EMG) signals were collected while their upper limbs were in 8 different static postures. Those signals were used to move, within a virtual cube, a small red sphere toward different targets. With 3 muscular synergies extracted from the 5 EMG signals, a classifier was trained to identify which synergy pattern was associated with a given static posture. Later, when a posture was recognized, the result was a displacement of a red sphere toward a corner of a virtual cube presented on a computer screen. The axes of the cube were assigned to the shoulder, elbow and wrist joint while each of its the corners was associated with a static posture. The goal for subjects was to reach, one at a time, the 4 targets positioned at different locations and heights in the virtual cube with different sequences of postures. The results of 12 normal subjects indicate that with the muscular synergies of the biceps brachii, it was possible, but not easy for an untrained person, to reach a target on each trial. Thus, as a proof of concept, we show that features of the biceps muscular synergy have the potential to facilitate the control of upper limb myoelectric prostheses. To our knowledge, this has never been shown before.

Keywords: Biceps brachii, muscle synergy, upper limb posture classification, target reaching, virtual cube, myoelectric prosthesis.

5.1. Introduction

Important progress has recently been made in the design of multiple degrees of freedom (DoF) upper limb myoelectric prosthesis (Lenzi et al., 2016) and this has led the production of commercially available units, such as the Luke Arm (Mobius Bionics, 2017). Such advanced prostheses can be most valuable to amputees in their daily living. Multiple DoFs implies that multiple control signals have to be derived from EMG signals. To that end, Daley et al. (2012) used a linear discriminant analysis (LDA) to classify 12 different wrist and hand movements of normal subjects using 8 optimally placed electrodes on the forearm. Similarly, Ameri et al. (2014) used an artificial neural network (ANN), where visual training was considered better than force training to simultaneously estimate intended movements of multiple joints. Comparing the classifiers performance, Adewuyi et al. (2016) found for non-amputees and partial-hand amputees that LDA and ANN perform better than the quadratic discriminant analysis. Betthauser et al. (2018) developed a robust sparsity-based adaptive classification method to get a classification system which is appreciably less sensitive to signal deviations between training and testing. When they tested it on 8 able-bodied and 2 transradial amputee subjects with 8 electrodes pairs regularly spaced around the proximal forearm, it was found that their approach significantly outperformed other movement classification methods.

In addition to such approaches, the concept of muscle synergy was proposed to examine how the brain could efficiently command various muscles to produce different movements. For instances, to understand the posture balancing reaction of humans on a platform submitted to various perturbations in the horizontal plane, Torres-Oviedo and Ting (2007) used muscle synergies between 16 leg and lower-back human muscles. Muceli et al. (2010) found synergy among 12 muscles of the upper limb of 8 subjects when reaching tasks were performed in the

horizontal plane. To extract muscle synergies, various approaches can be used such as principal component analysis (PCA), independent component analysis (ICA) and non-negative matrix factorization (NMF). Amongst those, Tresch et al. (2006) considered that the NMF algorithm (Lee and Seung, 2001) was more physiologically relevant than the others given that a muscle can only be active at various contraction levels (positive) but never below rest (negative).

Features of muscle synergies are often used for classification purposes (Delis et al., 2013). For instance, Naik and Nguyen (2015) used NMF processed data to classify the finger gesture of two forearm muscles. Similarly, Rasool et al. (2016) used forearm muscles for real-time classification of hand open/close, wrist flexion/extension and forearm pronation/supination. Antuvan et al. (2016) used extreme learning machines and muscle synergy features to classify upper limb postures involved in elbow flexion /extension and shoulder flexion/protraction/retraction and rest posture. Muscle synergy has also been applied to upper limb muscles for proportional control related to prosthetic applications (Jiang et al. 2009; Ma et al., 2015).

As for our research it is focused on the multifunctional biceps brachii muscle which is involved in shoulder elevation, elbow flexion, and forearm supination (Landin et al., 2008, Jarrett et al., 2012). There is also anatomical evidence to support its multifunctionality: besides its division into 2 heads, its inner surface appears to be further divided into up to 6 compartments which are each innervated by a branch of the musculocutaneous nerve (Segal, 1992)[3]. Multifunctionality is also supported by physiological evidence: ter Haar Romeny et al. (1984)

[3] Anatomically, compartments are not unique to the biceps brachii. They are also present in the deltoid, the pectoralis major and the latissimus dorsi at the shoulder level (Brown et al., 2007) which are less frequently studied than the biceps.

found that during different functional tasks of the upper limb, motor units of the biceps were activated at different locations within the muscle, probably due to activity in different compartments. These individual compartments can then be considered as muscles within a muscle working together to accomplish functional roles. This situation is somewhat similar to the one where anatomically different muscles work synergistically together (Bizzi and Cheung, 2013).

This paper reports on an experimental study where the biceps EMG signals are the only ones used to identify a static arm posture, out of 5 or 8. The study examines how successive postures could be used to develop a trajectory so as to reach a specified target in a virtual environment.

5.2. Materials and methods

The study was approved by the ethical committee of the Faculty of Medicine at the Université de Montréal and the 12 subjects signed a written informed consent form in accordance with the Declaration of Helsinki. To participate to the project, the inclusion criteria for each subject were: to be without any known history of neuromuscular disorders, be right-handed and aged between 20 and 35 years old; additional personal information is presented in Table 1.

For each subject, the borders of the biceps brachii were identified by palpation and the midpoint considered separating the short head (SH) from the long head (LH). As shown in Figure 1A, three pairs of surface electrodes were placed across the SH and two pairs across the LH while a reference electrode was placed over the acromion. To avoid the muscle's innervation zone, the upper row of electrodes was positioned 10 mm below the middle of the biceps.

Ag/AgCl disc electrodes of 10 mm in diameter (Kendall H69P) were used with a 2 cm vertical and horizontal distance between center to center distances. Acquisition of the 5 EMG signals was done with customized electronic circuits using a differential amplifier (AD8226, Analog Devices) with a gain of 200. The amplified signals were rectified with an op amp (TL084, Texas Instruments), high-pass (6.67 Hz) and low-pass (1240 Hz) filtered. Following the low-pass filter, a second gain of 10 was obtained using the same TL084 op amp. Following this analog processing, signals were digitized (2000 Hz, 12 bits) with a microcontroller (ROBOTIS OpenCM9.04). On an ARM Cortex-M3 processor (72 MHz clock), a root mean squared (RMS) function was implemented with a window width of 250 ms and a large 70 ms step size due to the communication rate of 15 Hz between the microcontroller and a laptop which hosted the MATLAB software that provided data processing and a graphical user interface (GUI) for interaction with the subject.

Table 5.1 Information on our 12 subjects with their body mass index (BMI) and mid-upper arm circumference (MUAC).

Subject ID	Height (cm)	Weight (kg)	BMI	MUAC (cm)
S1	169	50	17.5	23
S2	163	48	18.1	22
S3	167	55	19.7	24
S4	157	52	21.1	25
S5	160	58	22.7	24
S6	172	80	27.0	29
S7	183	70	20.9	28
S8	180	75	23.1	30
S9	170	72	24.9	28
S10	173	77	25.7	28
S11	179	83	25.9	32
S12	183	112	33.4	37
MEAN	**171.3**	**69.3**	**23.3**	**27.5**
±SD	**8.7**	**18.3**	**4.4**	**4.3**

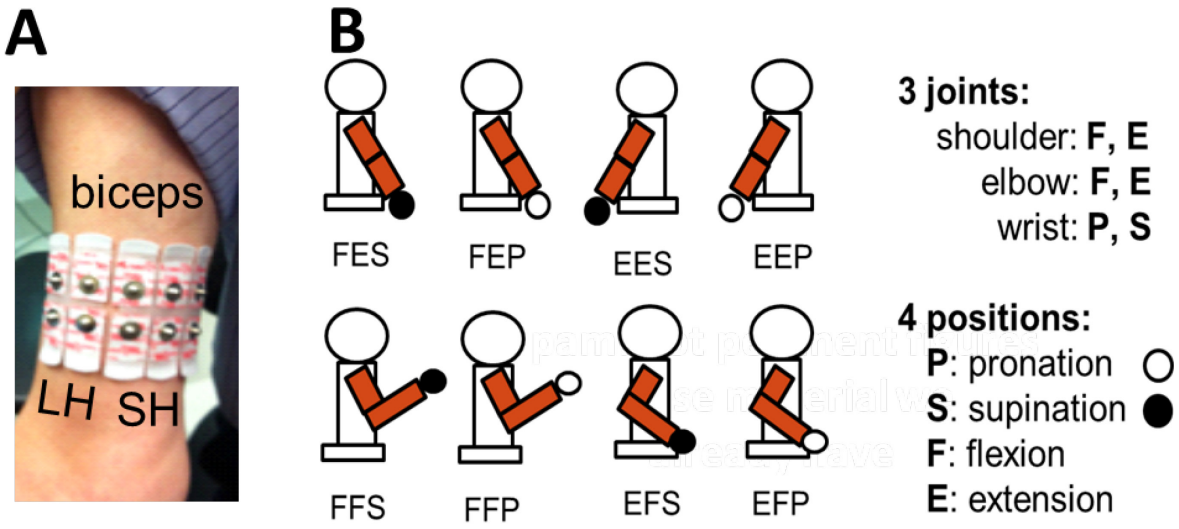

Fig. 5.1 Electrodes and postures. **(A)** Five bipolar surface electrodes were placed across the biceps brachii: 2 over the long head (LH) and 3 across the short head (SH). **(B)** Eight different static postures of the right upper arm were used. They are identified with a 3-tuple system [*,*,*] respectively representing shoulder, elbow, and wrist joints. For the first * it can be F (flexion) or E (extension) for shoulder joint posture, second * can be F or E for elbow joint posture, and third * can be P (pronation) or S (supination) for wrist joint posture.

While seated, subjects had to take one of eight different static postures (Figure 1B) while facing a computer screen where a cube was displayed. As shown in Figure 2A, each corner of the cube was assigned to one of the eight static postures (SP). The normalized axes of the cube were defined so the [-1 to 1] range represented the full excursion of the shoulder and elbow joints which were either extended or flexed and to the wrist joint which had the hand set either in pronation or in supination. Each intermediate position in the 3 axes is interpolated linearly. The distance measured between 0 and 1 on the vertical elbow axis is used as the unit against which each trajectory length and distance is measured within the cube. Before each trial (Figure 2B) the red sphere was positioned at the center of the cube and it has to be moved toward one of the targets and touch its grayish sphere (diameter: 0.2) within 120 s to be a success otherwise

the trial is a failure. The coordinates of each target are shown in Figure 2C. Each subject made three trials to reach a target.

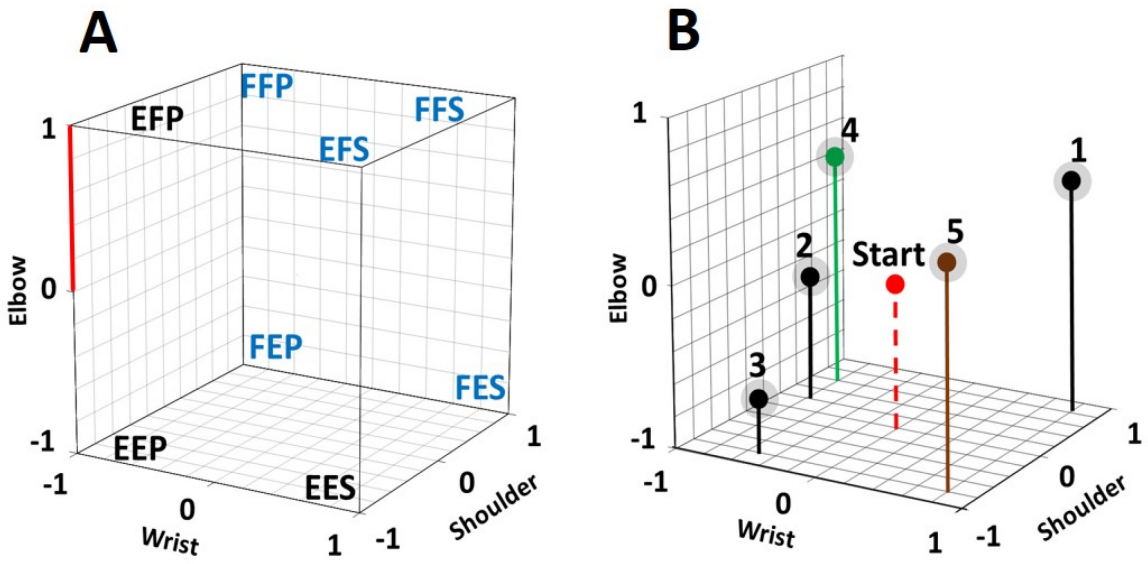

C

Targets	Coordinates [Wrist, Shoulder, Elbow]
1	[0.8, 0.8, 0.8]
2	[-0.75, 0.2, -0.05]
3	[-0.5, -0.8, -0.68]
4	[-0.8, 0.6, 0.8]
5	[0.75,-0.75, 0.8]

Fig. 5.2 Virtual target reaching. **(A)** Each of the 8 chosen static postures is assigned to a corner of a virtual cube displayed on a computer screen. Each axis of the cube represents the normalized angular changes at the shoulder, the elbow and the wrist joint. Experiments were done with the 8 illustrated postures and with a subset of 5 postures which are identified with a blue font. On the Elbow axis, the distance between 0 and 1 is used as the reference length to which distance, length and diameter measures are compared. **(B)** 3D view of the 5 targets within the cube. In each trial, the initial position of the red sphere is in the center of the cube and subjects have to move it so that it reaches one of the targets, which have a diameter of 0.2 including their greyed surrounding. The red sphere is only a point in the program, but it is displayed with a given diameter to make it visible to the subjects. **(C)** 3D coordinates of the 5 targets.

Figure 3 presents a flow chart of the MATLAB program used from EMG pre-processing up to displaying the position of the red sphere within the virtual cube. An NMF algorithm was used to extract muscle synergies from pairwise postures as done previously (He and Mathieu, 2018); details of the method are presented in Appendix 1 and 2. The muscle synergy is extracted from concatenated EMG signals of two different postures, and since no labeling information of the data is required, when a muscle synergy is extracted from concatenated EMG, the classifier should have the power to detect a difference between each paired posture. This power is determined by a signal-to-noise ratio (SNR) where the signal is the difference between paired

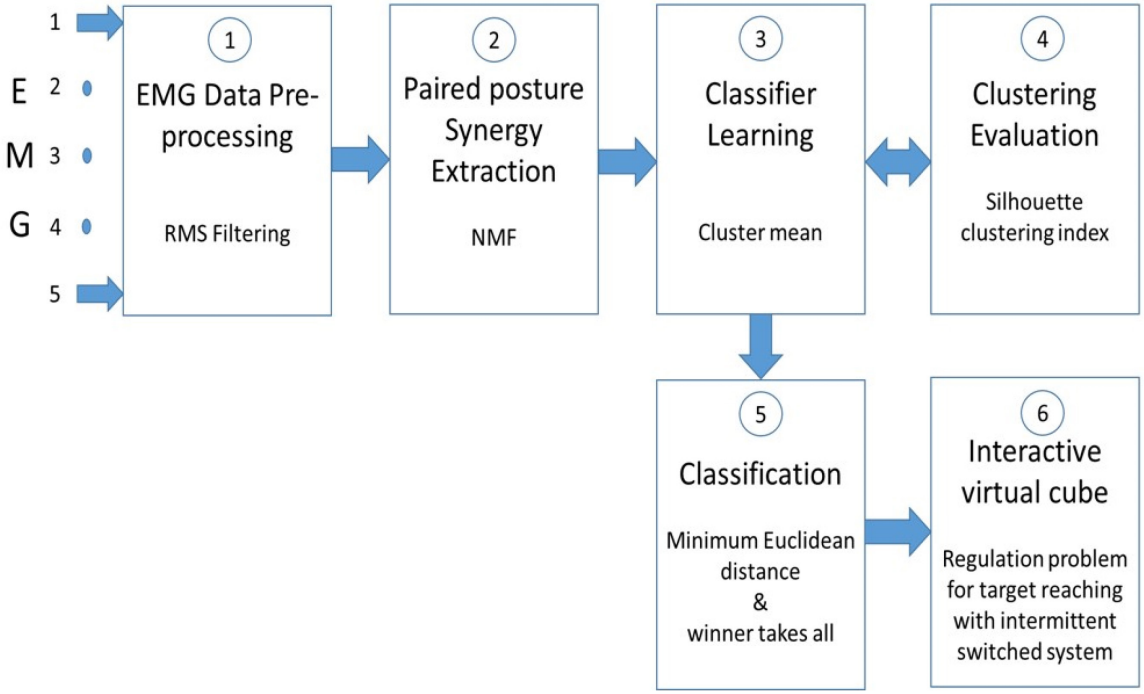

Fig. 5.3 Flow chart of computer program. Five raw EMG signals from the biceps are smoothed ① with a RMS filter. ② sEMG signals from paired postures are concatenated before extracting muscle synergy with a nonnegative matrix factorization (NMF) program. ③ Cluster mean values of the muscle synergy from pairwise postures are used to train a classifier. ④ To improve the classification accuracy, the clusters formation is evaluated with the silhouette clustering index. ⑤ Classification of paired postures is obtained using the minimum Euclidean distance between them. In stage ⑤ a "winner-takes-all" method is used to make simultaneous posture classifications. In ⑥, the virtual cube, a switched system is used to move the red sphere toward a target within the cube.

postures and noise is the dissimilarity of the clusters associated to each posture in the pair. The silhouette index of Rousseeuw (1987) was used to measure the discrimination power of the muscle synergy (i.e. how easy to identify different clusters). Some details of the silhouette index are also presented in Appendix 1. In the absence of a unique solution, the NMF algorithm was applied many times (n=30) on the same pairwise posture of EMG data to find the best solution, as shown in Appendix 2.

For an online classification of the 8 SPs of the upper limb, binary classifiers (Fürnkranz, 2002) were used with a round robin method (Park and Fürnkranz, 2007) which transforms binary classifiers into a posture classifier. The number of postures to be classified is a parameter of the classifier which determines the number of binary classifiers. With 8 static postures, the number

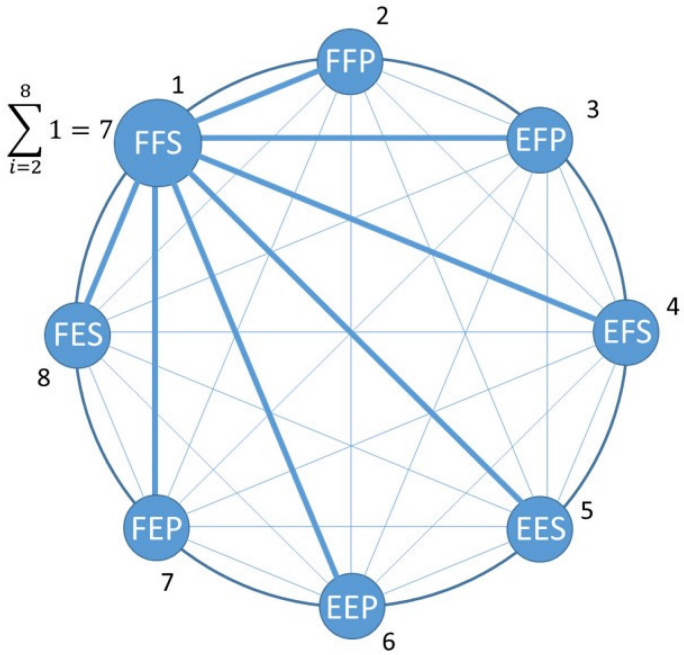

Fig. 5.4 Posture classification example where the maximum number of paired posture classification is 8*(8-1)/2=28. Out of those there are 21 thin blue lines representing paired posture classifier associated with postures other than FFS which were taken by a subject. Associated with FFS are 7 paired classifiers (large blue lines) which make correct classification with FFS.

of pairwise posture classifiers needed to obtain a posture classification is 8 x (8-1)/2= 28. The governing equation in the binary classifier is the measured Euclidean distance between the tested pattern and the learned class reference (Appendix 1, equations A1.3 and A1.4). In Figure 4, the 21 thin lines connecting a pair of 8 postures represent a trained binary classifier and the 7 thick lines related to the round robin method are used to identify a posture such as FFS. For the 5 SP condition (a subset of the 8 SPs), 10 pairwise posture classifiers are used. The posture identified with the posture classifier is fed to an intermittent controller.

5.2.1. Intermittent controller

For each trial, the initial location of the red sphere is at the center of the cube and when a first static posture taken by the subject to reach a target is identified by the classifier (Figure 5), the intermittent controller (Gawthrop et al., 2011) moves the red sphere toward the corner of the cube associated to the detected posture. If the target is not reached, additional posture changes are produced up to when the target is reached or when a 120 s time limit expires. Within the intermittent controller a discrete state switch control is used to compare the new joint posture with the previous one. Then, the activated joints are only those where a change had occurred. For example, in a FFS to FEP posture change, the shoulder joint (first F in both postures) will be inactivated and the red sphere will move, from flexion (F) to extension (E) along the elbow axis, and simultaneously on the wrist axis, from supination (S) to the pronation (P). When a change occurs simultaneously at the 3 joints as from EFS to FEP, the shoulder joint will only be activated and the red sphere will move, along the shoulder axis from extension (E) to flexion (F). As for the 2 other joints, they will remain inactive until the subject makes another posture change which does not involve the shoulder joint.

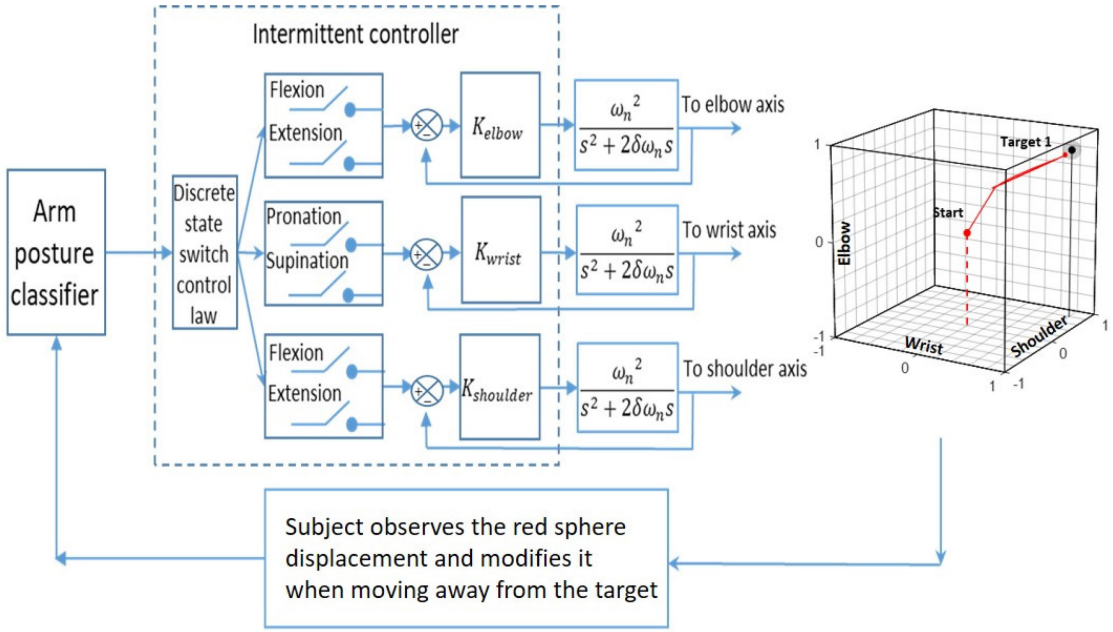

Fig. 5.5 Intermittent control with switch. The input of an arm posture classifier is fed to an intermittent controller that determines which switch to close in order to move the red sphere accordingly with the subject's posture. The movement of the red sphere in each of the three joint axes is produced with a 2nd order system whose transfer function is given by Equation 1. The subject used the movement of the red sphere within the cube as visual feedback to produce sequential posture changes, and the objective was to reach a target in the cube.

5.2.2. Red sphere displacement

The position of the red sphere in the cube corresponds to the position of the 3 joints of the upper limb of a subject and a static posture change is associated with a step function input to a second-order system and the output is a continuous displacement of the red sphere toward the appropriate corner. For this second-order system (Equation 1), the resistance to the movement of the red sphere is associated with ω_n (a large value produces a larger resisting force to the displacement) and resistance to speed change of the red sphere is associated with δ (a larger value produces a larger resisting force). The transfer function of the second-order system is:

$$\frac{C(s)}{R(s)} = \frac{{\omega_n}^2}{s^2+2\delta\omega_n s+{\omega_n}^2} \quad (1)$$

where C(s) is the output to the red sphere and R(s) is a step function associated with each static posture change made by the subject. The dynamic parameters of the red sphere's movement ($\omega_n = 0.39$ and $\delta = 1$) were the same for each subject. When a new posture is identified while the red sphere is still moving; the red sphere immediately changed its direction under the actuation of the intermittent controller. To move the red sphere anywhere within the cube, at least 4 static postures are needed.

5.2.3. Protocol

The day before the experiment, each subject came to the laboratory to view a short video demonstrating how to produce each of the 8 static postures illustrated in Figure 1B and during approximately 150 minutes, they practiced controlling the movements of the red sphere. The next day, during the experiment, targets 1, 2, 3, 4 had to be reached in succession with 5 SPs and targets 1, 2, 3, 5 with 8 SPs. Targets 1, 2, 3 were thus considered with both the 5 and 8 SP groups for comparison purposes. Performance of target reaching was measured with 4 measures: 1) time in seconds to reach a target; 2) trajectory length made by the red sphere from its initial position up to reaching a target, or in a failed trial, up to its end position when 120 s was reached; 3) number of posture changes taken to reach a target or to reach the 120 s for a failed trial; 4) the distance between the red sphere and the target when 120 s was reached for a failed trial. The Runge-Kutta 4 (RK4) method is used to obtain the trajectory length of the red sphere, which is obtained from the cumulative sum of Euclidean distances along the numerical solutions.

During the classifier training and evaluation, subjects kept their arm in each of the 8 static postures for 10 s, from which the muscular synergies were extracted for classifier training.

Next, they kept 3 times each of the 5 or 8 static posture for 5 s, from which the obtained synergies were compared online with the trained classifier. For each trial, 30 iterations were produced by the classifier and a percentage of good classification was obtained and a mean value obtained for each subject for the 5 and 8 SPs condition.

The NASA task load index (TLX) survey form (Appendix 3) was filled by each subject after the experiment. This is a self-evaluation of 6 items: mental, physical, temporal demand and level of effort, frustration and performance during the experiment. That feedback could provide valuable information to improve the experimental protocol and software programs used to process the information.

5.2.4. Statistics

A paired t-test was used to compare mean results obtained by the 12 subjects when 5 or 8 SPs were used. The tested hypothesis was that with 5 SPs, the mean classification results and the number of targets reached would be better than with 8 SPs because remembering how to reproduce with some fidelity 8 different postures is more mentally demanding than for only 5. Where numbers of subjects were different for targets or postures (Figure 7 and 8), independent sample t-test were used to test the difference between the compared results. A difference was considered significant when $p < 0.05$ and the IBM SPSS Statistics software was used.

5.3. Results

Classification % obtained during the training with 5 and 8 SPs are shown in Table 2A. With 5 SPs, the classification of 4 subjects was very good (> 90%), although it was quite poor for S12 (31%). With 8 SPs, the mean classification value (of 72 ± 20%) was significantly lower ($p = 0.001$) than with 5 SPs (82 ± 19 %). In Table 2B, each subject's ratio of the number of

reached targets out of 12 (3 trials x 4 targets) is presented. It can be observed that a good classification % in the training session was not always associated with a large ratio of reached targets. For instance, S2 and S8, who were among the 5 subjects with high classification performance, did not reach a single target in the 8 SP condition. As expected however, S12 with

Table 5.2 Classification and target reaching results. **(A)** In the training session, mean (± SD) classifier accuracy (%) for the 5 and 8 static postures (SP) conditions. Mean values of each subject are obtained from 3 trials of 5 s in each of the 5 or in each of the 8 static postures. The subjects are sorted from highest to lowest performance in the 5 SP condition. The difference between 5 and 8 SP results is significant ($p < 0.05$). **(B)** Success ratio (number of successful trials over total number of trials) of target reaching trials by each subject. The subjects are sorted from highest to lowers performance in the 5 SP condition. In each column the total number of trials is 12 (4 targets x 3 trials) for each subject. S3 was the best performer. Between the 5 and 8 SP results the paired t-test value is 0.281.

A

Subjects	5 SP	8 SP
	Mean±SD	Mean±SD
S5	99±2	87±20
S11	95±4	68±35
S1	94±6	88±25
S2	90±10	83±20
S8	89±9	79±21
S3	87±14	75±43
S4	87±21	90±11
S7	87±15	85±13
S9	85±15	72±26
S10	76±16	64±26
S6	60±36	49±45
S12	31±45	22±42
Mean ± SD	**82±19**	**72±20**

B

Subjects	5 SP	8 SP
	Ratio	Ratio
S3	0.67	0.75
S8	0.50	0.00
S7	0.50	0.25
S1	0.42	0.58
S6	0.33	0.33
S5	0.25	0.25
S9	0.25	0.25
S11	0.17	0.17
S4	0.17	0.17
S2	0.08	0.00
S10	0.08	0.08
S12	0.08	0.00
Mean ± SD	**0.29±0.18**	**0.24±0.23**

the lowest classification results could only reach 1 target with 5 SPs and 0 with 8 SPs (ratio: 0.08 and 0.00). For the group, the mean ratio of target reached was higher with 5 SPs (0.29 ± 0.18) than with 8 SPs (0.24 ± 0.23) but this difference was not significant ($p = 0.281$).

Figure 6 illustrates 2 trajectories of the red sphere which was controlled by S3 trying to reach target 2 with 5 SPs. In panel A, an example of a failed trial is shown, where in spite of 72 posture changes made during 120 s, the red sphere was still at a distance of 0.68[4] from target 2 after a trajectory length of 14.7[4]. The same subject was far more successful in another trial (panel B) where the same target was reached with only 4 posture changes within 9 s.

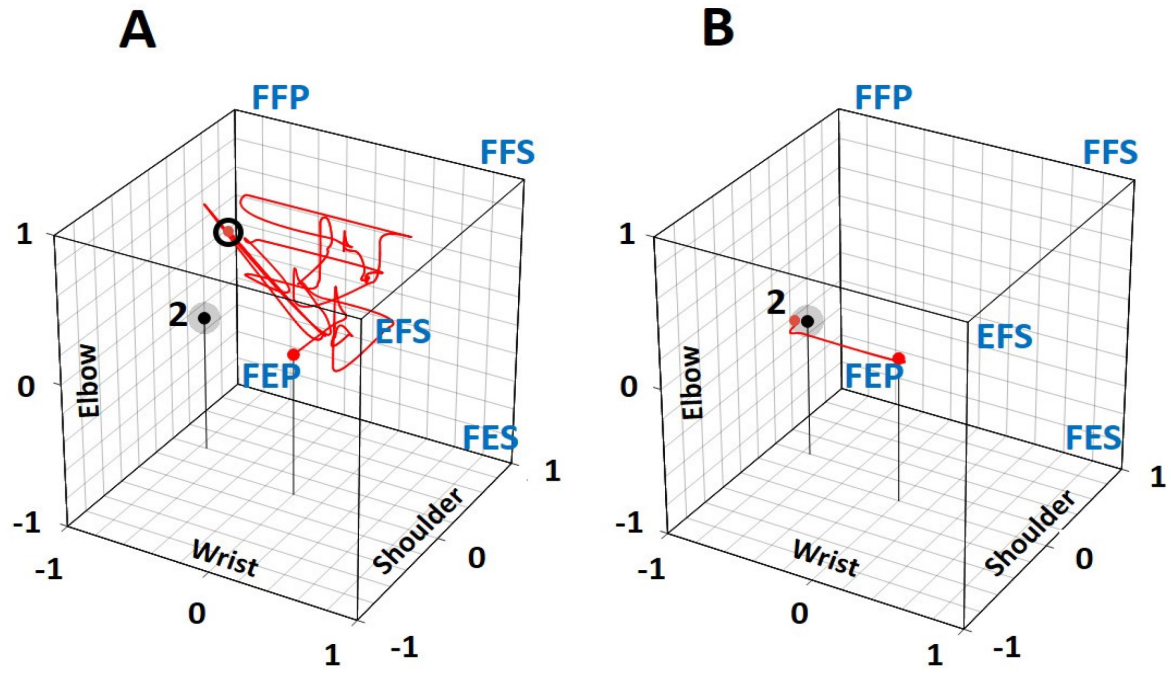

Fig. 5.6 Trajectories taken by S3 to move the red sphere toward target 2 in the 5 SP condition. **(A)** An unsuccessful 1st trial in spite of 72 posture changes where the final red sphere position after 120 s was at a distance of 0.68 (small black circle) from the target. **(B)** In the 3rd trial, the target was reached within 9 s with only 4 posture changes.

[4] Length is referenced to the 0 to1 distance on the elbow axis (Figure 2A).

The mean time to successfully reach the targets is shown in Figure 7A. Target 1 was the easiest to reach with a mean time of 38 s and 20 s for the 5 SP and 8 SP condition, respectively, and target 3 was the most difficult to reach with 59 s and 55 s. These mean values are the results of significant variations among the subjects and no significant difference was found between those results. Reaching target 1 was achieved with a smaller number of posture changes (panel B) than for the other targets. With 8 SPs, a significant difference was found between targets 1 and 2 and between 1 and 5. For trajectory length (panel C), a significant difference was obtained with 8 SPs between targets 1 and 3 and with 5 SPs between targets 2 and 3.

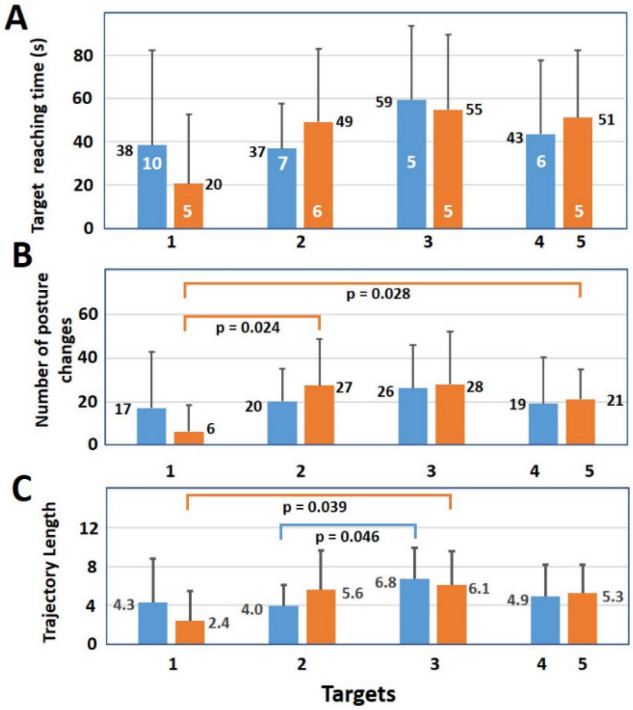

Fig. 5.7 Successful trials, mean results (+sd) of the 12 subjects with 5 (blue bars) and with 8 static postures (orange bars). **(A)** Mean time needed to reach each target. Number of subjects who reached a target at least once is shown in white. **(B)** Mean number of posture changes needed to reach each target. For 8 static postures, there is a significant difference in the number of posture changes between targets 1 and 2 as well as between target 1 and 5. **(C)** Mean trajectory length needed to reach each target. Differences between targets 1 and 3 are significant for 8 static postures as well as targets 2 and 3 for 5 postures. Significance of independent samples t-test level is $p \leq 0.05$.

Results for failed trials are shown in Figure 8. In panel A, it is seen that mean distances separating the red sphere from target 2 at the end of 120 s are smaller than those for the other targets. For the 5 SP condition the differences are significant between targets 1 2, 3 and 4 while for the 8 SP condition the difference is only significant between targets 2 and 3. While mean distance varied between 0.8 and 1.3, the smallest distance (0.1) was found with 5 SPs for target 2 and with 8 SPs for target 1 and the largest was 0.8 (white number) for the 8 SPs condition at target 3. As for the number of mean posture changes (panel B), they were always smaller with 5 SPs than with 8 SPs and the only significant difference was for 5 and 8 SPs at target 3. The mean trajectory lengths of the red sphere (panel C) were all equally elevated for 5 and 8 SPs.

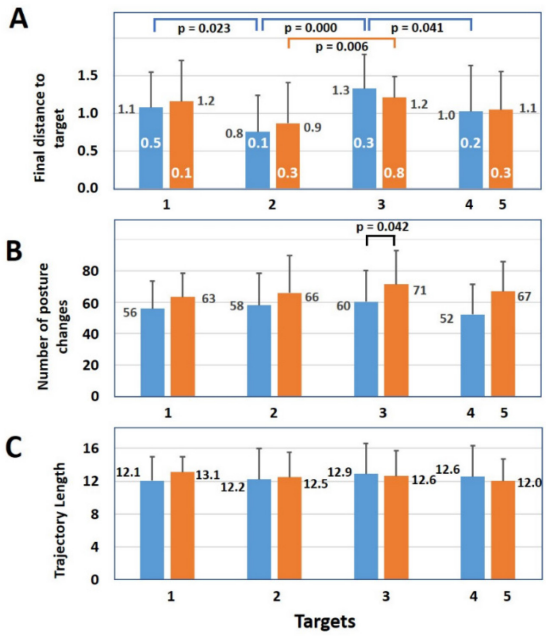

Fig. 5.8 Results of failed trials. **(A)** Mean distance (+sd) between the red sphere and a target at 120 s for 5 (blue bars) and for 8 static postures (orange bars). White numbers represent the minimum distance between the red sphere and a target at 120 s. For the 5 SP condition, differences between targets 1 and 2, targets 2 and 3 and targets 3 and 4 are significant. For the 8 SP condition, the difference between targets 2 and 3 is significant. **(B)** Mean number of posture changes at the end of each trial. For target 3 the difference between 5 and 8 SP conditions is significant. **(C)** For each target, the mean trajectory length of the red sphere during 120 s (independent samples t-test significance is $p \leq 0.05$).

The results of the NASA task load form are presented in Table 3. As a group, subjects considered that physical and mental demands to identify which static posture to choose to move the red sphere were high (15.3/20 and 14.0/20). As for the temporal demand, the limit of 120 s appeared adequate and the time spend in the lab not too long (10.4/20). In general, subjects were not very satisfied with their performance (7.2±3.7) and somewhat frustrated (12.8±4.9) from not having reached the targets more often. At the individual level, the best performer (S3) ranked both the physical and mental demands at a high 17/20 and frustration at the highest score of 20/20, for not being able to reproduce the postures correctly in order to reach more targets. While S2 got over 80% for the training classifier accuracy results (Table 2A), this subject could only reach one target (Table 2B). This subject considered the performance quite low (4/20) and

Table 5.3 NASA task load index (TLX) rates 6 factors (left column of the table) that are used to assess the subjective workload associated with the experiment. The three top factors are related to constraints associated with the tasks to be realized (demand) and the 3 bottom factors are related to the feelings associated with those tasks (own). Each factor is scaled from 0 to 20: higher values represents higher demand or higher performance. Mean values of the 12 subjects are shown in the second column of the table. Individual results are shown for the best performer and for the 2 lowest performing subjects.

TLX	Mean± SD (n=12)	Best performer (S3)	lowest performer 1 (S2)	lowest performer 2 (S12)
physical demand	15.3±2.8	17	14	13
mental demand	14.0±3.6	17	15	9
temporal demand	10.4±6.0	11	14	13
own performance	7.2±3.7	15	4	5
own frustration	12.8±4.9	20	16	8
own effort	12.4±3.4	15	13	11

was very frustrated (16/20). While the other low performer (S12) missed most of the targets, this subject considered, unexpectedly, that the experiment was not very mentally demanding and was not frustrating.

5.4. Discussion

Modern upper limb myoelectric prostheses are now able to produce many different movements. However, following an amputation, the number of available muscles to control them is reduced and strategies to alleviate that shortage have to be developed. When the biceps brachii is still functional, one strategy could be the extraction of more than one control signal from that muscle. To investigate that possibility with non-amputee subjects, 5 pairs of surface electrodes were put across this multifunctional muscle. With 2 postures for each shoulder, elbow and wrist joints 8 different static postures in the sagittal plane were used to control the displacement of a cursor toward different targets placed within a virtual cube. Results were obtained in 2 experimental conditions: one with 5 out of the 8 static postures and one with all 8 static postures.

To associate a red sphere direction to each of the 8 static postures, a training phase was used. After having done that with each subject, we verified the ability of a classifier to correctly recognize each of the 8 SPs. As shown in Table 2A, an important difference is observed between results of S5 at the top of the table and S12 at its bottom. Ability to remember how to reproduce with high fidelity 5 or 8 different static arm postures was thus quite variable among our subjects. With, a group mean value with 5 SPs being significantly larger than with 8 SPs ($p= 0.001$), this confirms that remembering how to duplicate 5 postures is significantly easier than duplicating 8 SPs.

Since the classifier accuracy of the above results were obtained online, no data was available for an offline cross-validation. However, the classifier training was with unsupervised synergies and their features formed nonoverlapping clusters. Thus, the discrimination capacity of the learned linear classifier is not an important concern since the receiver operating characteristic curve (ROC) of those features always occupies the upper half triangle. However, it is still possible that when a subject chooses a static posture, a misclassification occurs, causing the cursor to move in an unexpected direction, which is confusing for the subject. To prevent such situations, the use of a sparse representation of the classified postures as proposed by Betthauser et al. (2018) has to be added to our programs.

From the starting position of the red sphere (Figure 2B), targets 1 and 5 (which are located near a corner of the cube) could easily be reached by taking the FFS or EFS posture respectively because the initial posture that starts the movement of the red sphere actives movement in all three joint axes towards the corner corresponding to that posture. Those easy reaching strategies were used by only few subjects. Targets located at a distance from a corner were more difficult to reach since different postures had to be sequentially taken to reach them.

Among the 8 SPs, different subsets of 5 postures could have been chosen. The present choice was based on the main contribution of the biceps to the elbow flexion and forearm supination. As for the low mean target reaching ratios (< 0.30, Table 2B) and especially for subjects S2 and S12 who reached only one target over 12 trials with 5 SPs and 0 targets with 8 SPs, classification accuracy could be improved by replacing the present classifier by a support vector machine or an artificial neural network classifier. Also, the short training period the day before the experiment could be replaced by more training sessions as illustrated by one person

of the lab who, having repeated the protocol 4 times, reached a 90% success rate with 5 SPs and 58% with 8 SPs (unpublished results).

Classification results could also be improved by the addition of anatomical information on the biceps when the upper limb is in different postures. With an ultrasound probe placed at the biceps level where recording electrodes had been previously placed, changes in its shape and displacements relative to the skin surface were observed (unpublished results). In the future, with ultrasound images obtained before an experiment, position of the electrodes over the biceps could be optimized.

From the results of the NASA task load index, physical and mental demands have the highest scores indicating that our present approach to reach targets is not very intuitive. The difficulty of controlling their prostheses frequently leads amputees to leave them in a closet. Thus, it is suggested to replace the step by step cursor control of a red sphere in a virtual cube by a more realistic situation where the biceps' synergy would control a small humanoid robot for reaching objects within an arm's length. This would be a more realistic situation to the one shown in a video where the experimented person of the lab controlled a small humanoid robot arm with muscular synergies of the biceps (http://www.igb.umontreal.ca/).

5.5. Conclusion

We present a proof of concept that the muscular synergy extracted from a single muscle, the biceps brachii, could facilitate the control of an upper limb prosthesis. This was demonstrated by collecting 5 surface EMG signals of the biceps of 12 normal subjects who put their arm in 8 different static postures. Using a non-negative matrix factorization program, 3 muscular synergies were extracted and following a training session, a classifier could identify

each of those 8 postures. Then, within a virtual cube displayed on a screen, subjects could, with 5 and 8 different static postures, move a red sphere toward the targets. The number of targets reached was higher with 5 choices of posture than with 8 choices. The reasons for a low mean number of reached targets (around 30%) were a lack of training of our subjects before the experiment and a classifier that was not lenient enough. While the biceps may not be available for above elbow amputees, a muscular synergy may then be extracted from muscles near the shoulder such as the deltoid, the pectoralis major and the latissimus dorsi, which are also multifunctional.

5.6. Conflict of interest

The authors declare that the research was conducted in the absence of any commercial or financial relationships that could be construed as a potential conflict of interest.

5.7. Author contributions

LH developed the interactive control system for target reaching, conducted the data acquisition, compiled the results, and wrote the initial draft of the article. PAM designed the evaluation protocol, supervised the study, revised the article and obtained the funding. Each author approved the final version of the manuscript.

5.8. Funding

This research was supported by NSERC grants (156144-2010, RGPIN/06662-2018).

5.9. Acknowledgements

The authors thank Islam Krazdi for his participation in a pilot study, the preparation of a demonstration video for the subjects and his help during experiments with some of them. We also thank the 12 subjects involved in the protocol, Félix Veillette for statistical information, MB for precious feedback, and Paul Cisek for his revision of the manuscript.

5.10. References

Adewuyi, A.A., Hargrove, L.J., and Kuiken, T.A., Evaluating EMG feature and classifier selection for application to partial-hand prosthesis control. Front. Neurorobot., vol. 10, no. 15, pp. 1-11, 2016.

Ameri, A., Kamavuako, E.N., Scheme, E.J., Englehart, K.B., Parker, P.A., Real-time, simultaneous myoelectric control using visual target-based training paradigm. Biomed. Signal Process. Control, vol.13, pp. 8-14, 2014.

Antuvan, C.W., Bisio, F., Marini, F., Yen, S.-C., Cambria, E. and Masia, L., Role of muscle synergies in real-time classification of upper limb motions using extreme learning machines. J. Neuroeng. Rehabil., vol. 13, no. 76, pp. 1-15, 2016.

Betthauser, J.L., Hunt, C.L., Osborn, L.E., Masters, M.R., Lévay, G. Kaliki, R.R. and Thakor, N.V., Limb position tolerant pattern recognition for myoelectric prosthesis control with adaptive sparse repreentations from extreme learning. IEEE Trans. Biomed. Eng., vol. 65, no. 4, pp. 770–778, 2018.

Bizzi, E. and Cheung, V.C., The neural origin of muscle synergies. Front. Comput. Neurosci., vol. 7, no. 51, pp. 1-6, 2013.

Brown, J.M.M., Wickham, J.B., McAndrew, D.J., Huang, X.-F., Muscles within muscles: Coordination of 19 muscle segments within three shoulder muscles during isometric motor tasks. J. Electromyogr. Kines., vol. 17, no. 1, pp. 57-73, 2007.

Daley, H., Englehart, K., Hargrove, L. and Kuruganti, U., High density electromyography data of normally limbed and transradial amputee subjects for multifunction prosthetic control. J. Electromyogr. Kines., vol. 22, no. 3, pp. 478-484, 2012.

Delis, L., Berret, B., Pozzo, T., and Panzeri, S., Quantitative evaluation of muscle synergy models: a single-trial task decoding approach. Front. Comput. Neurosci. vol. 7, no. 8, pp. 1–21, 2013.

Fürnkranz, J., Pairwise classification as an ensemble technique. European conference on Machine learning, Helsinki, Finland, pp. 97-110, 2002.

Gawthrop, P., Loram, I., Lakie, M., and Gollee, H., Intermittent control: a computational theory of human control. Biol. Cybern., vol.104, pp. 31–51, 2011.

He, L. and Mathieu, P.A., Static hand posture classification based on the biceps brachii muscle synergy features. J. Electromyogr. Kines., vol. 43, pp. 201-208, 2018.

Jarrett, C.D., Weir, D.M., Stuffmann, E.S., Jain, S. Miller, M.C. and Schmidt, C.C., Anatomic and biomechanical analysis of the short and long head component of the distal biceps tendon. J. Shoulder Elb. Surg., vol. 21, pp. 942-948, 2012.

Jiang, N., Englehart, K. B. and Parker, P. A., Extracting simultaneous and proportional neural control information for multiple-DOF prostheses from the surface electromyographic signal. IEEE Trans. Biomed. Eng., vol. 56, no. 4, pp. 1070-1080, 2009.

Landin, D., Myers, J., Thompson, M., Castle, R. and Porter, J., The role of the biceps brachii in shoulder elevation. J. Electromyogr. Kines., vol. 18, no. 2, pp. 270-275, 2008.

Lee, D.D. and Seung, H.S., Algorithms for non-negative matrix factorization. In Leen, T.K., Dietterich, T.G. and Tresp, V. (Eds.), Advances in Neural Information Processing Systems 13, Cambridge, MA: MIT Press, pp. 556-562, 2001.

Lenzi, T., Lipsey, J., and Sensinger, J. W., The RIC arm - a small, anthropomorphic transhumeral prosthesis. IEEE ASME Trans. Mechatron., vol. 21, no. 6, pp. 2660–2671, 2016.

Ma, J., Thakor, N. V., and Matsuno, F., Hand and wrist movement control of myoelectric prosthesis based on synergy. IEEE Trans Hum. Mach. Syst., vol. 45, no. 1, pp. 74-83, 2015.

Mobius Bionics, Luke Arm System. from www.mobiusbionics.com/wp-content/uploads/2017/08/Mobius-Bionics-LUKE-Product-Spec-Sheet.pdf. 2017. Consulted on March 4, 2019.

Muceli, S., Boye, A. T., d'Avella, A., and Farina, D., Identifying representative synergy matrices for describing muscular activation patterns during multidirectional reaching in the horizontal plane. J. Neurophysiol., vol. 103, no. 3, pp. 1532–1542, 2010.

Naik, G.R. and Nguyen, H.T., Nonnegative matrix factorization for the identification of EMG finger movements: evaluation using matrix analysis. IEEE J. Biomed. Health inform, vol. 19, no. 2, pp. 478-485, 2015.

Park, S.H. and Fürnkranz, J., Efficnet pairwise classification. European conference on machine learning, Warsaw, Poland, pp. 658-665, 2007.

Rasool, G., Iqbal, K. Bouaynaya, N. and White, G., Real-time task discrimination for myoelectric control employing task-specific muscle synergies. IEEE. T. Neur. Sys. Reh. Eng., vol. 24, no. 1, pp. 98-108, 2016.

Rousseeuw, P.J., Silhouettes: a graphical aid to the interpretation and validation of cluster analysis. J. Comput. Appl. Math., vol. 20, pp. 53–65, 1987.

Segal, R.L., Neuromuscular compartments in the human biceps brachii muscle. Neurosci. Lett., vol. 140, no. 1, pp. 98-102, 1992.

ter Haar Romeny B.M., van der Gon J.J.D., Gielen C.C.A.M., Relation between location of a motor unit in the human biceps brachii and its critical firing levels for different tasks. Exp. Neurol., vol. 85, no. 3., pp. 631-650, 1984.

Torres-Oviedo, Gelsy and Lena H. Ting., Muscle synergies characterizing human postural responses. J. Neurophysiol., vol. 98, no. 4, pp. 2144-2156, 2007.

Tresch, M.C., Cheung, V. and d'Avella, A., Matrix factorization algorithms for the identification of muscle synergies: evaluation on simulated and experimental data sets. J. Neurophysiol., vol. 95, no. 4, pp. 2199-2212, 2006.

5.Appendix 1

Synergy extraction from pairwise postures

For muscle synergy extraction, EMG signals from concatenated pairwise postures are used. The process of muscle synergy extraction involves a dimensionality reduction where three muscle synergies are extracted from 5 EMGs of the biceps. Given a concatenated EMG dataset, E, two matrices H and W are obtained with the NMF algorithm

$$E^{5\times n} = W^{5\times 3} \cdot H^{3\times n} \tag{A1.1}$$

where $W^{5\times 3}$ is the muscle synergy matrix, and $H^{3\times n}$ is the matrix of muscle synergy coefficients. Given pairwise postures, the synergy coefficient from the first posture is defined as H_1 and the second is H_2. Their mean values i.e. $\bar{H}_1$ and $\bar{H}_2$ are used to train the minimum distance classifier. The muscle synergy matrix W is used for estimation of the synergy coefficient from the EMG signals acquired during evaluation as follows:

$$\hat{H}_i^{3\times 1} = W^{5\times 3^{-1}} E_i^{5\times 1} \tag{A1.2}$$

where i is the sample number in sequentially acquired EMG signals. The distance measured from the estimated synergy coefficient is given as follows

$$D_1^i = \left|\hat{H}_i - \bar{H}_1\right| \tag{A1.3}$$

$$D_2^i = \left|\hat{H}_i - \bar{H}_2\right| \tag{A1.4}$$

where the Euclidean distance is used as the metric measure. The minimum distance classifier determines the classification result as follows

$$if\ D_1^i < D_2^i, then\ the\ posture\ associated\ with\ \hat{H}_i\ is\ of\ 1^{st}\ class, otherwise\ 2^{nd} class$$

The classification presented here is called the pairwise posture classifier and it uses the muscle synergy coefficient obtained from the paired postures for classifier training and estimation of the muscle synergy from EMG using the pseudo inverse of the synergy matrix, $W^{5\times3}$.

Silhouette index (Rousseeuw, 1987)

To improve the discrimination power of the metric based classifier, the Silhouette clustering validation index, S, is used to evaluate the muscle synergy clustering from the pairwise postures. The Silhouette index is given as follows:

$$S_i = \frac{b_i - a_i}{\max(a_i, b_i)} \tag{A1.5}$$

where a_i is the average distance of synergy coefficient i in one cluster to all other synergy coefficient values in the same cluster, and b_i is the minimum average distance from synergy coefficient i in one cluster to all synergy coefficients in the other cluster. The value of S_i varies from -1 to 1. A large S_i value means the discrimination power is high. The average value of S_i is used to determine the discrimination power of muscle synergy coefficients obtained from pairwise postures:

$$S = \frac{1}{n}\sum_{i=1}^{n} S_i \tag{A1.6}$$

5.Appendix 2

Multiple synergy extraction

In Algorithm 1 (below), T is the predefined number of reinitiated NMF extractions, S is the Silhouette index value (initialized at -1), E is the concatenated EMG signal from paired

postures, L is the cluster label, and W and H are the synergy matrix and synergy coefficients from the NMF algorithm.

Algorithm 1 Clustering Validation Index for Paired Postures (Pos_1, Pos_2)

1: **procedure** CLUSER VALIDATION (T, S, E, L, W, H)
2: $T = 30$
3: $S = -1$
4: $\{E, L\} = \{Pos_1, Pos_2\}$
5: $\{W, H\} = \{\boldsymbol{I}, \boldsymbol{0}\}$
6: **for** each i in T **do**
7: $\{\text{new}W, \text{new}H\} = \text{NMF}(E)$
8: $\text{new}S = \text{Silhouette Index}(\text{new}H, L)$
9: **if** $\text{new}S > S$ **then**
10: $S = \text{new}S$
11: $\{W, H\} = \{\text{new}W, \text{new}H\}$
12: **end if**
13: **end for**
14: **Return** S, W, H, L
15: **end procedure**

5.Appendix 3

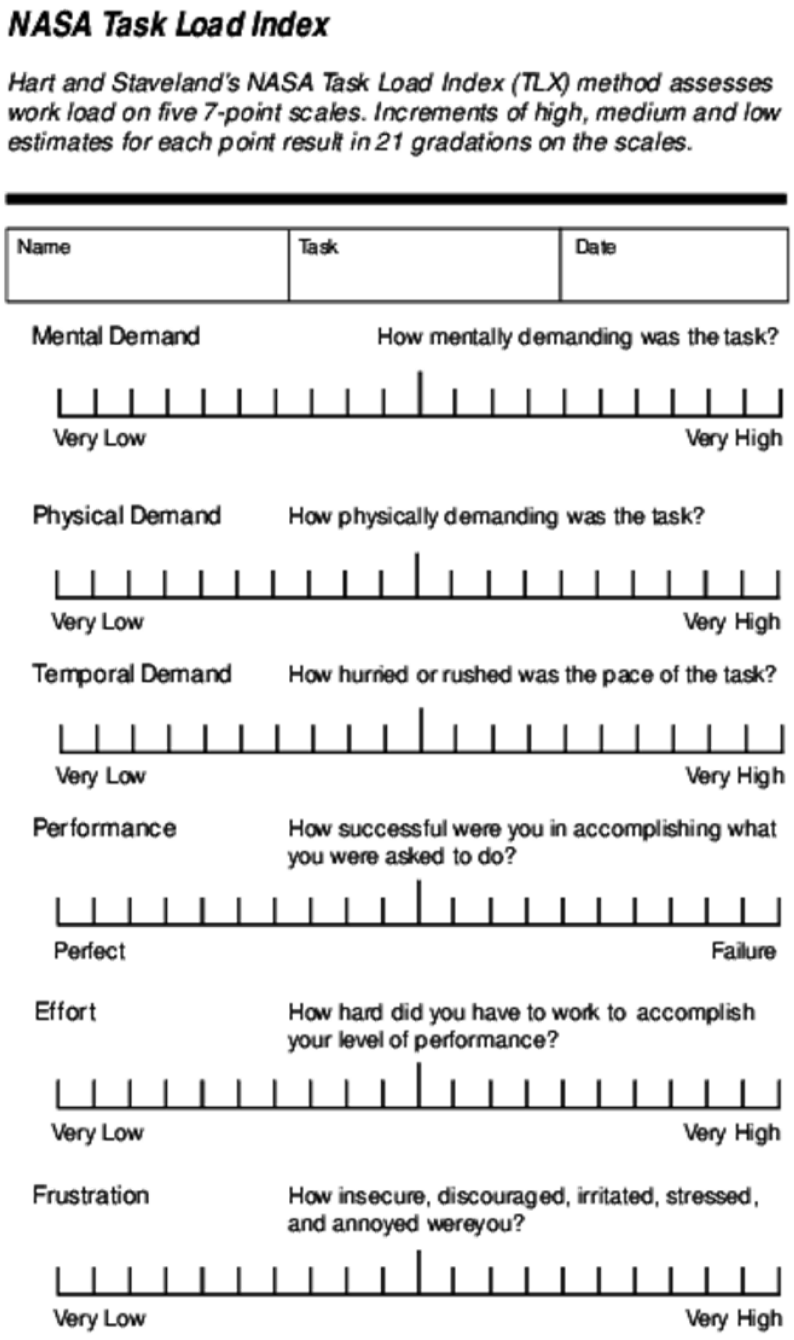

NASA Task Load Index

Hart and Staveland's NASA Task Load Index (TLX) method assesses work load on five 7-point scales. Increments of high, medium and low estimates for each point result in 21 gradations on the scales.

Name	Task	Date

Mental Demand — How mentally demanding was the task?

Very Low — Very High

Physical Demand — How physically demanding was the task?

Very Low — Very High

Temporal Demand — How hurried or rushed was the pace of the task?

Very Low — Very High

Performance — How successful were you in accomplishing what you were asked to do?

Perfect — Failure

Effort — How hard did you have to work to accomplish your level of performance?

Very Low — Very High

Frustration — How insecure, discouraged, irritated, stressed, and annoyed wereyou?

Very Low — Very High

6. Complementary Results

6.1. Effect of practice

With each of the 12 subjects, the static posture classification and target reaching experiment results were obtained from a single experimental session. Here, the results of an experienced subject, who had many practices with the program, are presented. All results were obtained with the subject's left arm and with the same protocol as the 12 subjects used. Each experimental session was separated from others by an interval varies from 1 day to 4 weeks. In Table 6.1, the results of successful trials obtained with 4, 5, and 8 static postures as control input are presented. The 4 postures (FFS, FFP, FES, and EFS) were included in the results because the subject had sufficient time to obtain those results in many laboratory sessions, but this was not the case for the 12 subjects who had only a few hours to complete their experiments.

Among those experiments, two types of electrode (Kendall H59P and Kendall H69P, Covidien, Dublin, Ireland) were used. The H59p electrodes were readily available in the laboratory, but they were replaced with H69p electrodes because of lack of sensitivity in the former due to long-term storage. In Table 6.1, the results demonstrate that as the number of postures used to control the red sphere movement in target reaching experiment increased, the H59p electrode reduced the subject's performance due to its low sensitivity. The low sensitivity of the electrodes reduced the discrimination power of the posture classifier. However, the performance was not affected when 4 postures were used as control input to reach targets.

As shown in Table 6.1, with 4 static postures from three experiments perfect results were obtained, and with 5 postures, targets 2 and 4 were more difficult to reach than targets 1 and 3. With 8 static postures the number of failed trials was higher with H59p electrodes. With those

Table 6.1 Number of successful trials (an experienced subject) with the experimental protocol. In each experiment (exp), 4, 5, and 8 static postures were used to reach the same targets as the 12 subjects tried to reach. Target numbers are T1…T5, and two types of electrodes (Electro) were tested (Kendall H59p and Kendall H69p). Only one type of electrode was used in a session. To be consistent with the results from 12 experimental subjects, no result is presented in the T5 column with 5 static postures or in the T4 column when 8 postures were used. With 4 static postures, all the targets were tested. The percentage of success (%) is shown in the lower right corner of each panel.

4 Static Postures

Electro	exp	T1	T2	T3	T4	T5	sum
H59P	1	3	3	3	3	3	15
H69P	2	3	3	3	3	3	15
H69P	3	3	3	3	3	3	15
	sum	9	9	9	9	9	45
	total	9	9	9	9	9	45
	%	100	100	100	100	100	100

5 Static Postures

Electro	exp	T1	T2	T3	T4	T5	sum
H59P	1	3	1	2	2		8
H59P	2	3	3	3	3		12
H69P	3	3	3	3	3		12
H69P	4	3	3	3	2		11
	sum	12	10	11	10		43
	total	12	12	12	12		48
	%	100	83	92	83		90

8 Static Postures

Electro	exp	T1	T2	T3	T4	T5	sum
H59P	1	0	2	0		2	4
H59P	2	0	3	1		1	5
H69P	3	3	1	3		3	10
H69P	4	3	1	2		3	9
	sum	6	7	6		9	28
	total	12	12	12		12	48
	%	50	58	50		75	58

electrodes, there were only 9 successful trials from two experiments out of a total of 24 trials. With H69p electrodes, there were 19 successful trials from two experiments. Targets 1 and 3 were more difficult to reach with H59p electrodes while target 2 was difficult to reach with H69p electrodes. Overall, the lower is the number of static postures used to reach targets, the higher the success rate becomes. Among the 25 unsuccessful trials, 19 were obtained when H59p electrodes (less sensitive ones) were used.

For successful trials, target reaching time, number of posture changes before reaching a target, and trajectory length are shown in Fig. 6.1 when 4, 5, and 8 postures were used as control input. The results include experiments when both types of electrode (i.e. H59P and H69P) were used.

As shown in Fig. 6.1A, the mean time required to reach a target is less when 4 postures were used as control input to reach targets 1, 2, 3, and 5.

The number of posture changes (mean + SD) before reaching a target is shown in Fig. 6.1B. For 4 postures as control input, the number of posture changes before reaching a target is smaller on average in targets 1, 4, and 5.

The trajectory length to reach each target (mean +SD) is shown in Fig 6.1C. For 4 postures as control input to reach targets, the average trajectory length is shorter when targets 1, 2, 3, and 5 were evaluated.

To summarize, 4 postures as control input require less reaching time, smaller number of posture changes, and shorter trajectory length on average for most of the targets in comparison with 5 or 8 postures as control input.

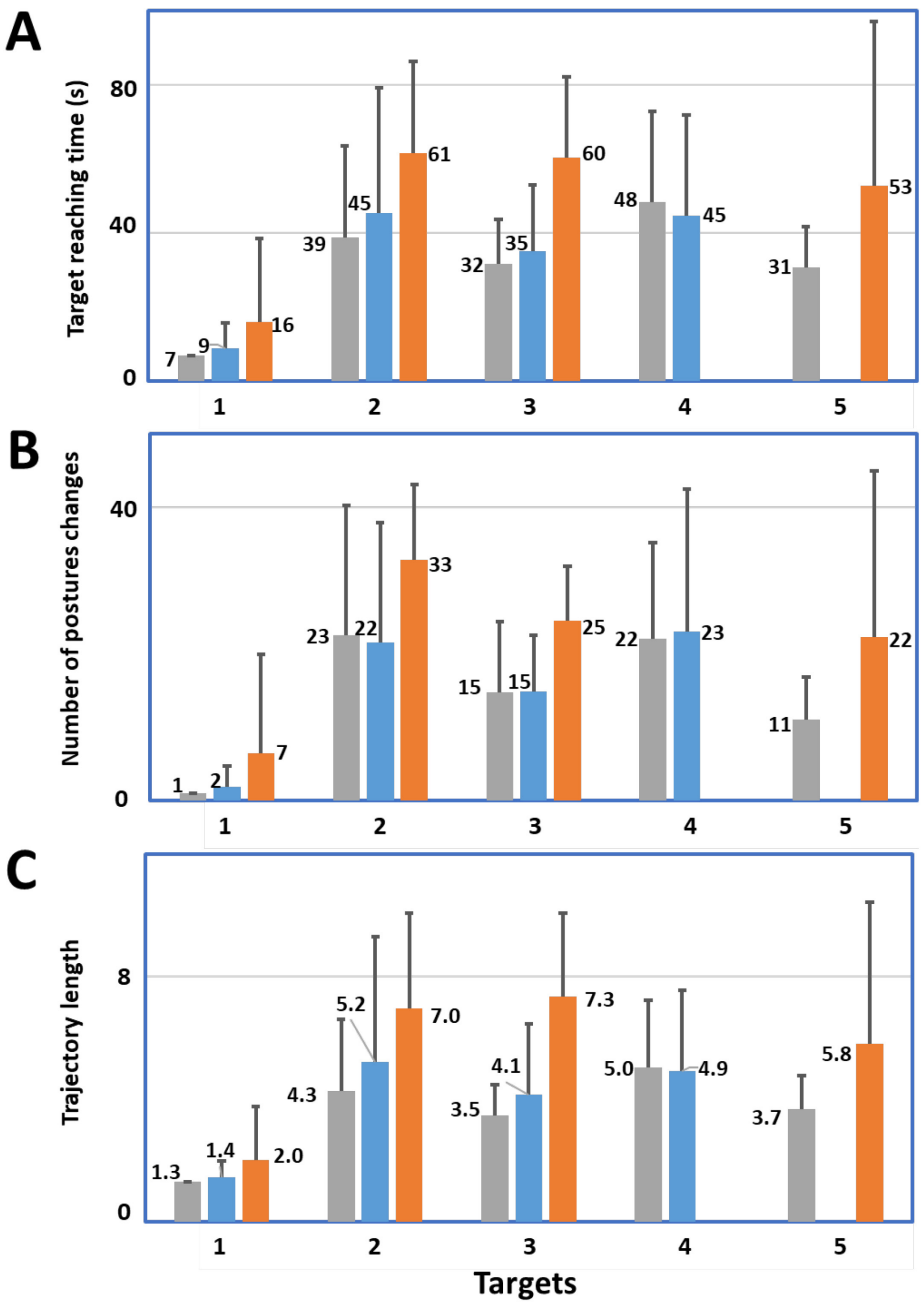

Fig. 6.1 Target reaching performance in the successful trials of one subject. The number of static postures, used as control input, are indicated with different colors (Gray: 4 Postures, Blue: 5 Postures, and Orange: 8 Postures). For target 4, the 8 postures condition was not presented, and for target 5, only 4 and 8 postures were presented. Results were obtained with both H59p and H69p electrodes. **A**: For mean target reaching time, it was the least with 4 postures for targets 1, 2, 3, and 5. **B**: For mean number of posture changes, it was the smallest with 4 postures for targets 1, 4, and 5. **C**: For mean trajectory length, it was also the shortest with 4 postures as control input, for targets 1, 2, 3, and 5.

6.2. Control of arm movement

To test the control algorithm for controlling an upper limb manipulator arm, 3D printing technology was used to construct a small humanoid manipulator as shown in Fig. 6.2. The manipulator was constructed by using the concept of reconfiguration from ROBOTIS Educational Kits (Kim, 2016). The humanoid manipulator was assembled from 3D printed components as shown in Fig. 6.2. Rivets (RS-10) and smart motors (DYNAMIXEL XL-320) were from ROBOTIS (Seoul, Republic of Korea). The number of DoFs of the humanoid arm manipulator is 6. There are three DoFs at the shoulder joint, one DoF at the elbow joint, and two DoFs at the wrist joint.

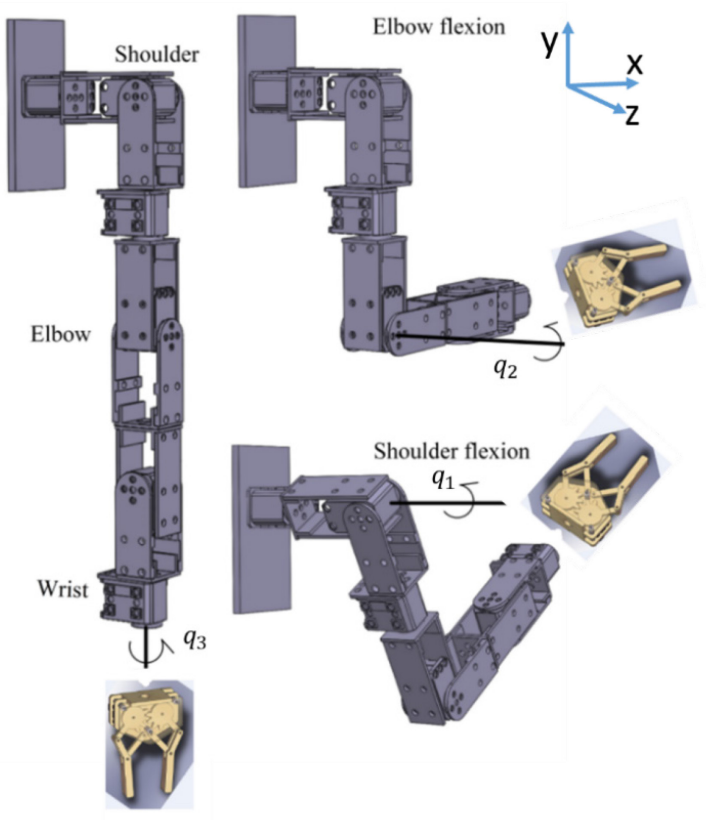

Fig. 6.2 3D printed humanoid manipulator arm (rivets and motors were from ROBOTIS): the assembled humanoid manipulator has three active joints, i.e. shoulder flexion and extension (q_1), elbow flexion and extension (q_2), and wrist supination and pronation (q_3).

The humanoid manipulator in 3 static postures is shown in Fig. 6.3. To activate the small manipulator, the 8 predefined static postures, as illustrated in Fig. 3.3A, were used, and a video was made when a subject took each of those 8 static postures (http://www.igb.umontreal.ca/). Out of the video, 3 frames are presented in Fig. 6.3 with a small icon illustrating each posture that the subject took.

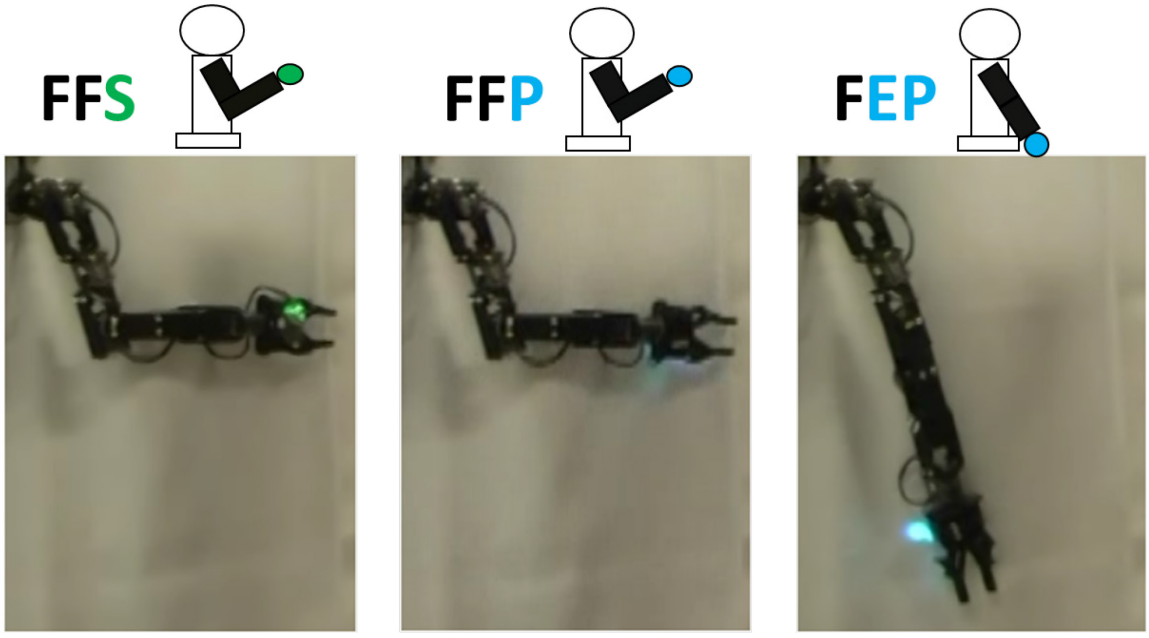

Fig. 6.3 Three postures taken by the small humanoid manipulator controlled by the 3 postures taken by a subject, shown as small icons. A colored LED is used to indicate the wrist position of the manipulator.

The small power of the motors used to activate the small manipulator was not enough to produce dynamic movements; therefore, a virtual environment was considered for upper limb dynamic movement simulation from a virtual avatar (Fig. 6.4). The movement of the three DoFs (q_1, q_2, q_3) of the upper limb was simulated with Runge-Kutta 4th order (RK4) method to obtained numerical solution, and the dynamic model parameters of the system were obtained from average anatomical values of human upper limb.

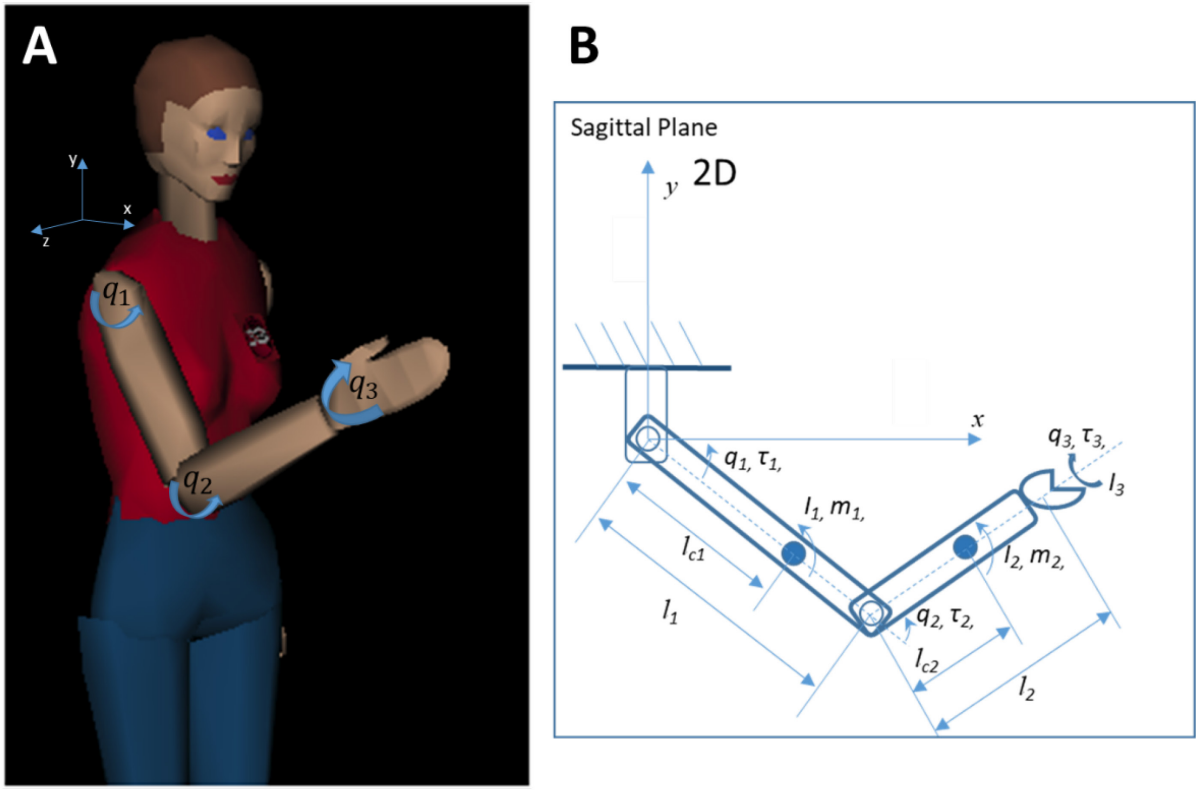

Fig. 6.4 Three joints upper limb model. **A**: 3D virtual avatar in MATLAB virtual world. **B**: All the movements of the upper limb of the avatar are constrained in sagittal plane: Shoulder flexion and extension (q_1), elbow flexion and extension (q_2), and wrist supination and pronation (q_3).

The 3D virtual avatar was developed by 3Name3D in the MATLAB virtual world (Fig. 6.4 A). It can perform three joint movements at shoulder (q_1), elbow (q_2), and wrist joint (q_3). For the extension and flexion at the shoulder joint, the movement range is limited to 45° at flexion and to -45° at extension. For the extension and flexion at the elbow joint, the movement range is between -45° at extension and 45° at flexion. For the pronation and supination at the elbow joint, the movement range is limited to -90° at the pronation and to 90° at supination.

The avatar arm movement is controlled by a nonlinear control law with feedback linearization (Slotine and Li, 1991) through the direct commands to the handle or joint node of the virtual world object, i.e. shoulder, elbow, and wrist joint. Upon receiving a command, the avatar changes its joint position, and it can be interfaced with other MATLAB programs that produce movement commands. For example, the MATLAB program that produces the red sphere trajectory can be interfaced with the avatar program to achieve online control of the avatar arm to produce dynamic movements that follow the specified red sphere trajectory in the virtual cube (by using parameter mapping provided in Fig. 3.7). A subject can use the virtual avatar as a mirror image on the computer screen to practice myoelectric control with control signal from biceps. For a right handed subject, the avatar's right arm posture is the target posture, and the subject needs to control the left arm of the avatar to produce a mirror image of avatar's right arm with reference to sagittal plane.

7. Discussion

In this research, two studies were pursued to determine whether muscle synergy exists in the single multifunction muscle, i.e. biceps brachii and whether the extracted muscle synergy can be used to provide control signals for movement production. In the first study, synergy was extracted from paired static forearm postures in two different body postures of 10 normal subjects. The significant finding from this study was that the synergies were present between paired static postures, and classifier trained with synergy features was able to produce a classification accuracy of greater than 80%. The result suggests that the synergy features extracted from biceps muscle are very robust and could be used to classify paired postures. In the second study, the muscle synergy features extracted from biceps muscle were used to classify 8 static upper limb postures from 12 normal subjects. The result shows that in a training session classification of 5 of the 8 postures was significantly more accurate than classification of all the 8 postures. The posture classification was subsequently used as control signals to control displacement of a red sphere in a virtual cube to reach targets. The results show that all the subjects were able to produce movement of the red sphere with the control algorithm presented in this research; however, to move the red sphere to a target in the cube was difficult (success rates: 29% for 5 SPs and 24% for 8 SPs) due to a steep learning curve of the interactive system. The effectiveness of practice was demonstrated with the results from one subject who had many practices with the system. The subject's results from 5 postures were better than those from 8 postures. With very short time of practice (i.e. one hour of familiarization of protocol on the day before the experiment), the results from 12 subjects also indicated that success trials were more numerous with 5 static postures than those with 8. In this research, the small robot manipulator was useful to demonstrate the effectiveness of static posture classifier.

7.1. Improvement to the existing method

In Chapter 4, the paired posture classifications provide evidence that muscle synergies can be obtained from the single multifunctional biceps brachii muscle. In Chapter 5, the posture classification accuracy needs to be improved in order to increase target reaching performance. One approach is to change the training strategy. As suggested by Cunningham and Ghahramani (2015), the NMF being nonlinear, the estimated synergy needs to be within the learned feature space. NMF being a non-convex optimization, solutions of the algorithm are not unique, and many local minima could coexist. Thus, to maintain the classification accuracy, retraining of the classifier is necessary when a classifier shows reduced performance. Another approach to improve accuracy of the posture classification is to use nonlinear classifiers, such as SVM. This classifier considers the nonlinearity of the data distribution and separates effectively different classes of data with unequal variance that could lead to misclassification of the MDC used in this research. To improve performance, the sparse representation of the classified postures as used by Betthauser et al. (2018) should be considered.

7.2. Comparison with previous research

Extraction of muscle synergy for myoelectric control was used by Jiang et al. (2009) to predict the force produced at hand joints of human subjects. In a subsequent work, Jiang et al. (2014) were able to demonstrate that with the proposed muscle synergy extraction method the 2 DoFs force prediction algorithm was able to effectively produce control in velocity and position mode of a virtual arrow displayed on a computer screen. This is different from our research where features of muscle synergy were considered as the origin of motion primitives associated with static postures. Thus, no matter where the red sphere is located in the virtual

cube, when a new static posture is detected by the posture classifier, the red sphere moves toward that static posture through position regulator associated with the corresponding motion primitive. With an intermittent control, these motion primitives are combined to produce a displacement of the red sphere in the virtual cube. With the movement estimation of two DoFs of the hand, Ma et al. (2015) used a force prediction method to extract muscle synergy features to control a virtual prosthetic hand's movement with good results. They used visual feedback to provide status information of the virtual prosthetic hand, which is similar to what we did to move the red sphere toward a target. They extracted a single synergy from a motion primitive and then combined the individual movement estimation to predict more complex movements. Different from theirs, our synergy extraction is task based, i.e. the synergy was obtained from static postures associated with positions of all the 3 arm joints. As for Nielsen et al. (2009), they included learning from complex movements to obtain simultaneous and proportional control of 3 DoFs. While they combined joint movement data to obtain force estimate, our method was to classify postures from features of muscular synergy for moving a red sphere based on the predefined motion primitive. Muscle activity from multifunctional muscle is not always proportional to the amplitude of recorded EMG signals, and this is a problem for the implementation of a proportional control (Fougner et al., 2012) with muscle synergy. This is why Ma et al. (2015) only tested their algorithm on discrete synergy levels instead of continuous ones.

Rasool et al. (2016) have extracted muscle synergy patterns from forearm muscles with a task based objective. Muscular synergy was assumed as a variable to be estimated with Kalman filtering from the collected sEMG signals. Thus, to predict the hand movement, they compared the similarity between the predicted value of muscle activity and actual value related to a

specific task. Instead of considering a single task, our muscle synergy extraction involved data from two different static postures of the upper limb. The resulting synergy matrix being shared by the two postures in the synergy subspace, they cannot be used to represent the spatial variance in the measurement model of the Kalman filter because transition between the two postures is not a random walk model. So, our synergy subspace covers the data generated from paired static postures, and the synergy coefficients thus extracted were used to classify only the corresponding paired static postures.

7.3. Explanation

Motor control and motor learning are not the same. In motor control, if the system parameters, such as those in the human skeletal and muscle system, are known, different motor control behavior can be predicted with a mathematical model. However, for motor learning, it is the parameters of the system model that need to be estimated in order to optimize task performance. In a simple motor learning task, it is suggested that two factors affect motor learning: one is learning factor and the other is forgetting factor (Haith and Krakauer, 2012). To learn a task is to learn the system parameter that requires collection of experimental data; in the case of human motor learning, it requires practice to assess the system parameter such that a change due to neuroplasticity or a completely new strategy adapted in cognitive level produces changes in performance level.

For the interactive program presented in Chapter 5, motor control and motor learning are both required to achieve good performance. For the motor control part, muscle synergy is considered as a strategy for the CNS to simplify the motor control. In this research, muscle synergies were extracted from a single multifunctional muscle, i.e. biceps brachii, while the

upper limb of the subject produces 8 static postures all have functional contributions by this muscle. A virtual cube with 8 corners associated with 8 static postures was thus developed to allow a subject to achieve dynamic motor control of the movement of a virtual sphere via biceps' muscle synergies. In addition to simple tasks, such as those used to reach the corners of the cube with a corresponding static posture, specific motor control tasks were also evaluated. These specific motor tasks are represented by target positions in the interior of the cube, and sequential combinations of simple motor controls, i.e. static postures, were required to complete those tasks. Motor learning is quite different from motor control because motor learning is the prerequisite for motor control. In other words, to produce motor control, a subject needs to learn first how to produce a desired motor control. Like learning any new tasks, such as riding a bicycle, playing basketball, etc., a learning period is required for a subject to produce skillful tasks. The learning period is used by a subject to adjust the adjustable parameters of their motor system to satisfy an optimization criterion, such as energy consumption for a specific motor task, error of force levels according to a force reference, etc. Not only a learning period is required for a subject to learn how to produce natural limb movement, but also it is required for a subject to learn how to control an interactive program, such as the system presented in this research.

With synergy-based motor control, if the target is associated with a learned static posture, the target should be less difficult to learn. For targets that require multiple postures as sequential commands, a subject need pre-plan the sequential commands; thus, it is more difficult to reach interior targets than those that require only a single static posture command.

The interactive program provides manual commands (i.e. 8 push buttons representing 8 identified postures) that allow a subject to control the movement of the red sphere to reach all

the targets. In the beginning of the experiment, each subject used both 5 and 8 push buttons as manual commands to reach all the required targets, and all the subjects obtained very good target reaching results. This preliminary test reduced the effects to the results due to the control system associated with the interactive program to minimum.

In this research, the primary concern is the motor control. In other words, how to extract control signals from biceps muscle that can move a robotic system to a predefined position in order to facilitate control of myoelectric prosthesis. In the future, the motor learning will be considered as a strategy to improve the control performance.

Without any previous myoelectric control experience, performance on target reaching of our 12 normal subjects was low because the posture classifier was trained with a winner-takes-all training method requiring that contraction of the biceps was similar to the one produced during the classifier's training. This was a difficult requirement to meet in a single session, and learning capability is not the same for everyone. To learn how to improve control skills, Powell and Thakor (2013) and Powell et al. (2014) found that their normal subjects and amputees needed multiple training sessions. In our research, an experimenting subject in the laboratory got success in over 90% of target reaching trials after many practices.

The results in the Chapter 6 were obtained by an experimenting subject after many practicing sessions with the interactive program. Despite many changes in target position and posture combination, consistent results (in terms of success percentage, Table 6.1) were obtained. The experimenting subject could have learned to perform well with the interactive program after many practicing sessions; however, the evaluation was designed entirely by someone else who had not used the interactive program. Thus, the results in Chapter 6 suggest

that the interactive program was not biased toward any evaluation tasks. When insensitive electrodes were used, large variation of the results was observed. We assume that the large variation in the results associated with the change of electrodes was caused by the noise contamination to the signal that reduced the discrimination power of the posture classifier.

Muscle synergy is usually extracted from multiple muscles with electrode attached to the surface of those muscles. In this research, synergies were extracted from a single muscle that has many compartments. Those compartments are not all located close to the skin, and some of those compartments could completely enclosed by other compartments as observed from the ultrasound image. When the electrodes were placed on top of the biceps, the measured sEMG can be contributed by several compartments of the biceps. This is not in contradiction with the conventional method used to extract muscle synergies from multiple muscles where the activity of individual muscle is a result of innervation of multiple synergies. Thus, the location of the compartments does not affect the extraction of muscle synergy; instead, it is the effect of the nerve innervation to all the compartments that produces discriminable patterns on the surface of the muscle that can be learned by the posture classification system.

In Chapter 4, 10 pairs of electrodes were placed across the biceps of all the subjects. To avoid the crosstalk effect from other muscles, only the inner 8 pairs, used for synergy extraction, gave the representation of biceps' activity. In both researches presented in Chapter 4 and 5, three synergies were used to reconstruct the measured muscle activities. Actually, as the number of paired electrodes decreases, the reconstruction accuracy of overall muscle activities, with same number of synergies, gets increased. The rational to use three synergies is associated with the muscle function. Since the biceps muscle of the upper limb is associated with the shoulder joint flexion, elbow flexion, and forearm supination, it is logical to assume that three nerve

innervations are contributed to the muscle when the muscle is active. Those nerve innervations could all be at rest corresponding to no activity of the muscle, or some nerve innervations occur while the muscle is performing a simple (e.g. forearm supination) or a combined (e.g. forearm supination and elbow flexion) motor task of the upper limb.

If the number of pairs of electrodes was to be increased, the VAF values would decrease with same number of synergies. In an initial study (He and Mathieu, 2017), 5 sEMG signals were used to extract muscle synergy from paired postures of all the available static upper limb postures. Results show that 5 sEMG signals were sufficient for synergy extraction and for subsequent use of posture classification.

Crosstalk is caused by the fact that EMG signals recorded from one muscle is interfered by the EMG signals from neighboring muscles propagating through the volume conductor. In this research, crosstalk is unavoidable at compartment level because the compartments of the biceps are packed together. The sEMG is a mixture as a result of multiple signal sources with their origins from those biceps compartments. Other than that, the crosstalk could also come from other muscles; however, having been compared with the participants with low classification results in Chapter 5, several subjects with smaller arm circumference produced above average classification results. This suggested that crosstalk from neighboring muscles may not be the cause of the low classification performance in certain participants.

In Chapter 4, the elbow joint was fixed at flexed position, and only forearm static postures were investigated (i.e. neutral, pronation, and supination). However, in the following research (Chapter 5), larger number of static postures was used. The change of elbow joint from extension to flexion could result in upward movement of the innervation zone of the biceps

muscle (Merletti and Muceli, 2019). If the electrodes were still placed above the middle portion of the biceps, they could pick up signals from the innervation zone, which according to literature should be avoid in the EMG measurement. Thus, the electrodes were placed below the middle length of the biceps to avoid the innervation zone when elbow was flexed.

The limitation of this research is that the extraction of muscle synergies does not assume that there is mechanical constraint that causes variation of the measured sEMG. In several studies about the sEMG of the biceps muscle, position change of the innervation zone was observed when the elbow was flexed in comparison with extended condition (Merletti and Muceli, 2019). This suggested that the partial changes of measured sEMG are caused by the mechanically shortened muscle while the electrodes were at fixed position of the skin surface. In the future, the mathematical model for sEMG production can be mitigated with consideration of mechanical changes of the muscle that cause the variation in the recorded sEMG. Subsequently, variation of muscle synergies can be better explained with the sampled sEMG.

Other limitations of this research can be divided into two parts. One part is associated with the software implementation, and the other is the hardware implementation. Both parts affected the results. For the software part, the MDC was used for posture classification. This could limit the performance of the posture classifier. In the future research, advanced classification algorithms, such as SVM or ANN should be considered to improve the posture classification performance. For the hardware part, customized analog circuits were built to preprocess the raw sEMG signals, which could limit the classification performance due to the circuits prone to noise contamination. In the future, commercially available signal preprocessing unit should be considered to reduce the effect of noise related performance deterioration. In this research, a laptop computer was used to implement the interactive program with limited CPU

and GPU power. Subsequently, delays were introduced to the interactive program. In the future, more powerful desktop computers will be used to provide sufficient computational power in order to reduce the computational delays caused by the hardware.

7.4. Application

In this research, the virtual environment was displayed on a conventional computer screen, and subjects interacted with the programs by using sEMG of their biceps. With fast development, virtual reality (VR) systems could provide fully immersed 3D experience to replace physical environment while augmented reality (AR) systems could be used to enhance the virtual experience. Virtual environment was investigated in 3D to study its effect on robot-assisted therapies in the rehabilitation of upper limb for stroke individuals (Norouzi-Gheidari et al., 2019). Those authors found that there was no significant difference when physical or virtual environment was used by both healthy and stroke individuals to reach targets with their arm. For prosthetic control training, Sharma et al. (2019) have implemented an AR prosthesis program to evaluate the performance of prosthetic control, and these authors found that normal subjects could improve their manipulation skills after training with AR system. Even without expensive goggles, a wide display (above 50 inches) could present an avatar in MATLAB virtual environment. If virtual display goggles (e.g. Oculus, VIVE, LENOVO, HoloLens, etc.) become available, the enhanced virtual experience could be obtained by using the MATLAB interfacing toolbox to stream the 3D signal from MATLAB to virtual display goggles. The VR and AR systems do not require significant investment and physical facilities, and their evaluation and training results are similar to those of the physical evaluation system. In addition, the simulation programs can be easily adapted for different training scenarios.

8. Conclusion

Muscle synergy is usually extracted from many muscles involved in a given motor task. Here, muscle synergy was applied to a single muscle, the biceps brachii, which has 2 heads and appears to be composed of up to 6 individually innervated compartments as viewed from its inner surface. So, the biceps brachii appears to be a muscle composed of many muscles. With a non-negative matrix factorization, three muscle synergies were extracted from 5 sEMG signals collected across this muscle when two different static postures of the upper limb contractions were paired. With features of muscular synergy extracted from this muscle, it was possible to have a good distinction among the 8 tested static postures. These functional muscle synergy features were used to support the second hypothesis of this research, i.e. the biceps muscle synergy features could be used to provide movement control. The results obtained from 12 subjects indicate that within a virtual cube, it is possible, with a succession of different static postures, to control the displacement of a sphere toward different targets.

Perfect target reaching results were obtained with 4 static postures by an experienced subject in 3 experimental sessions separated by days or months even with insensitive electrodes. This suggests that human adaptation and motor learning play a very important factor that limits the performance when many control parameters need to be learned in order to interact with a new control environment. The consistency of improved performance through multiple practice sessions will be investigated in the future research.

With an improved synergy-based control algorithm and a modern prosthesis available in the laboratory, normal subjects and below elbow amputees could then evaluate the performance of the control program and the prosthetic equipment in a quite realistic situation.

Bibliography

Andrews, J. R., Carson, W. G., Jr. and McLeod, W. D. (1985). "Glenoid labrum tears related to the long head of the biceps." Am. J. Sports. Med. **13**(5), 337-341.

Antuvan, C. W., Bisio, F., Marini, F., Yen, S. C., Cambria, E. and Masia, L. (2016). "Role of muscle synergies in real-time classification of upper limb motions using extreme learning machines." J. Neuroeng. Rehabil. **13**(76).

Athwal, G. S., Steinmann, S. P. and Rispoli, D. M. (2007). "The distal biceps tendon: footprint and relevant clinical anatomy." J. Hand Surg. Am. **32**(8), 1225-1229.

Atoufi, B., Kamavuako, E. N., Hudgins, B. and Englehart, K. (2014). "Toward proportional control of myoelectric prostheses with muscle synergies." J. Med. Biol. Eng. **34**(5), 475-481.

Atoufi, B., Kamavuako, E. N., Hudgins, B. and Englehart, K. (2015). Classification of hand and wrist tasks of unknown force levels using muscle synergies. Conf. Proc. IEEE Eng. Med. Biol. Soc. Milan, Italy.

Betthauser, J. L., Hunt, C. L., Osborn, L. E., Masters, M. R., Levay, G., Kaliki, R. R. and Thakor, N. V. (2018). "Limb position tolerant pattern recognition for myoelectric prosthesis control with adaptive sparse representations from extreme learning." IEEE Trans. Biomed. Eng. **65**(4), 770-778.

Bi, L., Feleke, A. G. and Guan, C. (2019). "A review on EMG-based motor intention prediction of continuous human upper limb motion for human-robot collaboration." Biomed. Signal Process. Control **51**, 113-127.

Bizzi, E. (2016). "Motor control revisited: a novel view." Curr. Trends Neurol. **10**, 75-80.

Bizzi, E. and Ajemian, R. J. (2015). "A hard scientific quest: understanding voluntary movements." Daedalus **144**(1), 83-95.

Bizzi, E. and Cheung, V. C. K. (2013). "The neural origin of muscle synergies." Front. Comput. Neurosci. **7**(51), 1-6.

Bizzi, E., Cheung, V. C. K., d'Avella, A., Saltiel, P. and Tresch, M. (2008). "Combining modules for movement." Brain. Res. Rev. **57**(1), 125-133.

Bizzi, E., d'Avella, A., Saltiel, P. and Tresch, M. (2002). "Modular organization of spinal motor systems." Neuroscientist **8**(5), 437-442.

Bizzi, E., Tresch, M. C., Saltiel, P. and d'Avella, A. (2000). "New perspectives on spinal motor systems." Nat. Rev. Neurosci. **1**(2), 101-108.

Buchanan, T. S., Almdale, D. P., Lewis, J. L. and Rymer, W. Z. (1986). "Characteristics of synergic relations during isometric contractions of human elbow muscles." J. Neurophysiol. **56**(5), 1225-1241.

Buchthal, F. and Schmalbruch, H. (1980). "Motor unit of mammalian muscle." Physiol. Rev. **60**(1), 90-142.

Cheung, V. C. K., d'Avella, A. and Bizzi, E. (2009). "Adjustments of motor pattern for load compensation via modulated activations of muscle synergies during natural behaviors." J. Neurophysiol. **101**(3), 1235-1257.

Cheung, V. C. K., d'Avella, A., Tresch, M. C. and Bizzi, E. (2005). "Central and sensory contributions to the activation and organization of muscle synergies during natural motor behaviors." J. Neurosci. **25**(27), 6419-6434.

Chiarapattanakom, P., Leechavengvongs, S., Witoonchart, K., Uerpairojkit, C. and Thuvasethakul, P. (1998). "Anatomy and internal topography of the musculocutaneous nerve: the nerves to the biceps and brachialis muscle." J. Hand Surg. Am. **23**(2), 250-255.

Côté, J. and Mathieu, P. A. (2000). "Mapping of the human upper arm muscle activity with an electrode matrix." Electromyogr. Clin. Neurophysiol. **40**(4), 215-223.

Cunningham, J. P. and Ghahramani, Z. (2015). "Linear dimensionality reduction: survey, insights, and generalizations." J. Mach. Learn. Res. **16**(89), 2859-2900.

d'Avella, A., Giese, M., Ivanenko, Y. P., Schack, T. and Flash, T. (2015). "Editorial: Modularity in motor control: from muscle synergies to cognitive action representation." Front. Comput. Neurosci. **9**(126), 1-6.

d'Avella, A. and Lacquaniti, F. (2013). "Control of reaching movements by muscle synergy combinations." Front. Comput. Neurosci. **7**(42), 1-7.

d'Avella, A., Portone, A., Fernandez, L. and Lacquaniti, F. (2006). "Control of fast-reaching movements by muscle synergy combinations." J. Neurosci. **26**(30), 7791-7810.

d'Avella, A., Saltiel, P. and Bizzi, E. (2003). "Combinations of muscle synergies in the construction of a natural motor behavior." Nat. Neurosci. **6**(3), 300-308.

d'Avella, A. and Tresch, M. (2006). Muscle synergies for motor control. In M. Akay, Handbook of Neural Engineering (pp. 449-465). Hoboken, NJ: John Wiley & Sons.

Dahmane, R., Djordjevic, S., Simunic, B. and Valencic, V. (2005). "Spatial fiber type distribution in normal human muscle histochemical and tensiomyographical evaluation." J. Biomech. **38**(12), 2451-2459.

De la Barrera, E. J. and Milner, T. E. (1994). "The effects of skinfold thickness on the selectivity of surface EMG." Electroencephalogr. Clin. Neurophysiol. **93**(2), 91-99.

Delis, I., Berret, B., Pozzo, T. and Panzeri, S. (2013). "Quantitative evaluation of muscle synergy models: a single-trial task decoding approach." Front. Comput. Neurosci. **7**(8), 1-21.

Duda, R. O., Hart, P. E. and Stork, D. G. (2001). Pattern Classification. New York, NY: John Wiley & Sons.

English, A. W., Wolf, S. L. and Segal, R. L. (1993). "Compartmentalization of muscles and their motor nuclei: the partitioning hypothesis." Phys. Ther. **73**(12), 857-867.

Farina, D., Merletti, R., Indino, B. and Graven-Nielsen, T. (2004). "Surface EMG crosstalk evaluated from experimental recordings and simulated signals: reflections on crosstalk interpretation, quantification and reduction." Methods Inf. Med. **43**(1), 30-35.

Fougner, A., Stavdahl, O., Kyberd, P. J., Losier, Y. G. and Parker, P. A. (2012). "Control of upper limb prostheses: terminology and proportional myoelectric control - a review." IEEE Trans. Neural. Syst. Rehabil. Eng. **20**(5), 663-677.

Fürnkranz, J. (2002). Pairwise classification as an ensemble technique. In T. Elomaa, H. Mannila and H. Toivonen, ECML 2002. Lect. Notes Comput. Sci., **2430** (pp. 97-110). Berlin/Heidelberg, Germany: Springer.

Gawthrop, P., Loram, I., Lakie, M. and Gollee, H. (2011). "Intermittent control: a computational theory of human control." Biol. Cybern. **104**(1-2), 31-51.

Gui, Q., Meng, M., Ma, Y. and Luo, Z. (2016). "Continuous estimation for joint movements of upper limb based on synergy activation model." Chinese J. Sci. Instrum. **37**(6), 1405-1412.

Haith, A. M. and Krakauer, J. W. (2012). Theoretical models of motor control and motor learning. In A. Gollhofer, W. Taube and J. B. Nielsen, Routledge Handbook of Motor Control and Motor Learning (pp. 7-28). Abingdon, United Kingdom: Taylor & Francis.

He, L. and Mathieu, P. A. (2017). Muscle synergy of biceps brachii and online classification of upper limb posture. Proc. Int. Conf. Virtual Rehabilitation (ICVR 2017). Montréal, Québec.

Henneman, E. (1957). "Relation between size of neurons and their susceptibility to discharge." Science **126**(3287), 1345-13477.

Henneman, E., Somjen, G. and Carpenter, D. O. (1965). "Functional significance of cell size in spinal motoneurons." J. Neurophysiol. **28**(3), 560-580.

Heywood, S., Pua, Y. H., McClelland, J., Geigle, P., Rahmann, A., Bower, K. and Clark, R. (2018). "Low-cost electromyography - Validation against a commercial system using both manual and automated activation timing thresholds." J. Electromyogr. Kinesiol. **42**, 74-80.

Hubal, M. J., Gordish-Dressman, H., Thompson, P. D., Price, T. B., Hoffman, E. P., Angelopoulos, T. J., Gordon, P. M., Moyna, N. M., Pescatello, L. S., Visich, P. S., Zoeller, R. F., Seip, R. L. and Clarkson, P. M. (2005). "Variability in muscle size and strength gain after unilateral resistance training." Med. Sci. Sports Exerc. **37**(6), 964-972.

Huxley, A. F. and Niedergerke, R. (1954). "Structural changes in muscle during contraction: interference microscopy of living muscle fibres." Nature **173**(4412), 971-973.

Huxley, H. and Hanson, J. (1954). "Changes in the cross-striations of muscle during contraction and stretch and their structural interpretation." Nature **173**(4412), 973-976.

Jarrett, C. D., Weir, D. M., Stuffmann, E. S., Jain, S., Miller, M. C. and Schmidt, C. C. (2012). "Anatomic and biomechanical analysis of the short and long head components of the distal biceps tendon." J. Shoulder Elbow. Surg. **21**(7), 942-948.

Jiang, N., Englehart, K. B. and Parker, P. A. (2009). "Extracting simultaneous and proportional neural control information for multiple-DOF prostheses from the surface electromyographic signal." IEEE Trans. Biomed. Eng. **56**(4), 1070-1080.

Jiang, N., Rehbaum, H., Vujaklija, I., Graimann, B. and Farina, D. (2014). "Intuitive, online, simultaneous, and proportional myoelectric control over two degrees-of-freedom in upper limb amputees." IEEE Trans. Neural Syst. Rehabil. Eng. **22**(3), 501-510.

Joergensen, K. (2006). "NMF DTU Toolbox." Retrieved on January 2016, from http://cogsys.imm.dtu.dk/toolbox.

Kim, B. S. (2016). Link mechanism and universal coupler based on the same. U. S. Patent. **US9500215B2**.

Kuiken, T. A., Lowery, M. M. and Stoykov, N. S. (2003). "The effect of subcutaneous fat on myoelectric signal amplitude and cross-talk." Prosthet. Orthot. Int. **27**(1), 48-54.

Landin, D., Myers, J., Thompson, M., Castle, R. and Porter, J. (2008). "The role of the biceps brachii in shoulder elevation." J. Electromyogr. Kinesiol. **18**(2), 270-275.

Lee, D. D. and Seung, H. S. (1999). "Learning the parts of objects by non-negative matrix factorization." Nature **401**(6755), 788-791.

Lee, D. D. and Seung, H. S. (2001). Algorithms for non-negative matrix factorization. In T. K. Leen, T. G. Dietterich and V. Tresp, Advances in Neural Information Processing Systems 13 (pp. 556-562). Cambridge, MA: MIT Press.

Ma, J., Thakor, N. V. and Matsuno, F. (2015). "Hand and wrist movement control of myoelectric prosthesis based on synergy." IEEE Trans. Hum. Mach. Syst. **45**(1), 74-83.

Malmivuo, J. and Plonsey, R. (1995). Nerve and muscle cells. In, Bioelectromagnetism: Principles and Applications of Bioelectric and Biomagnetic Fields (pp. 33-43). Oxford, United Kingdom: Oxford University Press.

Marieb, E. N. and Hoehn, K. (2007). Human Anatomy & Physiology. New York, NY: Pearson Education.

Merletti, R. and Muceli, S. (2019). "Tutorial. Surface EMG detection in space and time: Best practices." J. Electromyogr. Kinesiol. **49**(102363), 1-16.

Miyatani, M., Kanehisa, H., Ito, M., Kawakami, Y. and Fukunaga, T. (2004). "The accuracy of volume estimates using ultrasound muscle thickness measurements in different muscle groups." Eur. J. Appl. Physiol. **91**(2-3), 264-272.

Muceli, S., Boye, A. T., d'Avella, A. and Farina, D. (2010). "Identifying representative synergy matrices for describing muscular activation patterns during multidirectional reaching in the horizontal plane." J. Neurophysiol. **103**(3), 1532-1542.

Naik, G. R. and Nguyen, H. T. (2015). "Nonnegative matrix factorization for the identification of EMG finger movements: evaluation using matrix analysis." IEEE J. Biomed. Health Inform. **19**(2), 478-485.

Neilson, P. D., Neilson, M. D. and O'Dwyer, N. J. (1988). "Internal models and intermittency: A theoretical account of human tracking behavior." Biol. Cybern. **58**(2), 101-112.

Nejat, N. (2012). Study on the activation of the biceps brachii compartments in normal subjects. Montréal, Québec: Université de Montréal. **Master's Thesis**.

Nielsen, J. L., Holmgaard, S., Jiang, N., Englehart, K., Farina, D. and Parker, P. (2009). Enhanced EMG signal processing for simultaneous and proportional myoelectric control. Conf. Proc. IEEE Eng. Med. Biol. Soc. Minneapolis, MN.

Norouzi-Gheidari, N., Archambault, P. S. and Fung, J. (2019). "Robot-assisted reaching performance of chronic stroke and healthy individuals in a virtual versus a physical environment: a pilot study." IEEE Trans. Neural. Syst. Rehabil. Eng. **27**(6), 1273-1281.

Ogata, K. (2010). Modern Control Engineering. Upper Saddle River, NJ: Pearson Education.

Oliveira, A. S., Gizzi, L., Farina, D. and Kersting, U. G. (2014). "Motor modules of human locomotion: influence of EMG averaging, concatenation, and number of step cycles." Front. Hum. Neurosci. **8**(335), 1-9.

Osborne, A. W., Birch, R. M., Munshi, P. and Bonney, G. (2000). "The musculocutaneous nerve." J. Bone Joint Surg. Br. **82**(8), 1140-1142.

Papin, G. (2004). Le nerf musculo-cutane. Nantes, France: Université de Nantes. **Master's Thesis**.

Park, S.-H. and Fürnkranz, J. (2007). Efficient pairwise classification. In J. N. Kok, J. Koronacki, R. L. d. Mantaras et al., ECML 2007. Lect. Notes Comput. Sci., **4701** (pp. 658-665). Berlin/Heidelberg, Germany: Springer.

Powell, M. A., Kaliki, R. R. and Thakor, N. V. (2014). "User training for pattern recognition-based myoelectric prostheses: improving phantom limb movement consistency and distinguishability." IEEE Trans. Neural Syst. Rehabil. Eng. **22**(3), 522-532.

Powell, M. A. and Thakor, N. V. (2013). "A training strategy for learning pattern recognition control for myoelectric prostheses." J. Prosthet. Orthot. **25**(1), 30-41.

Rasool, G., Iqbal, K., Bouaynaya, N. and White, G. (2016). "Real-time task discrimination for myoelectric control employing task-specific muscle synergies." IEEE Trans. Neural Syst. Rehabil. Eng. **24**(1), 98-108.

Rousseeuw, P. J. (1987). "Silhouettes: a graphical aid to the interpretation and validation of cluster analysis." J. Comput. Appl. Math. **20**, 53-65.

Sabzevari, V. R., Jafari, A. H. and Boostani, R. (2017). "Muscle synergy extraction during arm reaching movements at different speeds." Technol. Health Care **25**(1), 123-136.

Saltiel, P., Wyler-Duda, K., d'Avella, A., Ajemian, R. J. and Bizzi, E. (2005). "Localization and connectivity in spinal interneuronal networks: the adduction-caudal extension-flexion rhythm in the frog." J. Neurophysiol. **94**(3), 2120-2138.

Sanders, D. B., Arimura, K., Cui, L., Ertaş, M., Farrugia, M. E., Gilchrist, J., Kouyoumdjian, J. A., Padua, L., Pitt, M. and Stålberg, E. (2019). "Guidelines for single fiber EMG." Clin. Neurophysiol. **130**(8), 1417-1439.

Schantz, P., Randall-Fox, E., Hutchison, W., Tyden, A. and Astrand, P. O. (1983). "Muscle fibre type distribution, muscle cross-sectional area and maximal voluntary strength in humans." Acta. Physiol. Scand. **117**(2), 219-226.

Scheme, E. and Englehart, K. (2011). "Electromyogram pattern recognition for control of powered upper-limb prostheses: state of the art and challenges for clinical use." J. Rehabil. Res. Dev. **48**(6), 643-659.

Segal, R. L. (1992). "Neuromuscular compartments in the human biceps brachii muscle." Neurosci. Lett. **140**(1), 98-102.

Sharma, A., Niu, W., Hunt, C. L., Levay, G., Kaliki, R. and Thakor, N. V. (2019). "Augmented reality prosthesis training setup for motor skill enhancement." arXiv:1903.01968 [cs.HC].

Sherman, E. D. (1964). "A Russian bioelectric-controlled prosthesis: report of a research team from the Rehabilitation Institute of Montreal." Can. Med. Assoc. J. **91**(24), 1268-1270.

Slotine, J.-J. E. and Li, W. (1991). Applied Nonlinear Control. Upper Saddle River, NJ: Prentice Hall.

Srinivasan, R. C., Lungren, M. P., Langenderfer, J. E. and Hughes, R. E. (2007). "Fiber type composition and maximum shortening velocity of muscles crossing the human shoulder." Clin. Anat. **20**(2), 144-149.

Staudenmann, D., Stegeman, D. F. and van Dieën, J. H. (2013). "Redundancy or heterogeneity in the electric activity of the biceps brachii muscle? Added value of PCA-processed multi-channel EMG muscle activation estimates in a parallel-fibered muscle." J. Electromyogr. Kinesiol. **23**(4), 892-898.

ter Haar Romeny, B. M., van der Gon, J. J. and Gielen, C. C. A. M. (1984). "Relation between location of a motor unit in the human biceps brachii and its critical firing levels for different tasks." Exp. Neurol. **85**(3), 631-650.

Theodoridis, S. and Koutroumbas, K. (2009). Pattern Recognition. Amsterdam, Netherlands: Elsevier.

Ting, L. H. and Macpherson, J. M. (2005). "A limited set of muscle synergies for force control during a postural task." J. Neurophysiol. **93**(1), 609-613.

Ting, L. H. and McKay, J. L. (2007). "Neuromechanics of muscle synergies for posture and movement." Curr. Opin. Neurobiol. **17**(6), 622-628.

Torres-Oviedo, G. and Ting, L. H. (2007). "Muscle synergies characterizing human postural responses." J. Neurophysiol. **98**(4), 2144-2156.

Tresch, M. C., Saltiel, P. and Bizzi, E. (1999). "The construction of movement by the spinal cord." Nat. Neurosci. **2**(2), 162-167.

Tresch, M. C., Saltiel, P., d'Avella, A. and Bizzi, E. (2002). "Coordination and localization in spinal motor systems." Brain Res. Brain Res. Rev. **40**(1-3), 66-79.